# Autonomous navigation of a wheeled mobile robot in farm settings

A Thesis Submitted to

the College of Graduate Studies and Research

in Partial Fulfillment of Requirements

for the Degree of Doctor of Philosophy

in the Department of Mechanical Engineering,

University of Saskatchewan, Saskatoon

Canada

By:

Seyede Fatemeh Heidari K.

## Permission to use

In presenting this thesis in partial fulfillment of the requirement for a postgraduate degree from the University of Saskatchewan, I agree that the Libraries of this University may make it freely available for inspection. I further agree that the permission for copying this thesis in any manner, in whole or in part for scholarly purposes, may be granted by the professors who supervised my thesis work or, in their absence, by the Head of the Department or Dean of the college in which my thesis work was conducted. It is understood that any copying or publication or use of this thesis or parts therefore for financial gain shall not be allowed without my written permission. It is also understood that due recognition shall be given to me and to the University of Saskatchewan in any scholarly use which may be made of any martial in my thesis.

Request for permission to copy or to make other use of material in this thesis, in whole or part, should be addressed to:

Head of the Department of Mechanical Engineering
University of Saskatchewan
College of Engineering
57 Campus Drive
Saskatoon, Saskatchewan, S7N 5A9
Canada

## Abstract:

This research is mainly about autonomously navigation of an agricultural wheeled mobile robot in an unstructured outdoor setting. This project has four distinct phases defined as: (i) Navigation and control of a wheeled mobile robot for a point-to-point motion. (ii) Navigation and control of a wheeled mobile robot in following a given path (path following problem). (iii) Navigation and control of a mobile robot, keeping a constant proximity distance with the given paths or plant rows (proximity-following). (iv) Navigation of the mobile robot in rut following in farm fields. A rut is a long deep track formed by the repeated passage of wheeled vehicles in soft terrains such as mud, sand, and snow.

To develop reliable navigation approaches to fulfill each part of this project, three main steps are accomplished: literature review, modeling and computer simulation of wheeled mobile robots, and actual experimental tests in outdoor settings. First, point-to-point motion planning of a mobile robot is studied; a fuzzy-logic based (FLB) approach is proposed for real-time autonomous path planning of the robot in unstructured environment. Simulation and experimental evaluations shows that FLB approach is able to cope with different dynamic and unforeseen situations by tuning a safety margin. Comparison of FLB results with vector field histogram (VFH) and preference-based fuzzy (PBF) approaches, reveals that FLB approach produces shorter and smoother paths toward the goal in almost all of the test cases examined. Then, a novel human-inspired method (HIM) is introduced. HIM is inspired by human behavior in navigation from one point to a specified goal point. A human-like reasoning ability about the situations to reach a predefined goal point while avoiding any static, moving and unforeseen obstacles are given

to the robot by HIM. Comparison of HIM results with FLB suggests that HIM is more efficient and effective than FLB.

Afterward, navigation strategies are built up for path following, rut following, and proximity-following control of a wheeled mobile robot in outdoor (farm) settings and off-road terrains. The proposed system is composed of different modules which are: sensor data analysis, obstacle detection, obstacle avoidance, goal seeking, and path tracking. The capabilities of the proposed navigation strategies are evaluated in variety of field experiments; the results show that the proposed approach is able to detect and follow rows of bushes robustly. This action is used for spraying plant rows in farm field.

Finally, obstacle detection and obstacle avoidance modules are developed in navigation system. These modules enables the robot to detect holes or ground depressions (negative obstacles), that are inherent parts of farm settings, and also over ground level obstacles (positive obstacles) in real-time at a safe distance from the robot. Experimental tests are carried out on two mobile robots (PowerBot and Grizzly) in outdoor and real farm fields. Grizzly utilizes a 3D-laser range-finder to detect objects and perceive the environment, and a RTK-DGPS unit for localization. PowerBot uses sonar sensors and a laser range-finder for obstacle detection. The experiments demonstrate the capability of the proposed technique in successfully detecting and avoiding different types of obstacles both positive and negative in variety of scenarios.

# Acknowledgment

First and foremost I would like to express my gratitude to my supervisor, Professor Reza Fotouhi who has been really supportive and given me the freedom to pursue various projects without objection. He has also provided insightful discussions about the research. Without his invaluable guidance, support and encouragement through my PhD program, this work would not have been possible. I also would like to thank the members of my PhD committee, Professors Rich Burton, Daniel Chen, and Aryan Saadatmehr for their helpful suggestions in general.

Financial support of this work provided by the University of Saskatchewan Graduate Scholarship and NSERC discovery grant and is gratefully acknowledged.

I am grateful to the Department of Mechanical Engineering for providing me a comfortable research environment.

# Table of Contents

# List of Acronyms

**AGV: Autonomous Ground Vehicle**

**LRF: Laser Range Finder**

**HIM: Human-Inspired Method**

**FLB: Fuzzy Logic Based**

**GPS: Global Positioning System**

**RTK-DGPS: Real-Time Kinematic Differential Global Positioning System**

# List of Figures

# List of Tables

# Chapter 1: Introduction

## 1.1 Background and motivation

Investigation on development of autonomous mobile robots for agricultural use is essential because of tedious, monotonous and very exhausting tasks for farmers. These tasks may include seeding, sowing, irrigating, weeding and harvesting. So usage of mobile robots in agricultural farms will result in raising the quality of the products, lowering production costs, and reducing the manual labors. While an increasing numbers of robots are being used in many different areas such as agricultural, manufacturing, medical care etc., there are also increasing needs for robots to be navigated robustly, reliably and accurately. Robust navigation of robots in outdoor and unstructured (unknown) environments is still a major challenge.

However, since the agricultural environments are very complex and mostly unstructured (unknown), navigation of mobile robots in these areas involve difficulties such as: robot operation in three dimensional continuously changing tracks, targets which are difficult to detect and reach, and targets may become hidden among leaves or branches. Hence, navigation and control of an agricultural autonomous mobile robot requires dynamic, real-time representation of the environment (localization and map-building), obstacle detection and collision avoidance, and path planning/ path following toward the goal. Therefore to design a system that can robustly navigate mobile robots in all conditions is really difficult.

Development of agricultural autonomous mobile robots is essential because of following reasons:

- Potential shortages of farmers in future

- Farming tasks are usually exhausting, and robots are not affected by age, unlike humans
- Farm setting are considered harsh and rough for a human, and may pose health hazards, thus using robots may be preferred in those settings

The research described in this thesis is a comprehensive study of navigation of a mobile robot on an inclined actual farm field (with maneuverable hill) using real-time differential global positioning system (RTK-DGPS) for localization. Two wheeled mobile robots (PowerBot and Grizzly) used for experiments are equipped with sonar sensors and laser range finders (LRF) to perceive the environments and shown in Fig. 1-1.

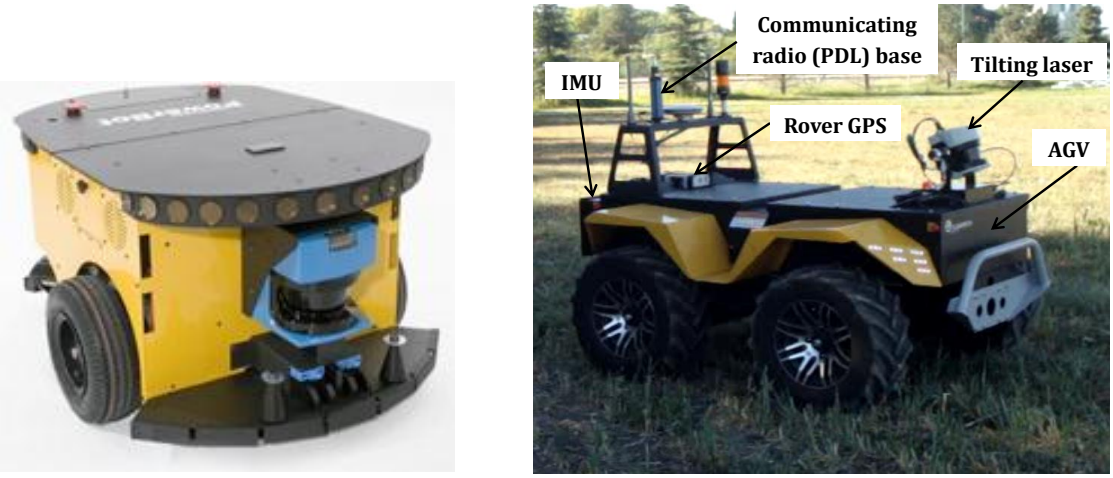


(a) (b)

Fig. 1-1: (a) PowerBot, (b) Grizzly mobile robots used for simulation and experimental tests

## 1.2 research objectives

The main objective of this research is autonomously navigation of an agricultural mobile robot. This project has four distinct parts defined as:

**1)** Navigation and control of a wheeled mobile robot for a point-to-point motion. In a farm setting a robot needs to navigate from a start point (home-position of the robot) to an end-point (where it starts to do its task).

**2)** Navigation and control of a wheeled mobile robot in following a given path (path following problem for seeding in a straight or curve path).

**3)** Navigation and control of a wheeled mobile robot, keeping a constant proximity distance with the given paths or plant rows (defined as parameter *d* in Fig. 1-1). This task is mainly for weed control and staying close enough to a row of crop for spraying.

**4)** Navigation of a mobile robot in rut following in farm fields. A rut is a long deep track formed by the repeated passage of wheeled vehicles in soft terrains such as mud, sand, and snow. Fig. 1-2 shows a typical rut made by the passage of manned vehicles in a farm field.

Fig. 1-2: A typical rut formed by the passage of vehicles in a farm field

These different aspects of the project are depicted schematically in Fig. 1-3.

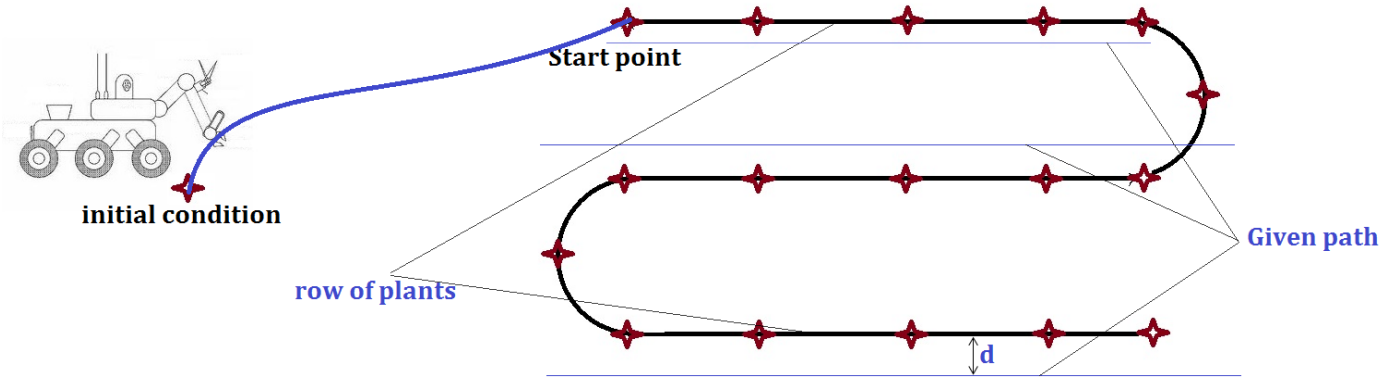


Fig. 1-3: Schematic of a navigation and control of wheeled mobile robot in farm field; first part of motion is a point-to-point motion while the second part are path following and proximity-following tasks.

## 1.3 Research methodology:

To choose the best appropriate navigation technique for this project, various kinds of methods for navigation of the mobile robots were studied comprehensively. Therefore, to develop an autonomous mobile robot that is capable of navigating in unstructured outdoor terrains such as a farm setting reliably, three main steps were accomplished: literature review, modeling and computer simulation of the wheeled mobile robots, and actual experimental tests in outdoor settings. An extensive literature search for information regarding navigation of wheeled mobile robots in outdoor terrains was performed. This resulted in a critical analysis of relevant published scholarly articles, research reports, books, theses etc. Then, kinematics, dynamics and navigation of two mobile robots, PowerBot and Grizzly, were simulated in MobileSim and Robot Operating System (ROS). Finally, the navigation of mobile robots was conducted on PowerBot and Grizzly robots in outdoor settings.

## 1.4 Synopsis of thesis

The chapters of this thesis were arranged in order to cover the research objectives explained in Section 1.3. In this research, navigation includes point-to-point motion planning, path following, proximity-following, and also rut-following of the mobile robot in off-road terrains. This thesis is organized as follows:

**Chapter 2:**

The contents of Chapter 2 were published in ASME conference under the title of "sensor-based navigation of agricultural autonomous mobile robots" [9]. In this chapter, the results related to the first objective were presented. A fuzzy-logic based (FLB) approach was proposed for real-time point-to-point motion planning of a mobile robot in complex and mostly unstructured environment. FLB approach required no prior knowledge of the environment and was able to cope with different dynamic and unforeseen situations by tuning a safety margin. The proposed method was validated using simulation and experimental tests. In Chapter 2, the results of FLB approach were compared with vector field histogram (VFH) and preference-based fuzzy (PBF) approaches; the comparison revealed that FLB approach produced shorter and smoother paths toward the goal in almost all of the test cases examined. To compare the results with PBF and VFH methods, two criteria were computed: the total path's length which robot traveled to reach its goal ($P_L$) and total bending energy of the trajectory ($B_E$). The total path length for the robot is calculated as summation of the distances between two consecutive points in robot's path from start point ($x_1$, $y_1$) to the goal point ($x_n$, $y_n$).

$$P_L = \sum_{i=1}^{n-1} \sqrt{(x_{i+1} - x_i)^2 + (y_{i+1} - y_i)^2} \qquad (1)$$

To consider smoothness of the paths produced by the proposed strategy, the total bending energy $B_E$ of the paths were computed as summation of square of curvatures.

$$B_E = \sum_{i=1}^{n-1} {\kappa_i}^2 \qquad (2)$$

where $k_i$ is the curvature of the path generated for the robot to follow. These two criteria were calculated for all paths produced by FLB, VFH, and PBF methods and are summarized in Table 1-I. It is seen from Table 1-I that the proposed navigation method produces shorter (lower value of $P_L$) and also smoother paths (lower $B_E$) compared with the PBF and VFH methods. Bending energy in FLB method for all cases except for the set-up3 was much smaller than the two other strategies; this means that our strategy provides much smoother paths with respect to the PBF and VFH approaches. FLB approach did not make abrupt changes in heading angle of the robot, and by providing shorter paths it decreased computational and execution times. The fuzzy approach developed in this chapter was applied on the mobile robot with other proposed approach in chapters 3, and 4.

Table 1-I: Comparison of the total path length ($P_L$) and bending energy ($B_E$) for the proposed FLB method with PBF and VFH

| Method / Set-up | **FLB** | | **PBF** | | **VFH** | |
|---|---|---|---|---|---|---|
| | **$P_L$ (cm)** | **$B_E$ (E-02)** | **$P_L$ (cm)** | **$B_E$ (E-02)** | **$P_L$ (cm)** | **$B_E$ (E-02)** |
| 1 | 510 | 0.750 | 571 | 4.510 | 573 | 5.330 |
| 2 | 680 | 0.610 | 943 | 68.420 | 966 | 10.500 |
| 3 | 675 | 0.530 | 399 | 1.930 | 390 | 3.700 |
| 4 | 570 | 0.670 | 433 | 4.620 | 380 | 3.620 |
| 5 | 375 | 0.060 | 513 | 3.250 | 713 | 5.940 |
| 6 | 450 | 3.400 | 469 | 2.820 | 425 | 5.550 |
| 7 | 590 | 0.820 | 539 | 2.510 | 458 | 7.120 |
| 8 | 575 | 0.510 | 466 | 7.320 | 456 | 10.170 |
| 9 | 555 | 0.730 | 437 | 2.800 | 237 | 4.600 |
| 10 | 425 | 0.520 | 444 | 2.040 | 400 | 5.010 |

**Chapter 3:**

The contents of Chapter 3 are under second review for publication in ASME journal of mechanisms and robotics under the title of "two new approaches for navigation of wheeled

mobile robots" [1]. This paper deals with point-to-point motion planning of the robot to fulfil the research objective 1. In this chapter a novel human-inspired method (HIM) was presented. HIM was inspired by human behavior in navigation from one point to a specified goal point. HIM endowed the robot a human-like ability for reasoning about the situations to reach a predefined goal point while avoiding any static, moving and unforeseen obstacles; this made the proposed strategy efficient and effective [8].

The HIM used distance-based sensory data from a laser range-finder for navigation of a wheeled mobile robot in unknown and cluttered settings. No prior knowledge from the environment was needed for the navigation. HIM gave the robot a human-like ability of reasoning about the environment which provided uncertainty management ability for the system. HIM enabled the robot to deal with imprecise and uncertain information, therefore the navigation system handled the error from laser readings and GPS data. Experimental evaluation of HIM indicated that HIM was capable of creating smooth (no oscillations) paths for safely navigating the mobile robot, and coping with fluctuating and imprecise sensory data from uncertain environment. HIM specified the best path ahead, according to the situation of encountered obstacles, preventing the robot to get trapped in deadlock and impassable conditions. This deadlock detection and avoidance is a significant ability of HIM. The simulation and experimental results of HIM and fuzzy logic method were presented and compared. HIM was computationally fast and efficient, since it used very simple and easily applicable rules for real-time robot navigation. The proposed approach in this chapter (HIM) was implemented for obstacle avoidance in chapters 4, and 5 for the navigation of the robot.

**Chapter 4:**

The content of Chapter 4 is a submitted paper to the ASME Journal of Mechanical Design under the title of "A biologically inspired approach for point-to-point and path-following navigation of mobile robots" [5].

In Chapter 4, the second part of the research objectives was realized. A navigation system was developed for path following control of a wheeled mobile robot in outdoor (farm) settings and off-road terrains. The proposed system was composed of four main actions which are: sensor data analysis, obstacle detection, obstacle avoidance, and goal seeking. Using these actions, the navigation method is capable of autonomous row-detection, row-following and path planning motion in outdoor settings such as farms. In order to drive the robot in off-road terrain safely, obstacle detection and obstacle avoidance modules were developed in navigation system. These modules enabled the robot to detect holes or ground depressions (negative obstacles), that are inherent parts of farm settings, and also over ground level obstacles (positive obstacles) in real-time at a safe distance from the robot. Other main originality of this chapter was that the robot could accurately identify the end of the rows of trees/bushes in farm/orchard and enter the next row to continue its tasks. The mobile robot utilizes a tilting unit which carries a laser range-finder to detect objects and perceive the environment, and a RTK-DGPS unit for localization. Diverse experimental tests were carried out using a differential wheeled mobile robot in farm fields to evaluate the navigation system. The experiments demonstrated that the proposed technique was capable of successfully detecting and following rows (path following) as well as robust navigation of the robot in point-to-point motion control.

**Chapter 5:**

The content of Chapter 5 was submitted for possible publication in Journal of Robotica under the title of "A new 3D laser-based method for proximity-following and rut following in orchard rows" [6].

The goal of this chapter was to fulfill the third and fourth parts of the research objectives. The navigation system developed in Chapter 4 was successfully extended to detect and follow the rows of bushes for proximity-following. In this system, while the robot followed the plant rows, it also kept a proximity distance with the rows. The plant rows were recognized based on Hough transform (a line recognition technique). The novelty of this chapter is in introducing a new curve fitting technique for row following. The proposed method generated piecewise smooth path for the robot to follow; this technique did not carry the shortages of Hough transform in line recognition. Rut following technique is also included in this chapter. This technique was carried out successfully to detect and follow different shapes and sizes of ruts (curvy, S-shape, and shallow ruts) and two ruts simultaneously in farm fields. In addition, data from a 3D laser range finder (LRF) was used to analyze the terrain and to detect negative obstacles. In this chapter, the navigation system was positively conducted to detect and avoid different holes in real-time in outdoor settings. The experimental evaluations conducted on a 4x4 differential drive 16.5 KW autonomous ground vehicle (AGV) in different field setups showed the accuracy and robustness of the proposed system in rut detection and tracking, proximity-following, and negative obstacle detection and avoidance tests.

**Chapter 6:**

In this chapter the summary and conclusions of the thesis are presented. Also, the directions for the possible expansions and future study of the research were discussed in this chapter.

The candidate's research on topics not related to this thesis resulted in publications [2 to 4] and [9]. The abstracts of these publications are included in Appendix.

## References

**Candidate's papers:**

**Published journal articles:**


1. **Heidari F.**, Fotouhi R., and Vakil, M., "Two New Approaches for Navigation of Wheeled Mobile Robots", ASME Journal of Mechanisms and Robotics, under review with minor revision **2013.**

2. Vakil M., Sharbati E., Vakil A., **Heidari F.**, Fotouhi R. "Vibration analysis of a Timoshenko beam on a moving base", Journal of Vibration and Control, DOI: 10.1177/ 1077546313492808, **2013**.

3. **Heidari F.**, Vakil M., Fotouhi R., Nikiforuk P. N., "Truncation error of assumed mode modeling for flexible-link manipulators", Journal of Mechanical Engineering Science, 226 (11), 2627-2644, **2012**.

4. Vakil M., Fotouhi R., Nikiforuk P. N., **Heidari, F.** "A study on the free vibration of flexible-link flexible-joint manipulators", Journal of Mechanical Engineering Science, 225(6), 1361-1371, **2011.**

**Unpublished journal articles (submitted for publication):**

5. **Heidari F.**, Fotouhi R., "A biologically inspired approach for point-to-point and path-following navigation of mobile robots", submitted to ASME Journal of Mechanical Design, **2013**.

6. **Heidari F.**, Fotouhi R., Bitner D., "A new 3D laser-based method for proximity-following in orchard rows", submitted to Journal of Robotica, **2013**.

**Published conference articles:**

7. **Heidari F.,** Vakil M., Fotouhi R., "A human-inspired method for mobile robot navigation", ASME 2013 International Design Engineering Technical Conferences, Portland, USA, August 4- 7, **2013**.
8. **Heidari, F.**, Vakil M., Fotouhi R., "Sensor-Based Navigation of Agricultural Autonomous Mobile Robots", ASME 2012 International Design Engineering Technical Conferences, Chicago, IL, USA, August 12-15, **2012**.
9. **Heidari, F.**, Vakil M., Fotouhi R., "On the Accuracy of Assumed Mode Modeling For Flexible Manipulators", ASME 2011 International Design Engineering Technical Conferences, Washington, DC, USA, August 29-31, **2011**.

# Chapter 2: Sensor-based navigation of agricultural autonomous mobile robots

The contents of this chapter were published in ASME conference, 2012:

**Heidari, F.**, Vakil M., Fotouhi R., "Sensor-Based Navigation of Agricultural Autonomous Mobile Robots", ASME 2012 International Design Engineering Technical Conferences, Chicago, IL, USA, August 12-15, **2012**.

## Abstract

Investigation on development of autonomous mobile robots for agricultural use in a complex and mostly unstructured environment is studied. An approach that uses fuzzy-logic control and distance-based sensory data for real-time navigation of a mobile robot in an unknown farm setting is proposed. This approach requires no prior knowledge of the environment and adjusts a safety margin to cope with dynamic and unforeseen conditions. The simulation and experimental results indicate that the proposed strategy navigates robot in different conditions safely and efficiently. Comparing our results with vector field histogram and preference-based fuzzy approaches revealed that the approach suggested here produces shorter and smoother paths toward goal in almost all of the test cases examined.

## 2.1. Introduction

Investigation on development of autonomous mobile robots for agricultural use is essential because of potential shortages of farmers in the future. Robots' tasks in the farm setting are monotonous and repetition. These tasks may include seeding, weeding and harvesting. Use of mobile robots in farm setting may result in lowering production costs, and reducing the manual labors.

However, since farm environments are very complex and mostly unstructured (unknown), navigation of robots involve difficulties such as: robot operation in changing tracks, and targets which are difficult to detect and reach.

In Europe and North America, particularly in Canada crop production has significant economic value, with millions of dollars of annual revenue. An autonomous mobile robot capable of navigating through rows of crops for intra-row weeding is a promising alternative for conventional weeding [1].

To the authors' knowledge only a few researchers have reported works in navigation of agricultural autonomous mobile robots. In [2] motion of a four-wheel-steering (4WS) mobile robot moving in farm land was modeled and controlled. They considered sliding and slippery conditions to attain both lateral deviation of the robot from desired path and the heading (orientation) of the vehicle with respect to a reference value. Outdoor navigation of a wheeled mobile robot was also discussed in [3]; navigation process was performed in four stages: Map-building, laser scanning and data processing, robot localization, and robot motion control.

Managing the uncertainty and altering conditions is one of the most challenging problems in navigating mobile robots in an unknown and unstructured environment. Several approaches were suggested for robot navigation, such as the artificial potential field [4], the vector field histogram (VFH) [5], the edge detection [6], the obstacle boundary following [7], the goal oriented recursive path planning (GORP) [8], the curvature velocity method [9], the dynamic window approach [10], and the fuzzy-logic and neural-network based reactive methods [11]. The model-based approaches use a map or model of the environment to generate a path for the robot to follow toward goal point. In [12] an online approach to define an obstacle free path for an outdoor mobile manipulator was suggested. Measurements using ultrasonic and laser sensors were used to generate a map of the terrain and to define an obstacle free path for the robot. The uncertainty of parameters

computed in map building process was minimized using combination of adaptive Kalman filter and a fuzzy interface mechanism. But the model-based approaches would have difficulty dealing with the real time navigation of a mobile robot in outdoor environment. This is because it is usually difficult or maybe impossible to obtain an accurate model of a dynamic outdoor environment. Sensor-based approaches [13] use data from different sensors such as sonar, laser range finder or visual camera in real time to generate control commands for the mobile robot motion. The main advantage of sensor-based approaches is that a robot can navigate safely in a dynamic environment by reacting to unforeseen obstacles.

The potential field method suffers from getting trapped in local minima; unintended stoppage happens between closely spaced obstacles; oscillations (circulating around) in the presence of multiple obstacles; and oscillations in narrow passages [4].

Dynamic window approach computes the optimum velocity of a robot and satisfies the kinematic and dynamic constraints of a robot, and maximizes a given cost function. This cost function is usually defined as a distance to a goal and obstacles in the environment [14]. In the GORP method a longest straight-path segment is first found; then the approach tries to direct the robot to the goal while keeping shortest distance to the predefined path and avoiding the obstacles [7]. This method produces paths in an open area with convex objects, but may have difficulty in the presence of non-convex obstacles and cannot plan the shortest path. To develop algorithms for real-time mobile robot navigation in unstructured and unknown outdoor environments, fuzzy-logic and neural-network approaches were proposed. Real time adaptive motion planning (RAMP) was developed for simultaneously planning and execution of motion of high degree of freedom mobile

manipulators [15]. Due to simplicity of implementation, fuzzy logic control is well suited for autonomous mobile robots. Fuzzy logic has been utilized in navigation systems for mobile robots for sometimes [16]. In navigating mobile robot in an obstacle free path hierarchical fuzzy controller [17] and preference-based fuzzy behavior method [18] were used. The navigation problem was broken down into two control actions: heading control and speed control. Obstacle avoidance was performed in speed control stage. Application of a hierarchical Fuzzy-Genetic system to produce an autonomous outdoor mobile robot controller capable of online learning and implementing was introduced in [19].

Use of fuzzy-logic in mobile robot navigation [13] revealed flexible capability of fuzzy control results in producing smooth path for the robot motion; fuzzy-logic is also robust to face the errors and fluctuations in sensory data. The problems of deadlock, when there is no passable space for the robot to go through and the robot get trapped and goal-unreachable were dealt with reinforcement learning to adjust parameters in fuzzy navigator. Fuzzy-logic approaches were also combined with other algorithms, such as genetic algorithms [20], potential fields [21], and neural networks [22].

In fuzzy-logic control and navigation of mobile robot the number of rules and input/outputs increase exponentially with the number of variables; hence performance time of real-time control of robot will increase dramatically. To solve this problem, a hierarchical fuzzy-logic strategy was proposed to break down the input space for analysis by sharing this space amongst multiple low level behaviors. Each behavior is designed to respond to specific types of situations, and then the recommended outputs of these behaviors are integrated via a high level coordination layer [23].

This paper introduces a new fuzzy based approach for mobile robot navigation in an

agricultural farm setting with unforeseen and challenging conditions. The premise of the proposed method is its robust results for uncertain and changing environments which is inherent characteristic of the farm fields. In this research, tuning a safety factor enables the robot to cope with fluctuating and imprecise sensory data from uncertain environment. In this method no prior knowledge about the environment is needed, consequently it is appropriate and easy to implement for real-time navigation in mobile robotics. The proposed navigation method is experimentally tested in a laboratory setting, and is compared with previous methods such as Vector Field Histogram (VFH) and preference-based fuzzy (PBF) [18].

## 2.2. Proposed fuzzy strategy for mobile robot navigation

### 2.2.1. Robot Model

In this study, an automated guided vehicle (AGV) mobile robot is employed to investigate the performance of the designed fuzzy navigation approach. The robot is equipped with two sonar arrays, one in front and the other one in the rear. These sonar arrays provide 360 degrees of seamless sensing. The robot moves in one plane and can identify its own pose in the world by GPS and IMU (Inertial Measurement Unit) data in outdoor environment or integrating the encoder's information for indoor navigation. Each drive shaft is equipped with a high resolution optical quadrature shaft encoder for precise position, direction, and speed sensing and advanced dead-reckoning.

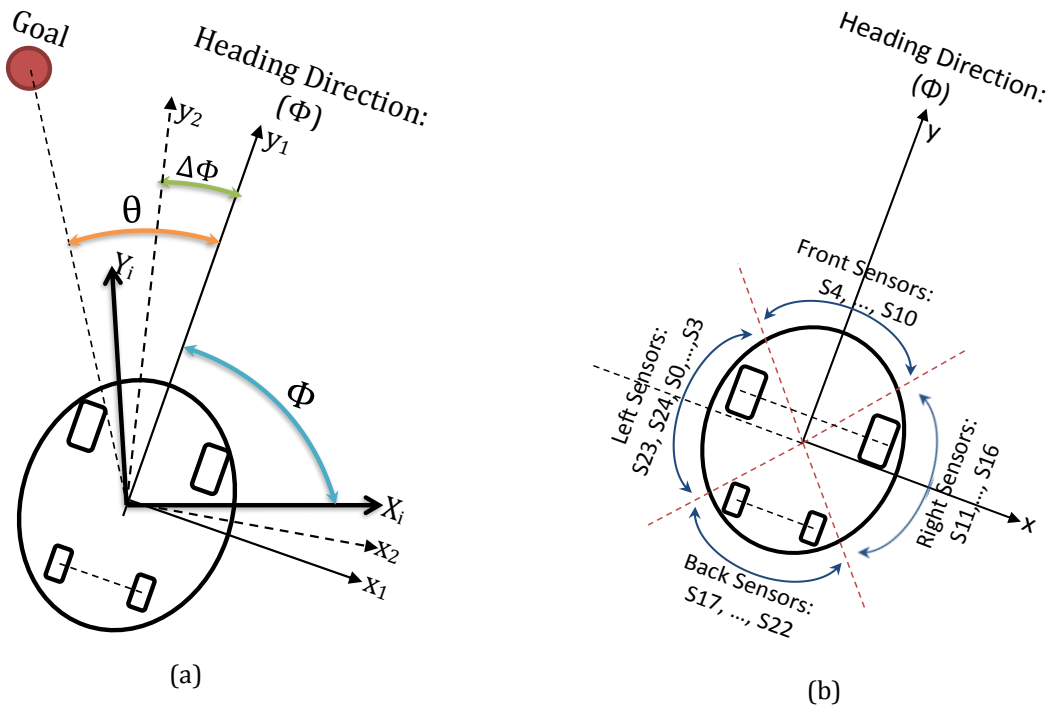


Fig. 2-1: Schematic of (a) the mobile robot and (b) the sonar arrangements on the robot

In Fig. 2-1 a schematic of top view of the AGV and the sonar system are depicted. These sonar sensors are divided into four groups of left (sensors S23, S24, S0, S1, S2, S3), front (sensors S4, S5,…, S10), right (sensors S11, S12, …, S16) and back (sensors S17, S18,…, S22). The obstacle distances detected in right, front, left, and back of the robot are represented by dR, dF, dL and dB respectively. These parameters are defined as:

$$\begin{cases} dL = \min\{distance\ data\ of\ sensors:\ (\mathrm{S23}, \mathrm{S24}, \mathrm{S0}, \dots, \mathrm{S3})\} \\ dF = \min\{distance\ data\ of\ sensors: (S4, S5, \dots, S10)\} \\ dR = \min\{distance\ data\ of\ sensors: (S11, S12, \dots, S16)\} \\ dB = \min\{distance\ data\ of\ sensors: (S17, S18, \dots, S22)\} \end{cases} \quad (1)$$

There exists an inertial coordinate system ($X_i$-$Y_i$) attached to the ground and a robot coordinate system (x-y) attached to the centre of the robot base. The angle between heading of the robot and $X_i$ axis is defined as angle (Φ), the angle between orientation of goal in x-y coordinate system and heading of the robot is defined as (θ). Control action

includes heading control, which provides change in heading angle of the robot ($\Delta\Phi$), and speed control which provides robot linear speed (v).

## 2.3. Fuzzy Navigation Strategy

The proposed navigation strategy in this research is based on fuzzy-logic control. Different behaviour blocks are suggested; each behaviour block is composed of sets of fuzzy-logic rule statements designed for achieving appropriate values for control parameters ($\Delta\Phi$ and v). The motion control variables of the mobile robot are the translational speed of the robot (v) and the change in the heading angle of the robot ($\Delta\Phi$). These navigation blocks are composed of fuzzy rules and statements. Inputs for the navigation blocks are sensor reading information. For example in obstacle avoidance behaviour, this information is obstacle's distances to the robot: sonar sensors' measurement in right, front and left sectors of the robot to determine the distances to obstacles in each sector according to equation (1). These distances are mapped in to fuzzy membership functions {Far, Medium, Close} as shown in Fig. 2-2. Then according to the defined fuzzy rules, control outputs ($\Delta\Phi_j$ and $v_j$) for each rule are produced. The final control output will be obtained using defuzzification for each fuzzy rule's output.

The change in the robot heading angle is represented using five linguistic fuzzy sets {NB, NS, ZE, PS, PB}; these membership functions are illustrated in Fig. 2-3. NB is negative-big, NS negative-small, ZE zero, PS positive-small, and PB positive-big. The positive and negative terms mean counter-clock wise and clock wise rotation of the robot, respectively.

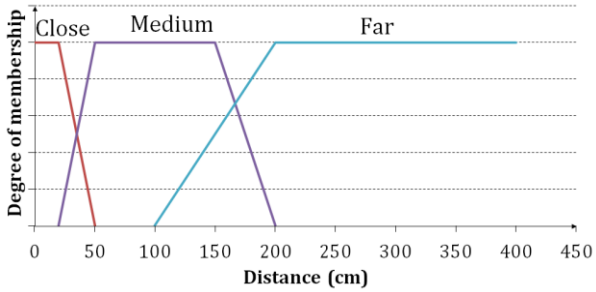


Fig. 2-2: Fuzzy membership functions for measured distance

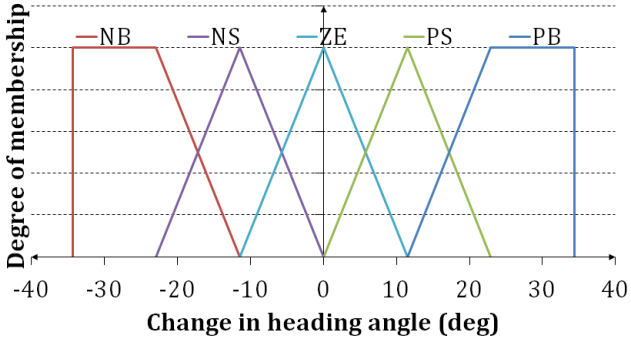


Fig. 2-3. Fuzzy membership functions for change in the robot heading angle

## 2.4. Integration of the Fuzzy Outputs

In some cases, the final fuzzy output for the change in heading angle of the robot has almost symmetrical shape about zero axis. For example if there is an obstacle in front area of the robot, there are two appropriate choices for the robot: to turn right or to turn left and the zero turning (straight motion of the robot) is not recommended. In this case the centroid defuzzification strategy gives a command: to go straight directly toward the obstacle. Therefore blending of the output rules that occur, during centroid defuzzification method can give a prohibited control command. In such situations the final control output for the robot may be: approaching an obstacle or even colliding with it. The mean of maximum (MOM) defuzzification strategy, while it guides the robot appropriately for this specific

case, it may produce abrupt transitions in the control command for other cases. To handle this problem, the Centre-of-the-Largest-Area (CLA)[24] defuzzification strategy was implemented here.

In CLA strategy, the fuzzy control output is divided into n distinct control areas (ΔΦ). Then a threshold value (Trsh) is used as a criterion to take into account or ignore these control areas; control areas with ΔΦ more than Trsh are selected in the fuzzy control output and other areas are ignored. Then the centroid method is used to obtain the final fuzzy control outputs ΔΦ and v:

$$\Delta\Phi = \frac{\sum_{j=1}^{n} \alpha_j(\Phi_j).\Delta\Phi_j}{\sum_{j=1}^{n} \alpha_j(\Phi_j)} \quad (2)$$

$$v = \frac{\sum_{j=1}^{n} \alpha_j(v_j).v_j}{\sum_{j=1}^{n} \alpha_j(v_j)} \quad (3)$$

where $\alpha_j$ (.) is the weighting factor for the rule j computed by product method and $\Delta\Phi_j$ is area under the truncated membership function for change in the heading angle of the robot (ΔΦ), while $v_j$ is the corresponding value for the velocity (v) fuzzy sets.

Changing the threshold value (Trsh) affects behaviour and outputs of the fuzzy navigation system. The (Trsh) shows the least value for control outputs to be calculated in final outputs of the navigation system. Effect of changing the (Trsh) parameter on navigation of the robot is also studied and depicted in simulation results. Choosing (Trsh=0) will give the same results as using centroid defuzzification strategy (robot is considered a point) and using (Trsh=1) is equal in using MOM approach for defuzzification (robot actual size is considered). The smaller the Trsh value means the smaller the robot, or the obstacle.

Consequently, smaller Trsh produce shorter path.

## 2.5. Simulation Results

The proposed navigation strategy was simulated in different environments: both static and dynamic (moving obstacles) configurations. An AGV mobile robot was used for this strategy. The AGV robot size is (660mm × 900mm × 480mm) and is shown in Fig. 2-4.

Fig. 2-4: AGV mobile robot used for simulation and experiment

## 2.6. Static Environment

The performance of the algorithm is tested in different conditions, first for an unknown static environment with fixed position obstacles. In Fig. 2-5 a typical static setting with stationary obstacles and the mobile robot, which is equipped to sonars and laser range finder, is depicted; the obstacles are shown by black lines.

Fig. 2-6 shows a typical result for an unknown static environment. Here obstacles are depicted by full circles and ellipses and the path which robot travelled is shown with a solid line.

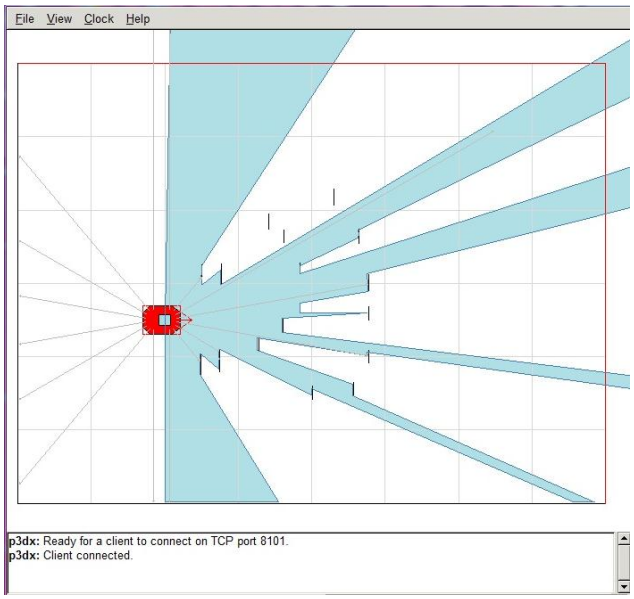


Fig. 2-5: A view of AGV, static obstacles, and sonar rays

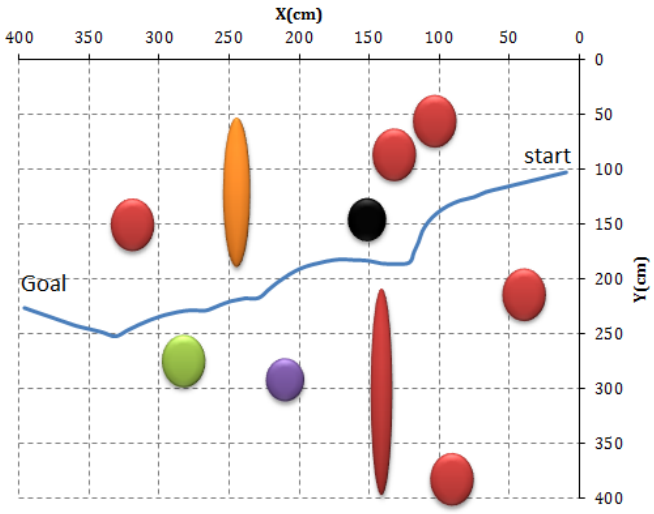


Fig. 2-6. Path of the AGV in an unknown static environment

## 2.7. Dynamic Environment

In order to implement the planned navigation algorithm for a dynamic setting, some of the obstacles are set to move with constant velocities in different directions. As we do not use

any map or prior information of the environment in the navigation algorithm, these moving obstacles are considered unforeseen. Figs. 2-7 and 2-8 show two cases of dynamic settings, in which motion of the obstacles are illustrated by arrows. These figures represent complex conditions and the ability of our algorithm to navigate the robot in dynamic environments. In these setups, the goal position is chosen such that the robot must maneuver around obstacles in order to reach goal position. The path which robot traversed from start point to reach the goal point is shown in blue solid curve.

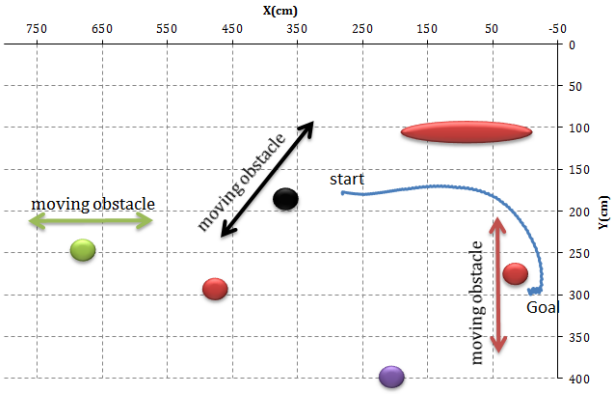


Fig. 2-7. Navigation of the AGV in an unknown dynamic setting1

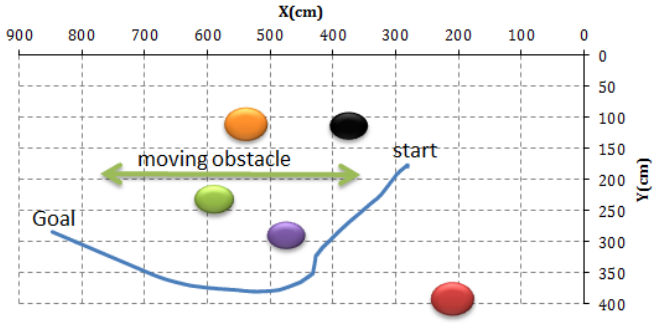


Fig. 2-8. Navigation of the AGV in an unknown dynamic setting2

## 2.8. Comparison of the Results

To investigate the effectiveness of our navigation algorithm, this method is compared with preference-based fuzzy (PBF) method and VFH method represented in [18]. To obtain comparable results with PBF and VFH methods, locations of the obstacles, initial pose of the robot, position of the goal points and also dimensions of the test environment are chosen same as [18].Ten situations for two categories, single-path and multi-path setups are implemented. As mentioned before, the sensory data for the AGV robot are supplied by sonar sensors.

First test situation is depicted in Fig. 2-11; obstacles are arranged in such a way to make a narrow passage for the robot. By changing the threshold value (Trsh) for CLA defuzzification approach, the motion of the robot will change and the robot goes through a different path. As shown in Fig. 2-11 performance of the proposed method for two values of Trsh= 0.6 and 0.3 are shown. The results of the VFH and PBF approaches for four cases are shown in Fig. 2-9 for comparison with our results.

In Fig. 2-11, a more cluttered environment is demonstrated in which the robot had to navigate through very crowded setting, for two threshold values (Trsh= 0.6 and 0.3). Performances of our navigation strategy for different settings with diverse obstacle configurations are depicted in Figs. 2-11 to 2-20 all in static obstacle settings.

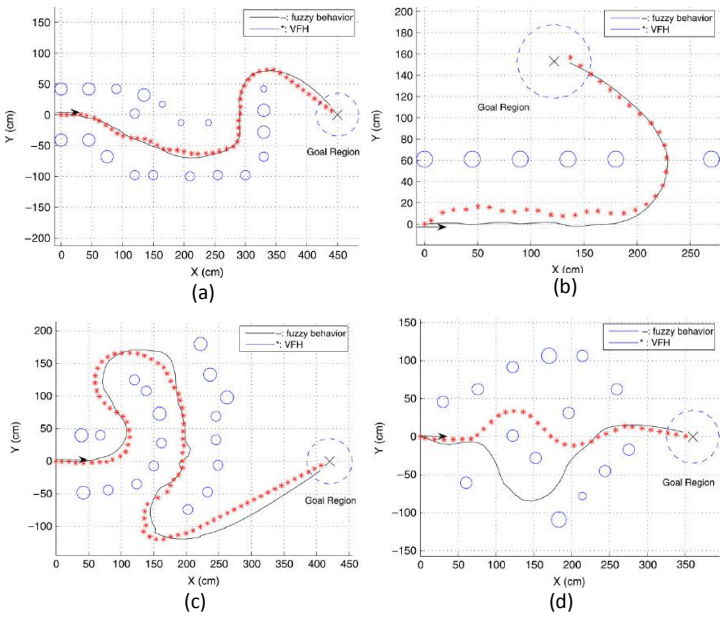


Fig. 2-9. Navigation results for VFH and PBF approaches for four set-ups: (a): set-up1, (b): set-up2, (c): set-up3 and (d): set-up4. Red dots are the paths generated by VFH and solid lines are the paths generated by fuzzy behavior[18].

To compare the results with PBF and VFH methods, two criteria used in [18], are computed: the total path's length which robot traveled to reach its goal (PL) and total bending energy of the trajectory (BE). The total path length for the robot is calculated as summation of the distances between two consecutive points in robot's path from start point ($x_1$, $y_1$) to the goal point ($x_n$, $y_n$).

$$P_L = \sum_{i=1}^{n-1} \sqrt{(x_{i+1} - x_i)^2 + (y_{i+1} - y_i)^2} \qquad (4)$$

To consider smoothness of the paths produced by the proposed strategy, the bending energy $B_E$ of the paths are computed as summation of square of curvatures. To find the curvature of the path through points, the equation of the circle passing through three successive points in the path was obtained and then the curvature of this circle was computed. Coordinate of the center of the circle passing through three points, shown in Fig.

2-10, with coordinates: $P_1(x_1, y_1)$, $P_2(x_2, y_2)$, $P_3(x_3, y_3)$, joined by lines with slopes $m_1$ and $m_2$ is given by:

$$x_c = \frac{m_1.m_2(y_1 - y_3) + m_2(x_1 + x_2) - m_1(x_2 + x_3)}{2(m_2 - m_1)} \quad (5)$$

$$y_c = \frac{-1}{m_1}.\left(x_c - \frac{x_1 + x_2}{2}\right) + \frac{y_2 + y_1}{2} \quad (6)$$

where slopes of lines $m_1$ and $m_2$ are computed as following:

$$m_1 = \frac{y_2 - y_1}{x_2 - x_1} \quad (7)$$

$$m_2 = \frac{y_3 - y_2}{x_3 - x_2} \quad (8)$$

Finally, the radius of the circle $R_i$ can be calculated by finding the distance between the center of the circle C and any one of the points on the circle.

$$R_i = \sqrt{(x_2 - x_c)^2 + (y_2 - y_c)^2} \quad (9)$$

The curvature of the path through points $P_1$, $P_2$, and $P_3$, $\kappa_i$, is equal to:

$$\kappa_i = \frac{1}{R_i} \quad (10)$$

The total bending energy of the path is defined as summation of all curvature of pieces of path:

$$B_E = \sum_{i=1}^{n-1} {\kappa_i}^2 \quad (11)$$

The objective is to find the sum of the smallest radius of curvature.

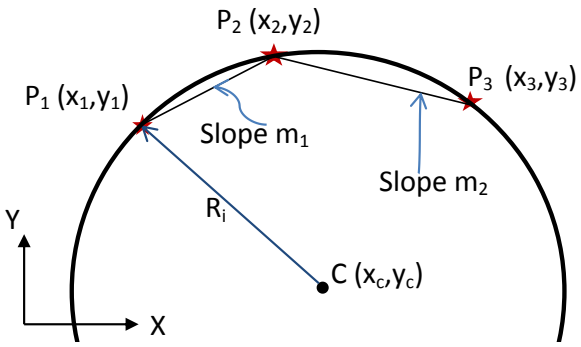


Fig. 2-10. Radius of circle $R_i$ passing through three points $P_1$, $P_2$, $P_3$

These two criteria are calculated for all paths produced by the suggested navigation method and are summarized in Tables 2-I and 2-II.

It is inferred from Table 2-I and 2-II that the proposed navigation method produces shorter (lower value of $P_L$) and also smoother paths (lower $B_E$) compared with the PBF and VFH methods. Bending energy in the proposed method for all cases except for the set-up3 is much smaller than the two other strategies; this means that our strategy provides much smoother paths with respect to the PBF and VFH approaches. In the proposed approach the robot does not turn abruptly, and by providing shorter paths it will decrease computational and execution times.

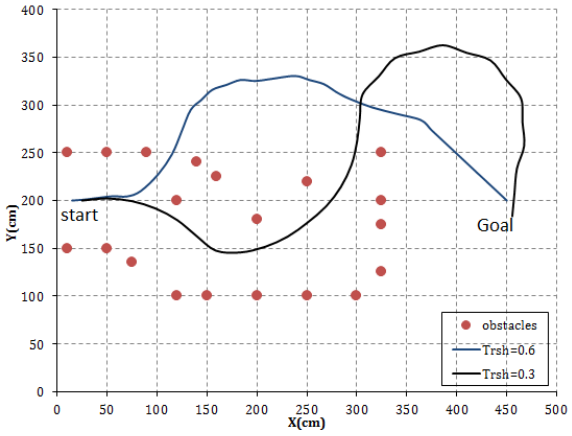


Fig. 2-11. Navigation of the AGV for set-up1

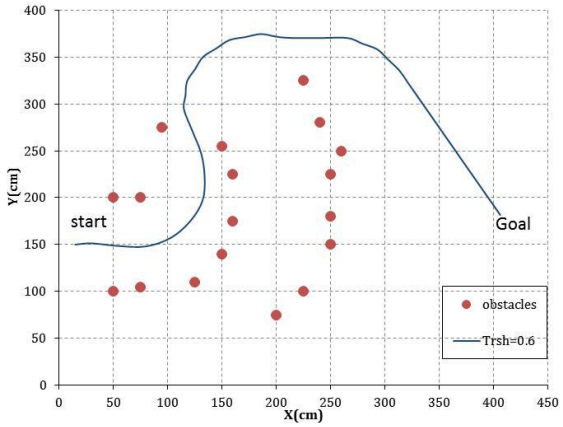


Fig. 2-12. Navigation of the AGV for set-up2

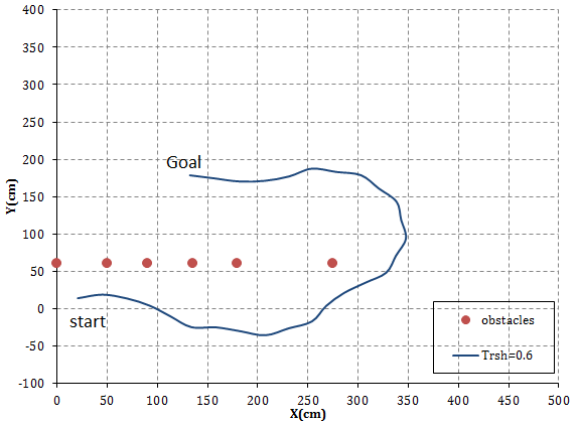


Fig. 2-13. Navigation of the AGV for set-up3

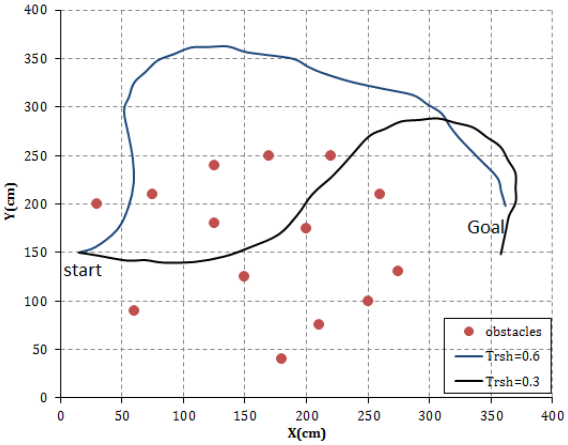


Fig. 2-14: Navigation of the AGV for set-up4

## 2.9. Experimental Test Results

The performance of the proposed navigation method was also evaluated using tests implemented on AGV shown in Fig. 2-4. The robot is equipped with sonars and also laser range finder. In this navigation strategy, sonar sensors are used for obstacle detection and determining the distance to the obstacle. Ten different snapshots of one test are demonstrated in Fig. 2-21. During the test, robot avoids obstacles which appear in its way safely and tries to reach its goal point. As it is depicted in Figs. 2-21 to 2-23 the robot reaches the target position successfully.

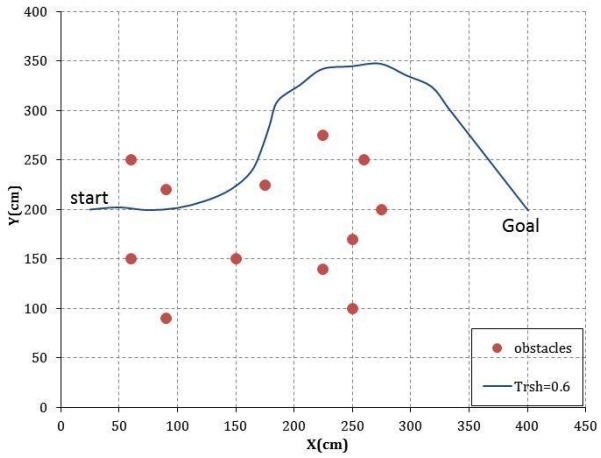


Fig. 2-15: Navigation of the AGV for set-up5

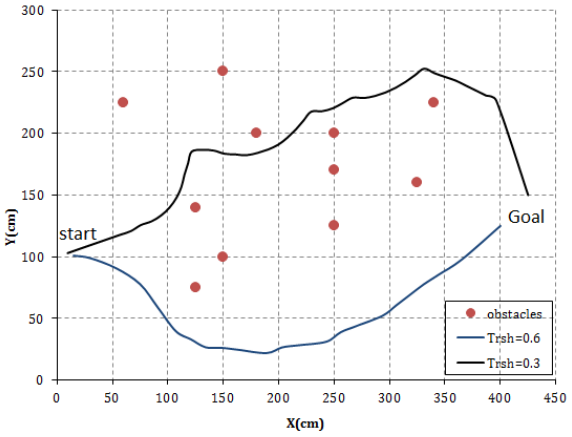


Fig. 2-16: Navigation of the AGV for set-up6

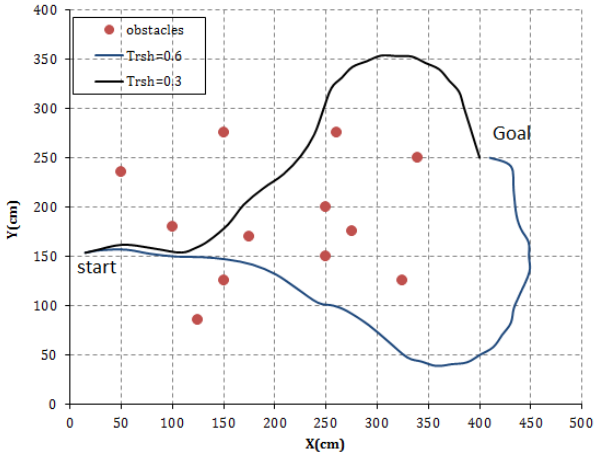


Fig. 2-17: Navigation of the AGV for set-up7

## 2.10. Conclusion

A strategy for mobile robot navigation in an uncertain and unforeseen setting was introduced. This approach is based on fuzzy-logic statements and sensory data from environment. It does not require prior information from the robot's environment and was able to be implemented for real-time navigation. Tuning a safety margin enabled the robot to travel in different paths and cope with different conditions. Comparing our results with the published results in [18] showed that the proposed method produced smoother and also shorter paths in almost all of the test cases examined. Therefore this work represents a time-efficient and computationally cost-efficient approach for outdoor mobile robot navigation.

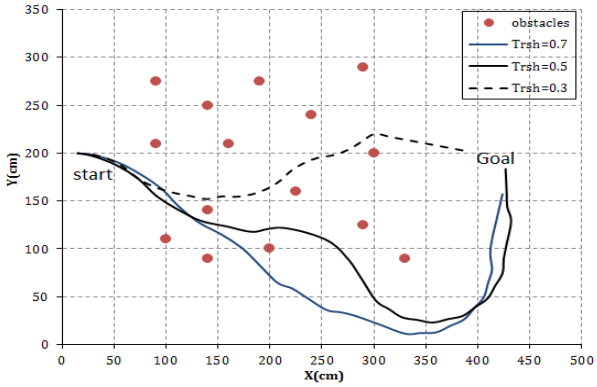


Fig. 2-18: Navigation of the AGV for set-up8

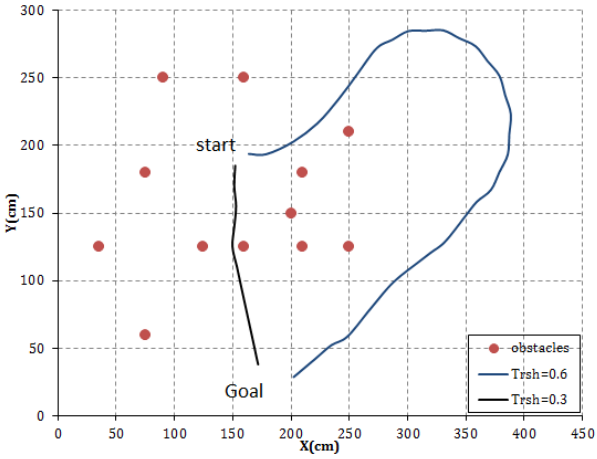


Fig. 2-19: Navigation of the AGV for set-up9

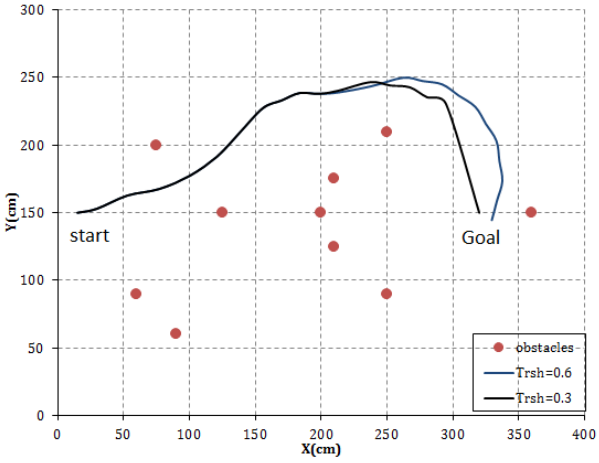


Fig. 2-20: Navigation of the AGV for set-up10

Table 2-I: comparison of the total path length ($P_L$) for the proposed method with PBF and VFH

| | $P_L$(cm) | | | |
|---|---|---|---|---|
| Method / Set-up | **Our Method** | | **PBF** | **VFH** |
| | **Trsh=0.3** | **Trsh=0.6** | | |
| 1 | 450 | 510 | 571 | 573 |
| 2 | 375 | 680 | 943 | 966 |
| 3 | - | 675 | 399 | 390 |
| 4 | 530 | 570 | 433 | 380 |
| 5 | 525 | 375 | 513 | 713 |
| 6 | 395 | 450 | 469 | 425 |
| 7 | 544 | 590 | 539 | 458 |
| 8 | 405 | 575 | 466 | 456 |
| 9 | 135 | 555 | 437 | 237 |
| 10 | 663 | 425 | 444 | 400 |

Table 2-II: Comparison of the total bending energy ($B_E$) for the proposed method with PBF and VFH

| | $B_E$ (E-02) | | | |
|---|---|---|---|---|
| Method / Set-up | **Our Method** | | **PBF** | **VFH** |
| | **Trsh=0.3** | **Trsh=0.6** | | |
| 1 | 0.219 | 0.750 | 4.510 | 5.330 |
| 2 | 0.110 | 0.610 | 68.420 | 10.500 |
| 3 | - | 0.530 | 1.930 | 3.700 |
| 4 | 0.600 | 0.670 | 4.620 | 3.620 |
| 5 | 0.270 | 0.060 | 3.250 | 5.940 |
| 6 | 0.300 | 3.400 | 2.820 | 5.550 |
| 7 | 0.560 | 0.820 | 2.510 | 7.120 |
| 8 | 0.580 | 0.510 | 7.320 | 10.170 |
| 9 | 0.100 | 0.730 | 2.800 | 4.600 |
| 10 | 0.350 | 0.520 | 2.040 | 5.010 |

Fig. 2-21: Snapshots of the AGV used for experiments: top-left image shows start point of the robot and bottom-right image indicates goal achievement. Image sequence proceeds to the right and down.

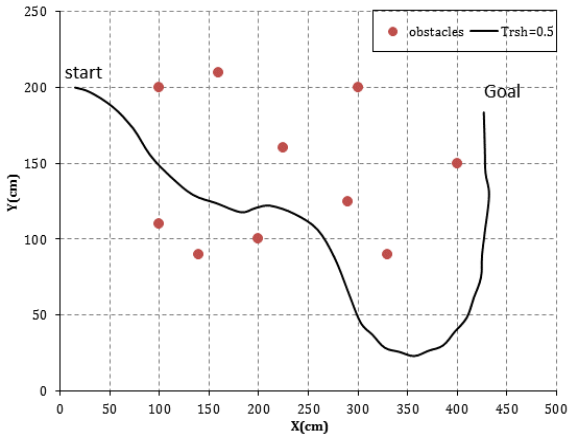


Fig. 2-22: Navigation of real mobile robot for set-up11

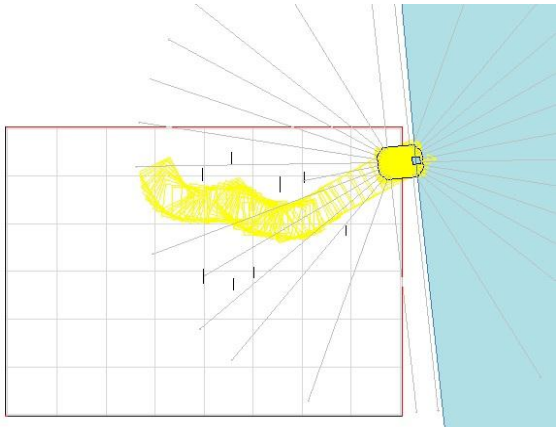

Fig. 2-23. Navigation of the AGV for set-up11

## References


[1] Khot, L R; Tang, L, Blackmore, S; Nrremark, M, Navigational context recognition for an autonomous robot in a simulated tree plantation, Trans of the ASABE, v49, n5, 1579-1588, 2006

[2] Cariou, C.; Lenain, R.; Thuilot, B.; Berducat, M., Automatic Guidance of a Four-Wheel-Steering Mobile Robot for Accurate Field Operations. Journal of Field Robotics, v26, n 6-7, p 504-18, June 2009

[3] Morales, Y.; Carballo, A.; Takeuchi, E.; Aburadani, A.; Tsubouchi, T., Autonomous Robot Navigation in Outdoor Cluttered Pedestrian Walkways. Journal of Field Robotics, v 26, n 8, p 609-635, 2009

[4] Y. Koren, J. Borenstein, Potential field methods and their limitations for mobile robot navigation, in: Proceedings of the IEEE International Conference on Robotics and Automation, 1991, pp. 1398-1404.

[5] J. Borenstein, Y. Koren, Real-time obstacle avoidance for fast mobile robot in cluttered environments, in: Proceedings of the IEEE Int. Conference on Robotics and Automation, 1990, pp. 572-577.

[6] 1. Boren, Y. Koren, Obstacle avoidance with ultrasonic sensors, IEEE Journal of Robotics and Automation 4 11988) 213-218.

[7] H. Noborio, T. Yoshioka, T. Hamaguchi, On-line deadlock-free path-planning algorithms by means of a sensor-feedback tracing, in: Proceedings of the IEEE International Conference on System, Man and Cybernetics, 1995, pp. 1291-1296.

[8] S.M. Noorhosseini, A,S. Malowany, GORP: a new method for mobile robot path planning problem. SPIE 183 I, Mobile Robots VII (1992) 37-44.

[9] R. Simmons, "The curvature-velocity method for local obstacle avoidance.," in IEEE Int. Conf. on Robotics and Automation (ICRA), April 1996, pp. 3375–82.

[10] D. Fox, W. Burgard, and S. Thrun, "The dynamic window approach to collision avoidance," IEEE Robotics and Automation Magazine, vol. 4, March 1997.

[11] W. Li, A hybrid neuro-fuzzy system for sensor based robot navigation in unknown cnvironments, in: Proceedings of the American Control Conference, 1996, pp. 2749-2753.

[12] Najjaran, H.; Goldenberg, A., Real-time motion planning of an autonomous mobile manipulator using a fuzzy adaptive Kalman filter. Robotics and Autonomous Systems, v 55, n 2, p 96-106, 2007.

[13] X. Yang, R. V. Patel, and M. Moallem, "A fuzzy-Braitenberg navigation strategy for differential drive mobile robots," in Proc. 3rd IFAC Symp. Mechatronic Systems, Sydney, Australia, Sep. 2004.

[14] Teimoori, H., Savkin, A., V. " Distance-only based navigation of wheeled mobile robots with obstacle avoidance" IEEE International Conference on Robotics and Biomimetics, ROBIO 2008, p 1956-1961, 2008

[15] Vannoy, J.; Xiao, J., Real-Time Adaptive Motion Planning (RAMP) of Mobile Manipulators in Dynamic Environments with Unforeseen Changes. IEEE TRANSACTIONS ON ROBOTICS, Vol. 24, No. 5, 2008

[16] Yang, Xiaoyu, Moallem, M.; Patel, R., V. "A layered goal-oriented fuzzy motion planning strategy for mobile robot navigation" IEEE Transactions on Systems, Man, and Cybernetics, Part B: Cybernetics, v 35, n 6, p 1214-1224, December 2005

[17] Canning, J., R.; Edwards, D., B.; Anderson, M., J., Development of a Fuzzy Logic Controller for Autonomous Forest Path Navigation. Transactions of the ASAE, American Society of Agricultural Engineers ISSN 0001-2351, 2004.

[18] Selekwa, M.F.; Dunlap, D.D.; Dongqing, S.; Collins, E.G., Robot navigation in very cluttered environments by preference-based fuzzy behaviors. Robotics and Autonomous Systems, v 56, n 3, p 231-46, 2008.

[19] Hagras, H; Colley, M; Callaghan, V; Carr-West, M, Online learning and adaptation of autonomous mobile robots for sustainable agriculture, Autonomous Robots, v 13, 1, 37-52, 2002

[20] S. I. Lee and S. B. Wang, "Emergemt behaviors of a fuzzy sensory motor controller evolved by genetic algorithm," IEEE Trans. Syst., Man,Cybern. B, Cybern., vol. 31, no. 6, pp. 919–929, Dec. 2001.

[21] N. Tsourveloudis, K. Valavanis, and T. Hebert, "Autonomous vehiclenavigation utilizing electrostatic potential fields and fuzzy logic," IEEE Trans. Robot. Autom., vol. 8, no. 6, pp. 9–17, Dec. 2001.

[22] C. Ye, N. H. C. Yung, and D.Wang, "A fuzzy controller with supervised learning assisted reinforcement learning algorithm for obstacle avoidance," IEEE Trans. Syst., Man, Cybern. B, Cybern., vol. 33, no. 1, pp.17–27, Feb. 2003

[23] Hagras, H.A., "A hierarchical type-2 fuzzy logic control architecture for autonomous mobile robots" , IEEE Transactions on Fuzzy Systems, v 12, n 4, p 524-39, Aug. 2004

[24] Pfluger, N.; Yen, J.; Langari, R., "A defuzzification strategy for a fuzzy logic controller employing prohibitive information in command formulation." IEEE Int Conf Fuzzy Syst FUZZ-IEEE, p 717-723, 1992

# Chapter 3: Two New Approaches for Navigation of Wheeled Mobile Robots

The content of this chapter is under second review for publication in ASME journal of mechanisms and robotics, 2013.

**Heidari F.**, Fotouhi R., and Vakil, M., "Two New Approaches for Navigation of Wheeled Mobile Robots", ASME Journal of Mechanisms and Robotics, under review with minor revision **2013.**

**Abstract:**

Development of new methods for real-time navigation of mobile robots in a complex and mostly unstructured environment is studied. Two novel approaches are proposed here: fuzzy logic based (FLB) and human-inspired method (HIM). These approaches use distance-based sensory data from a laser range finder for navigation of a wheeled mobile robot in unknown and cluttered settings. The approaches require no prior knowledge from the environment thus they are easy to be implemented for real-time navigation of mobile robots. The FLB method enables the robot to cope with dynamic and unforeseen conditions by tuning a safety margin (Trsh). FLB produces smoother and shorter paths in almost all of the test cases examined in comparison with other approaches. Also it uses fewer numbers of fuzzy rules for navigation. Therefore this technique represents a time-efficient and computationally effective method for outdoor mobile robot navigation. HIM is inspired by human behavior. HIM endows the robot a human-like ability for reasoning about the situations to reach a predefined goal point while avoiding any static and moving or unforeseen obstacles; this makes the proposed strategy efficient and effective. Results indicate that HIM is capable of creating smooth (no oscillations) paths for safely navigating the mobile robot, and coping with fluctuating and imprecise sensory data from uncertain environment. HIM specifies the best path ahead, according to the situation of encountered obstacles, preventing the robot to get trapped in deadlock and impassable conditions. This deadlock detection and avoidance is a significant ability of HIM. The simulation and experimental results of HIM and FLB are presented and compared.

**Keywords**: wheeled mobile robot navigation, human-inspired method, fuzzy logic approach

## 3.1. Introduction:

Increasingly, robots are being used in different applications such as agriculture, manufacturing, health care and so on; there is also increasing needs for these robots to be navigated robustly, reliably and accurately. Navigation of robots in outdoor and unstructured environments reliably, is still a major challenge. Since agricultural fields are very complex and mostly unknown; navigation of robots involves difficulties such as operation of the robot in continuously changing tracks and targets, which are difficult to detect and reach.

This research is part of a bigger project in control and navigation of an autonomous mobile robot in agricultural farm for sowing, weeding, and harvesting. To choose the best appropriate navigation technique for this project, various kinds of methods for navigation of mobile robots were studied comprehensively. This study is mainly about reliable navigation of an outdoor wheeled mobile robot. First we worked on navigation of an automated guided vehicle (AGV), a mobile robot, for point-to-point motions, in which the robot tries to go to the goal point while avoiding any collision with static and moving (unforeseen) obstacles. Second, the mobile robot navigation to follow a given path is being carried out. This research is under development, and results will be reported later.

Navigation of mobile robots in outdoor environments has been studied previously. In [1] motion of a four-wheel-steering (4WS) mobile robot moving in farm land was modeled. Trajectory planning was considered for a wheeled platform in [2]; None of these two works considered uncertainties such as moving (unforeseen) obstacles that are inherent of outdoor setting.

Managing the uncertainty and altering conditions is one of the most challenging problems in navigating mobile robots in an unknown and unstructured environment. Several approaches were suggested for robot navigation, such as the artificial potential field [3], the vector field histogram [4], the edge detection [5], the obstacle boundary following [6], the goal oriented recursive path planning (GORP) [7], the curvature velocity method [8], the dynamic window approach [9], and the fuzzy-logic and neural-network based reactive methods [10]. The potential field method [3] suffers from getting trapped in local minima; unintended stoppage happens between closely spaced obstacles; oscillations (circulating around) in the presence of multiple obstacles; and oscillations in narrow passages also may occur. Dynamic window approach [9] computes the optimum velocity of a robot and satisfies the kinematic and dynamic constraints of a robot, and maximizes a given cost function. This is usually defined as a function of distances to the goal and to obstacles. In GORP [7] method the longest straight-path segment is first found; then the approach tries to direct the robot to the goal, while keeping shortest distance to the predefined path, and to avoid obstacles. This method produces paths in an open area with convex objects, but may have difficulty in the presence of non-convex obstacles and cannot plan the shortest path. Fuzzy-logic and neural-network approaches for navigation were proposed in [11]. Optimum trajectory planning for group of mobile robots was studied in [12]; each robot moved from its start point to its goal position while minimizing its own energy. Navigation of mobile robots in rough terrain was discussed in [21, 22], in which power consumption of the robot was optimized in [21], and slip and skid of the robot in terrain was considered in [22]. These model-based approaches use a map or model of the environment to generate a path for the robot to follow toward a goal point.

In [13] an online approach to define an obstacle-free path for an outdoor mobile robot was suggested. Measurements using ultrasonic and laser sensors were used to generate a map of the terrain and to define an obstacle-free path for the robot. But model-based approaches would have difficulty dealing with the real time navigation of a mobile robot in outdoor environment. It is usually difficult or impossible to obtain an accurate model of an outdoor environment. Sensor-based approaches [14] use data from different sensors such as sonar, laser range finder or visual camera in real time to generate control commands for the mobile robot motion. The main advantage of a sensor-based approach is that it can navigate the robot in a changing environment by seeing unforeseen obstacles. Fuzzy logic has been utilized in navigation systems for mobile robots [15-16]. For navigating mobile robot in an obstacle-free path, hierarchical fuzzy controller [17] and preference-based fuzzy behavior method [18] were used. The navigation problem was broken down into two control actions: heading control and speed control. Obstacle avoidance was performed in speed control stage. Application of a hierarchical Fuzzy-Genetic system to produce an autonomous outdoor mobile robot controller capable of online learning and implementing was introduced in [19]. Stereo cameras and laser range finders have been used for autonomous navigation of the mobile robots. For example in [20] a SICK laser range finder and vision-based method was used for obstacle detection and collision avoidance for a Yamaha robot. The vision-based navigation techniques deeply depend on environment's light and color which varies with seasons and day or night time. In practice, reliable and effective automated analysis of images from visual sensors is challenging. Similarly, techniques that successfully interpret on-line sensor data for several settings begin to fail past short ranges as the density and accuracy for such computation quickly reduce.

We proposed a self-supervised human-inspired method (HIM) to navigate the robot in different terrains and perceive traversable paths in unstructured outdoor settings. Mobile robots will be able to associate their observations of the terrain with learning signals using HIM. The difference between robot and human navigation is in the perceptual capabilities. Humans can detect, classify, and identify environmental features under widely varying environmental conditions, independent of relative orientation and distance [23]. To control a wheeled mobile robot that is capable of navigating in unstructured outdoor environments such as a farm setting reliably, we used inspiration from human skills. In this research, robots mimic how humans move in unknown environment when seeking goal and avoiding obstacles. This implies that the robot has to deal with unknown static and moving obstacles in outdoor settings. To do so, the robot has to sense, extract and process sensory data in real time. Also the robot must be able to detect the passable and non-passable spaces in its path due to unexpected moving obstacles.

In this research, sensory data from the environment is perceived by a laser range finder mounted on the mobile robot. The performance of the human-inspired navigation method (HIM) is tested and compared with results from a fuzzy logic based (FLB) algorithm on an AGV in real world conditions. Because of environmental challenges (snow on the ground) tests were carried out indoor, but no prior information (map) of the environment was used for navigation of the robot. The premise of the proposed methods is their robust results for uncertain and changing environments which are inherent characteristics of the farm fields. We assumed that the mobile robot performs in situations and settings that there is always ways to reach a goal point.

## 3.2. System architecture

### 3.2.1. Methodology and Approach

There are several different approaches for autonomous navigation of the mobile robot for point-to-point motion in outdoor setting. At first, in this research, a new fuzzy logic based (FLB) approach is designed to navigate the robot. We also introduced a novel human-inspired method (HIM) for navigation with moving obstacles and rough settings. The simulation and experimental results of HIM and FLB are presented and compared here.

### 3.2.2. Robot model used for simulation and experiments

The navigation strategies are tested on an AGV. The robot size is (660mm × 900mm × 480mm), and it is shown in Fig. 3-1. Our AGV is equipped with two sonar arrays, one in front and the other one in the rear. Also there is one SICK LMS200 laser range finder mounted in front of the robot. The laser range finder can sense objects within 50 meters away from the robot of 180° view in a single plane. Because the laser beam is highly focused and not readily distorted or absorbed by reflecting medium, the precision of the laser range finder is much superior to the sonar with many fewer false readings. Moreover, laser can detect objects much farther away from the robot compared to sonars. Therefore we decided to use laser range finder for navigation of the AGV and obstacle avoidance algorithms. The robot moves in a plane and can identify its own pose in the world coordinate system by GPS and Inertial Measurement Unit (IMU) data in outdoor environment, or integrating the encoder's information for indoor navigation as done in [30].

Fig. 3-1: AGV mobile robot used for simulation and experiment tests

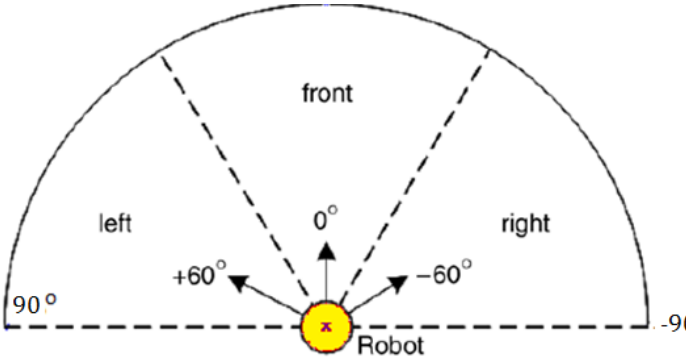


Fig. 3-3: Sectors of the perceptible region detected by the laser range finder

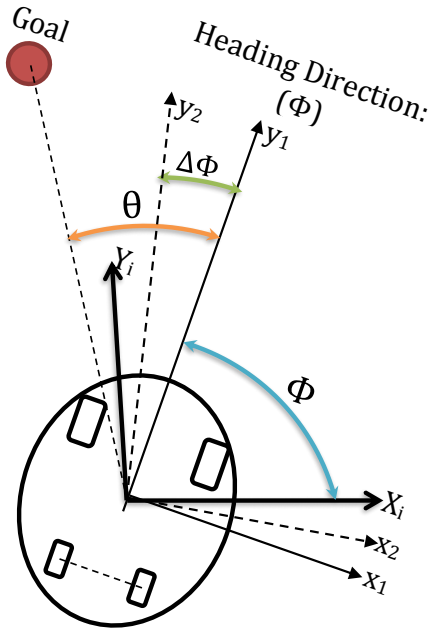


(a)

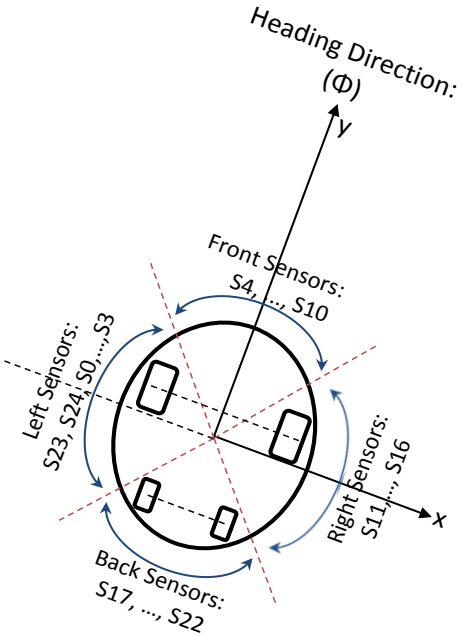


(b)

Fig. 3-2: Schematic of (a) the mobile robot and (b) the sonar arrangements on the robot

In Fig. 3-2 (b), a schematic of top view of the AGV and the sonar sensors is depicted. These sonar sensors are divided into four groups of left (sensors S23, S24, S0, S1, S2, S3), front (sensors S4, S5,..., S10), right (sensors S11, S12, ..., S16) and back (sensors S17, S18,..., S22). As shown in Fig. 3-2, there is an inertial coordinate system ($X_i$-$Y_i$) attached to the ground (reference system) and a robot coordinate system (x-y) attached to the center of the robot base. The angle between current heading of the robot (y) and $X_i$ axis is defined as angle (Φ), the angle between orientation of goal in x-y coordinate and heading of the robot is defined

as (θ). Control action includes heading control, which provides change in heading angle of the robot (ΔΦ), and speed control which provides robot linear speed (v).

The perceptible region viewed by the laser range finder is illustrated in Fig. 3-3; this area is divided into three 60° circular sectors. The radius of the circular sector is the laser's range. The size of this radius is 50 m for the laser used here.

The distances to the objects detected by laser in right, front, and left, of the robot are represented by dR, dF, and dL respectively. These parameters are defined as following equation:

$$\begin{aligned} dR &= \min \{\text{distance data reading for } -90 \le \text{angle} \le -30\} \\ dF &= \min \{\text{distance data reading for } -30 \le \text{angle} \le +30\} \\ dL &= \min \{\text{distance data reading for } +30 \le \text{angle} \le +90\} \end{aligned} \quad (1)$$

These (dL, dF, dR) readings are used for obstacle avoidance and navigation behaviors.

### 3.2.3. Kinematics of the robot

The AGV used for experiments is a Hilare-type mobile robot, which has two differentially actuated wheels and two caster wheels as shown in Fig. 3-1; its schematic is shown in Fig. 3-4. In this figure, $T$ is the width of the robot and $r$ is the radius of the differential wheels. ($x_1$ - $x_2$) is inertial coordinate system, ϕ is the heading angle of the robot; ($x_{r1}$ - $x_{r2}$) is the coordinate system fixed to the mobile robot and $o$ is the origin of the ($x_{r1}$ - $x_{r2}$). The center of mass of the mobile robot is C.G., as shown in Fig. 3-4. The drive mechanism of the robot has two independent motors. The actual kinematic inputs that drive the robot and affect its speed and direction of motion are the two wheel speeds.

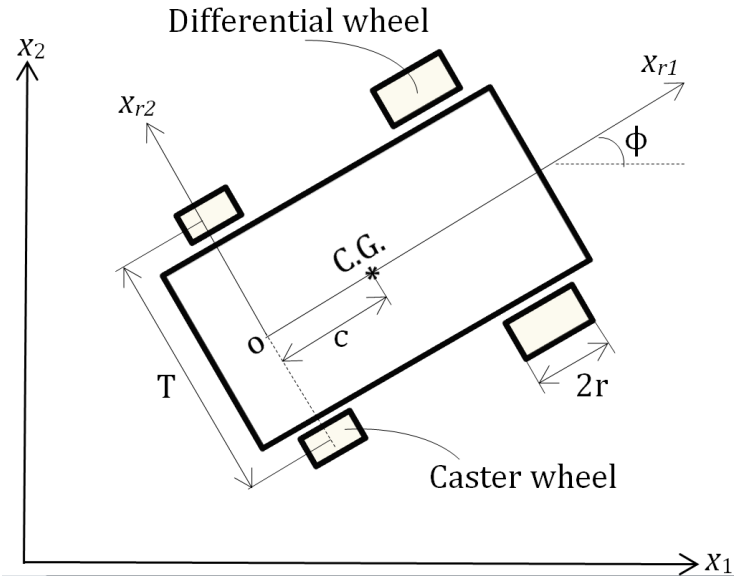


Fig. 3-4: Schematics of a Hilare-type mobile robot

The vector q describes the configuration (position and orientation) of the robot at any time:

$$q = \begin{bmatrix} x_1 & x_2 & \phi \end{bmatrix}^T \tag{2}$$

($x_1$ , $x_2$) are the coordinates of the robot (point *o*) in the inertial frame. If the linear speed and angular velocity of the robot are *v* and ω, respectively, assuming no-slip on wheels, the velocity components can be written as:

$$\begin{aligned} \dot{x}_1 &= v\cos\phi \\ \dot{x}_2 &= v\sin\phi \\ \dot{\phi} &= \omega \end{aligned} \tag{3}$$

The kinematics of the robot can be written as follows:

$$\dot{q} = \begin{bmatrix} \cos\phi & 0 \\ \sin\phi & 0 \\ 0 & 1 \end{bmatrix} .u \tag{4}$$

where $u = \begin{bmatrix} v & \omega \end{bmatrix}^T$ is the control input. Angular velocity of the robot can be written in terms of velocities of the right and the left wheel centers ($v_r$, $v_l$):

$$\omega = \frac{v_r - v_l}{T} \tag{5}$$

### 3.2.4. Dynamics of the mobile robot

The dynamics equations of motion of the Hilare-type mobile robot (Fig. 3-4) are presented as [29]:

$$\overline{M}(q).\dot{u} + \overline{C}(q,\dot{q})u = \overline{B}(q).\tau \tag{6}$$

where matrices are defined as following:

$$\overline{M}(q) = \begin{bmatrix} \frac{r.m}{2} + \frac{I_w}{r} & \frac{r.I}{T} + \frac{T.I_w}{2.r} \\ \frac{r.m}{2} + \frac{I_w}{r} & \frac{-r.I}{T} - \frac{T.I_w}{2.r} \end{bmatrix}$$

$$\overline{C}(q,\dot{q}) = \begin{bmatrix} \frac{r}{T} m_c.c.\dot{\phi} & -\frac{r}{2} m_c.c.\dot{\phi} \\ -\frac{r}{T} m_c.c.\dot{\phi} & -\frac{r}{2} m_c.c.\dot{\phi} \end{bmatrix} \tag{7}$$

$$\overline{B}(q) = \begin{bmatrix} 1 & 0 \\ 0 & 1 \end{bmatrix} \qquad \tau = \begin{bmatrix} \tau_r \\ \tau_l \end{bmatrix} \qquad u = \begin{bmatrix} v \\ \omega \end{bmatrix} \tag{8}$$

, ,

which $\tau_r$ and $\tau_l$ are torques applied at the right and the left driving wheels of the robot respectively. We let $m = m_c + 2m_w.$ and $I = m_c c^2 + m_w.\frac{T}{2}^2 + I_c + 2.I_m.$ where, $m_c$ is the mass of the robot body, $m_w$ is mass of each differential wheel including its motor, $I_c$ is the mass moment of inertia of the robot body about the vertical axis passing through C.G., $I_w$, is for

each wheel about its horizontal rotational axis, and $I_m$ is for each wheel about a vertical axis passing through its center.

## 3.3. Algorithms

This section is composed of two parts. In the first part, HIM for navigation of mobile robots is described in details. Then a description of FLB approach is given.

### 3.3.1. Human-inspired method (HIM)

This method is inspired from human behavior [23]. In this method, the robot makes decisions similar to a wise adult human in dynamic environments. HIM is designed to imitate behavior of an adult human to reach a goal point while avoiding any static and moving unforeseen obstacles. First, information about the environment is obtained using the laser range finder which is mounted on the robot. Data of the laser scanner are recorded in terms of the scanning angle and the distance between the robot and obstacles. HIM uses this data to find the closest traversable path toward the goal point.

I. Check direct path to the goal

Using laser data, HIM detects if there is any obstacle in a direct path from robot's current position to the goal point. This behavior is called "Check Direct Path"; if there is no obstacle in the direct path, then the robot moves toward the goal point until it detects an obstacle (moving or stationary) on its way. Once an obstacle is detected in the path to the goal, HIM tries to find all possible *scape-points* in robot's current position. Scape-points are positions that are travelable (safe and feasible) for the robot according to the predefined safety factor and the actual size of the robot.

II. Scape-point finding behavior

Scape-points (also known as free-space) are safe and traversable positions for the robot. To find these scape-points in the robot environment, first the raw data from the laser are decoded into a list of points in polar coordinates. Afterward, those are mapped to the Cartesian (x-y) coordinates and are used for navigation and obstacle avoidance. Then lines, objects' boundaries and free-spaces are obtained. This behavior is called Scape-Point Finding. Then, the total length of the path from the current pose of the robot to each scape-point and from the scape-point to the goal point is computed. After that, the scape-point with the shortest total path length is chosen as a transitional goal point. The robot goes directly toward the transitional goal point; afterward the robot turns its heading toward the final goal point and repeats all previous behaviors until no obstacle is detected in the direct path to the goal point. Later the robot moves to the goal position.

The resolution of the laser scanner used for tests, is 1.0 degree per point (i.e., 181 points for 180 degrees). The accuracy of each measurement is ±5 cm in 50m. Fig. 3-5 shows one sample of the laser scanner measurements from the environment (blue dots are laser range finder (LRF) data). The occupancy grid for LRF data is determined; possible attributes for each grid are: occupied, free, and unknown. If any obstacle is detected at distance R then the grid at R is set as occupied. If no obstacle is observed then the region will be set as *free*. The region behind the occupied area is labeled as *unknown*. Fig. 3-6 shows the grid occupancy for a region of angular sector θ. If the free-space between two consequent end-points of obstacles is traversable for the robot, those end-points are determined as scape-points. All passable scape-points ($S_1$, $S_2$, $S_3$, $S_4$, and $S_5$, shown in Fig. 3-7) for the robot are detected in the setting. After all passable scape-points are detected, the best traversable

path to the goal point is found. Total distance to reach the goal point via each scape-point is calculated as $D_i = L_i + P_i, i = 1,...,5$ . Fig. 3-8 (a) and (b) are illustrations of the performance of HIM for navigation. By using the minimum of $D_i$s, the best scape-point ($S_3$ here) is calculated, thus the robot moves to $S_3$ and then to the goal point. The paths that robot traversed to reach the goal is shown as solid line.

The advantage of HIM is that it can navigate the robot in a very dense, cluttered and complex environment. Also this method avoids local minima or local trap because HIM chooses passable ways and avoids very narrow passages in advance. Fig. 3-9 summarizes the basic structure of navigation process in HIM.

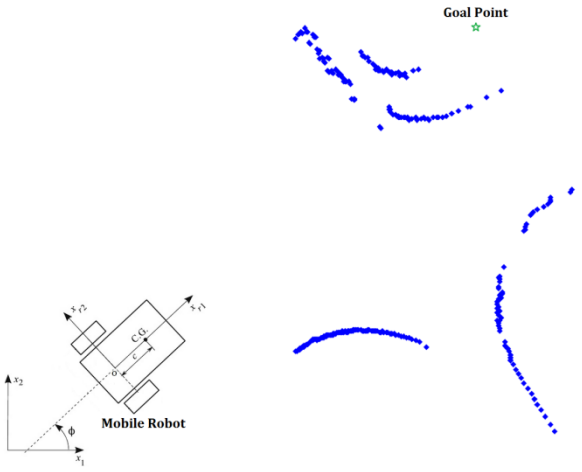


Fig. 3-5: A sample 2D laser scanner data from the environment. Blue dots are obstacles detected by laser scanner.

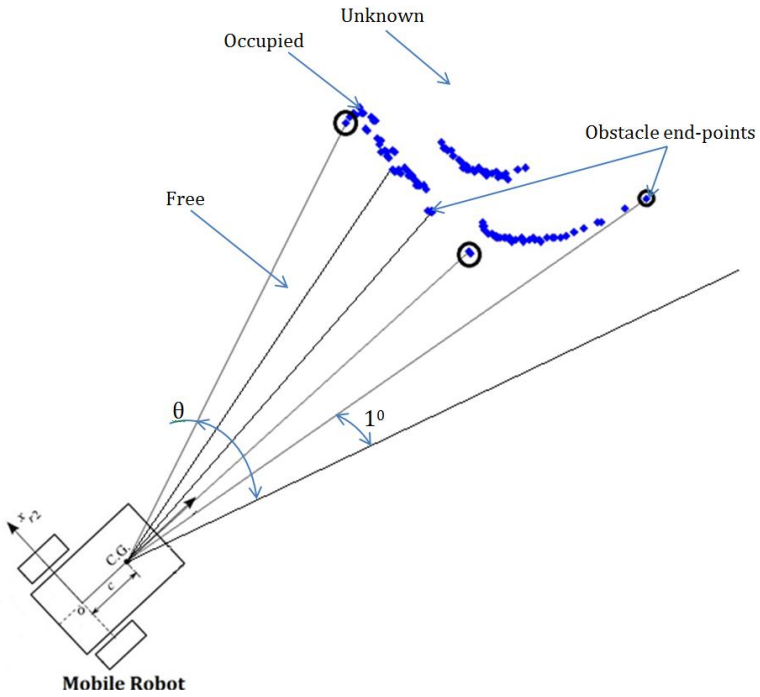


Fig. 3-6: Different regions in the laser scanner view.

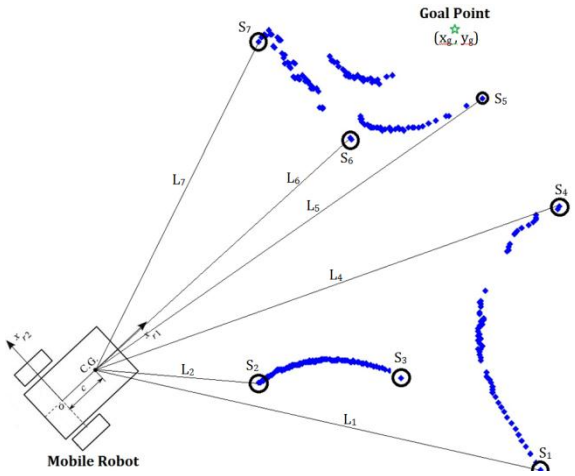


Fig. 3-7: Scape-points are defined as $S_i$. $L_i$ is the distance from the scape-point $S_i$ to the robot position.

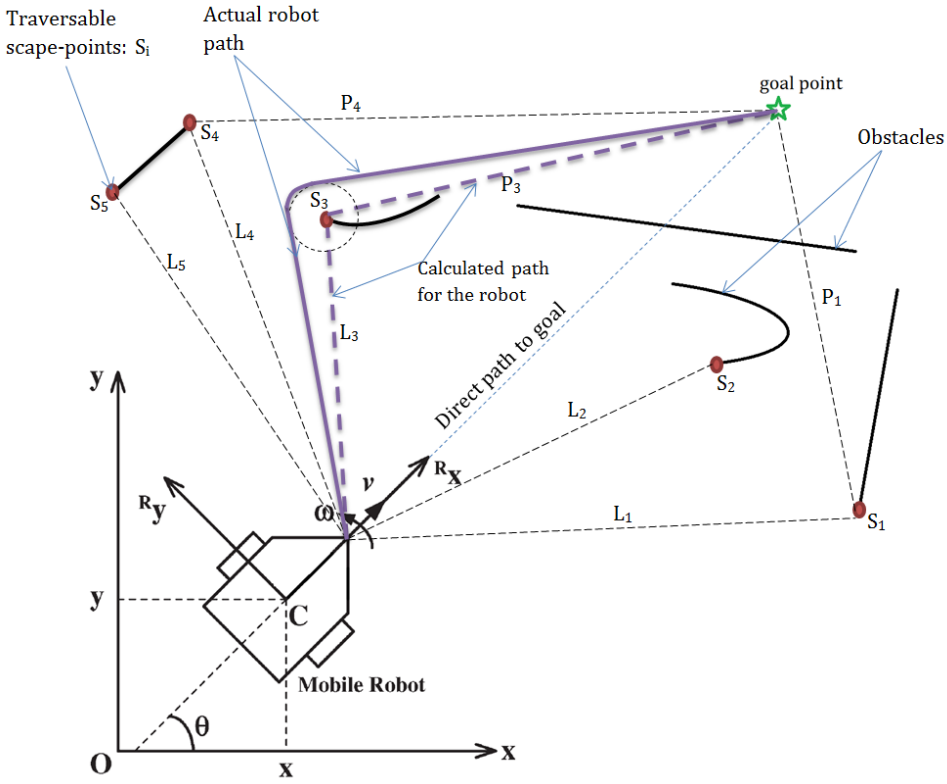


(a)

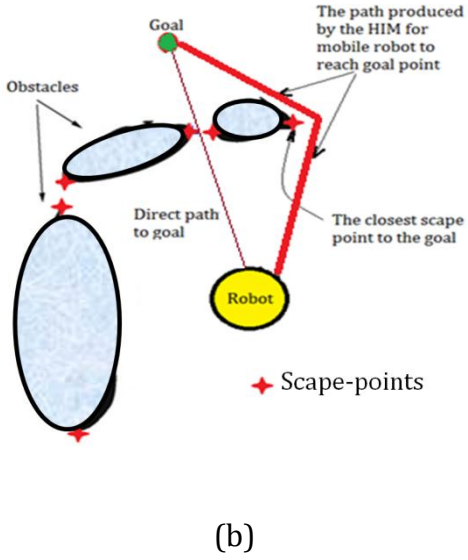


(b)

Fig. 3-8: Two typical performances of HIM for mobile robot navigation

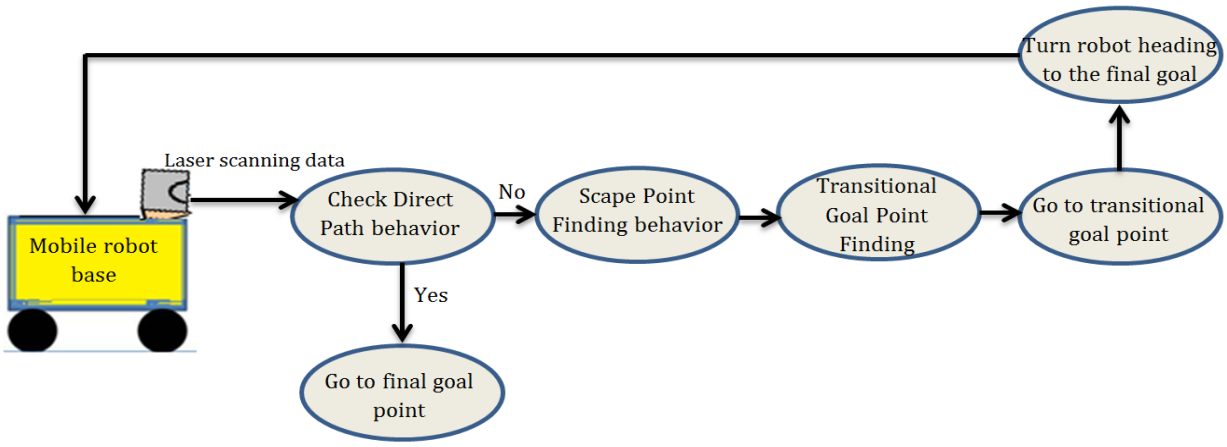


Fig. 3-9: Path finding behaviors of HIM for mobile robot navigation

### 3.3.2. Fuzzy logic based (FLB) approach

Because of the simplicity of application, fuzzy logic control is a common technique for autonomous mobile robots navigation. In this study, fuzzy logic is utilized to navigate the AGV. The FLB strategy used here is based on different behavior blocks. Each behavior block is composed of sets of fuzzy logic rule statements designed for achieving appropriate values for control parameters: heading angle ($\Delta\Phi$) and velocity (v) of the robot. The motion control variables are the translational speed (v), and the change in the heading angle ($\Delta\Phi$) of the robot. These navigation blocks are composed of fuzzy rules and statements. Inputs for the navigation blocks are laser range finder data (distances detected by the laser). For example in obstacle avoidance behavior, this information is obstacle's distances to the robot; and laser's measurements in left, front and right sectors of the robot are defined according to the equation (1). These (dL, dF, dR) distances which are laser measurements in left, front and right sides, respectively, are mapped into trapezoidal fuzzy membership functions {Far, Medium, Close} (shown in Fig. 3-10)[26, 27]. Because piecewise linear functions are evaluated faster and more efficiently by computers, the triangular and

trapezoidal membership functions were used in our navigation system. These functions are such that the obstacle avoidance behavior becomes effective when an obstacle is observed by the robot. The values assigned to {Far, Medium, Close} functions are determined according to the size of the robot and safe distance in navigation. The distance is normalized by the AGV size. Then according to the defined fuzzy rules, control outputs ($\Delta\Phi_j$ and $v_j$) are produced for each rule. The overall control outputs $\Delta\Phi$ and v are obtained using defuzzification from each fuzzy rule's control outputs.

The robot speed is represented by three fuzzy sets {STOP, SLOW, FAST}. In Fast mode, $v_j$ is equal to the maximum speed of the robot ($V_{max}$); in SLOW, $v_j$ is equal to 0.2× $V_{max}$ (for safe navigation), and in STOP mode, $v_j$ is equal to zero. Similarly, change in the robot heading angle is represented using five linguistic fuzzy sets {NB, NS, ZE, PS, PB}; these membership functions are shown in Fig. 3-11 and are as follow: NB is negative-big, NS negative-small, ZE zero, PS positive-small, and PB positive-big. The positive and negative terms mean counter-clock wise and clock wise rotation of the robot, respectively.

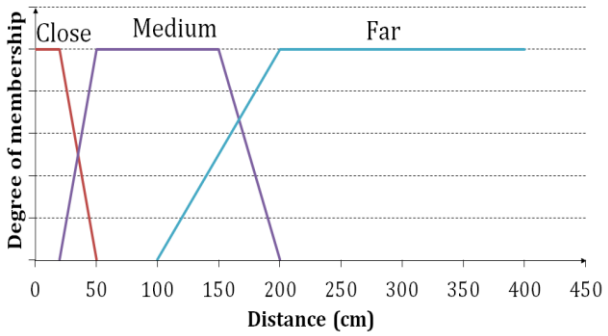


Fig. 3-10: fuzzy membership functions for measured distance

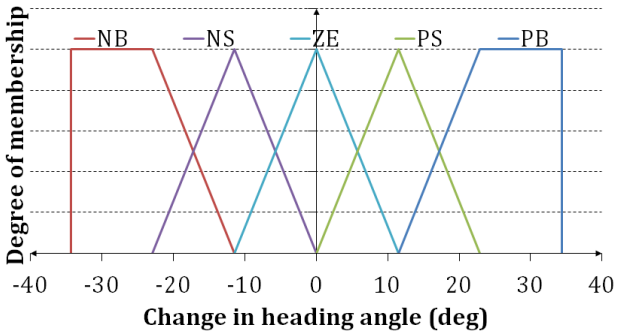


Fig. 3-11: fuzzy membership functions for change in the robot heading angle

I. Fuzzy rules:

The fuzzy rules for determination of the robot turn angle and speed ($\Delta\Phi_j$ and $v_j$) are based on human reasoning. The main objectives of these rules are to avoid collision with obstacles and guiding the robot toward the goal. If the robot is far from obstacles in all three sectors, then the robot moves toward the goal with its maximum speed. If the goal is not in front of the robot and there exist obstacles, then the robot approaches the nearest obstacle in the right or left side, according to the smallest distance to the obstacle. If the goal and obstacles are both in front of the robot, then the robot approaches the nearest obstacle on its right or left while seeking the goal. The robot speed is based on the closest obstacle distance in the three sectors. If there is any close obstacle in front sector of the robot then the robot speed is zero. If there is any obstacle with medium distance in front sector then the robot speed is slow ($0.2\times V_{max}$). If the front sector of the robot is free from obstacles but there are obstacles in the right and/or left sides then the robot speed is slow ($0.2\times V_{max}$). But if obstacles are far from the robot (all sectors' distances are far) then the robot speed is $V_{max}$. The fuzzy rules for turn angle and speed of the robot ($\Delta\Phi_j$ and $v_j$) are summarized in Table 3-I.

In some cases, the total fuzzy output for the change in heading angle of the robot ($\Delta\Phi$) has almost symmetrical shape about zero axis. For example, if there is an obstacle in front area of the robot, there are two appropriate choices for the robot, to turn right or left, but straight motion is not recommended. In this case, the centroid defuzzification strategy gives a prohibited command such as: go straight toward the obstacle ($\Delta\Phi=0$). Therefore, blending of the outputs of the rules that occur, during centroid defuzzification method can give a prohibited control command. In such situations the final control output for the robot

may be approaching an obstacle or even colliding with it. Another approach is the mean of maximum (MOM) defuzzification strategy, which guides the robot appropriately for this specific case. To solve this problem, the Centre-of-the-Largest-Area (CLA) approach was applied here for defuzzification [24]. In this strategy, the fuzzy control output (ΔΦ) is divided into two or more distinct control areas. Then the output with the largest area is chosen and taken into account for defuzzification using the standard Centroid technique. This technique resolves the prohibited responses of the Centroid method. If the control output for ΔΦ has equal areas for right and left turning, then either right or left turning direction is chosen according to the goal position as the "GOAL" turn direction. Thus by selection of the "GOAL" as turning direction, the final outputs that result in moving the robot straight into the local obstacle or the impassable terrain segment are avoided. The centroid method is used to obtain the overall fuzzy control outputs ΔΦ and v as follow:

$$\Delta\phi = \frac{\sum_{j=1}^{n} \alpha_j.(\phi_j).\Delta\phi_j}{\sum_{j=1}^{n} \alpha_j.(\phi_j)}. \tag{19}$$

$$v = \frac{\sum_{j=1}^{n} \alpha_j.(v_j).v_j}{\sum_{j=1}^{n} \alpha_j.(v_j)}. \tag{20}$$

where $\alpha_j$ (.) is the weighting factor for the rule jth, and $\Delta\Phi_j$ is area under the truncated membership function for change in the heading angle of the robot (ΔΦ), while $v_j$ is the corresponding value for the velocity fuzzy sets.

This FLB method enables the robot to cope with fluctuating and imprecise sensory data from uncertain environment. In this technique no prior knowledge of the environment is

needed, consequently it is easy to implement for real-time navigation of the mobile robot. Comparing FLB approach with the published results in [18] showed that the FLB method produced smoother and also shorter paths in almost all of the test cases examined and also it uses fewer numbers of rules for navigation (more details are given in next section). Therefore this technique represents a time-efficient and computationally cost-efficient method for outdoor mobile robot navigation.

Table 3-I: Fuzzy rules used in FLB

| | |
|---|---|
| 1) | IF (dL, dF, dR) is (C, C, C) THEN $v_1$ is ZE and $\Delta\Phi_1$ is PB |
| 2) | IF (dL, dF, dR) is (C, C, M) THEN $v_2$ is ZE and $\Delta\Phi_2$ is NS |
| 3) | IF (dL, dF, dR) is (C, C, F) THEN $v_3$ is ZE and $\Delta\Phi_3$ is NB |
| 4) | IF (dL, dF, dR) is (C, M, C) THEN $v_4$ is ZE and $\Delta\Phi_4$ is ZR |
| 5) | IF (dL, dF, dR) is (C, M, M) THEN $v_5$ is ZE and $\Delta\Phi_5$ is NS |
| 6) | IF (dL, dF, dR) is (C, M, F) THEN $v_6$ is ZE and $\Delta\Phi_6$ is NS |
| 7) | IF (dL, dF, dR) is (C, F, C) THEN $v_7$ is ZE and $\Delta\Phi_7$ is ZR |
| 8) | IF (dL, dF, dR) is (C, F, M) THEN $v_8$ is ZE and $\Delta\Phi_8$ is NS |
| 9) | IF (dL, dF, dR) is (C, F, F) THEN $v_9$ is ZE and $\Delta\Phi_9$ is NS |
| 10) | IF (dL, dF, dR) is (M, C, C) THEN $v_{10}$ is $0.2\times v_{max}$ and $\Delta\Phi_{19}$ is PS |
| 11) | IF (dL, dF, dR) is (M, C, M) THEN $v_{11}$ is $0.2\times v_{max}$ and $\Delta\Phi_{11}$ is GOAL |
| 12) | IF (dL, dF, dR) is (M, C, F) THEN $v_{12}$ is $0.2\times v_{max}$ and $\Delta\Phi_{12}$ is NS |
| 13) | IF (dL, dF, dR) is (M, M, C) THEN $v_{13}$ is $0.2\times v_{max}$ and $\Delta\Phi_{13}$ is PS |
| 14) | IF (dL, dF, dR) is (M, M, M) THEN $v_{14}$ is $0.2\times v_{max}$ and $\Delta\Phi_{14}$ is ZR |
| 15) | IF (dL, dF, dR) is (M, M, F) THEN $v_{15}$ is $0.2\times v_{max}$ and $\Delta\Phi_{15}$ is NS |
| 16) | IF (dL, dF, dR) is (M, F, C) THEN $v_{16}$ is $0.2\times v_{max}$ and $\Delta\Phi_{16}$ is PS |
| 17) | IF (dL, dF, dR) is (M, F, M) THEN $v_{17}$ is $0.2\times v_{max}$ and $\Delta\Phi_{17}$ is ZR |
| 18) | IF (dL, dF, dR) is (M, F, F) THEN $v_{18}$ is $0.2\times v_{max}$ and $\Delta\Phi_{18}$ is NS |
| 19) | IF (dL, dF, dR) is (F, C, C) THEN $v_{19}$ is $0.2\times v_{max}$ and $\Delta\Phi_{19}$ is PB |
| 20) | IF (dL, dF, dR) is (F, C, M) THEN $v_{20}$ is $0.2\times v_{max}$ and $\Delta\Phi_{20}$ is PS |
| 21) | IF (dL, dF, dR) is (F, C, F) THEN $v_{21}$ is $0.2\times v_{max}$ and $\Delta\Phi_{21}$ is GOAL |
| 22) | IF (dL, dF, dR) is (F, M, C) THEN $v_{22}$ is $0.2\times v_{max}$ and $\Delta\Phi_{22}$ is PS |
| 23) | IF (dL, dF, dR) is (F, M, M) THEN $v_{23}$ is $0.2\times v_{max}$ and $\Delta\Phi_{23}$ is PS |
| 24) | IF (dL, dF, dR) is (F, M, F) THEN $v_{24}$ is $0.2\times v_{max}$ and $\Delta\Phi_{24}$ is GOAL |
| 25) | IF (dL, dF, dR) is (F, F, C) THEN $v_{25}$ is $0.2\times v_{max}$ and $\Delta\Phi_{25}$ is PS |
| 26) | IF (dL, dF, dR) is (F, F, M) THEN $v_{26}$ is $0.2\times v_{max}$ and $\Delta\Phi_{26}$ is ZR |
| 27) | IF (dL, dF, dR) is (F, F, F) THEN $v_{27}$ is $v_{max}$ and $\Delta\Phi_{27}$ is ZR |

## 3.4. Results

The proposed navigation strategies (HIM and FLB) were verified on a mobile robot (the AGV shown in Fig. 3-1). The evaluation of the performance of methods was conducted using computer simulation and actual experiments. For the computer simulation a program

in Visual C++ was developed and two-dimensional visualization of the robot motion was given using MobileSim. In Fig. 3-12, a typical simulation setting with stationary obstacles and the mobile robot, which is equipped with sonars and laser range finder, is depicted. For actual experiments the AGV shown in Fig. 3-1 was used at the engineering building of University of Saskatchewan. Because of cold weather and existence of snow on the ground, we were unable to do experiment outdoor. Although experiments were carried out indoor, any prior information (such as a map) of the environment was not used for navigation. We plan to do our tests in actual outdoor settings when weather permits. Experiments were performed as the robot was navigating outdoor in a sense, except that floor was flat. For comparing the results of navigation strategies, energy consumption, path length and total time spent for the robot to reach the goal are measured.

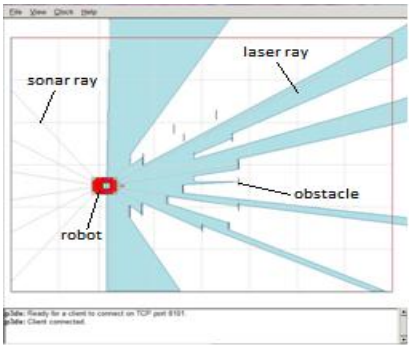

Fig. 3-12: A view of the mobile robot, static obstacles, sonar and laser rays in MobileSim

### 3.4.1. Simulation results

The proposed navigation strategies (FLB and HIM) are tested for different setups. In each situation, the results of FLB and HIM are both illustrated for comparison. The mobile robot was set at a specific start point (0,0) for each test, and goal point position and final heading of the robot were also defined. The path of the robot and its velocity during motion is recorded and is shown in Fig. 3-13 for four different setups. In these figures, solid black line

shows the path produced by HIM and dashed line is the path created by FLB approach. In each setup, the robot avoids obstacles and reaches the goal point successfully. As it is inferred from Fig. 3-13, in complex environments FLB may have some oscillations and create longer path to navigate the robot to reach the goal compared with HIM. Therefore, the simulation tests confirm the advantage of HIM in terms of path length, smoothness (no oscillations), and efficiency (less energy and time). The results of the tests in both simulation and experiments are based on empirical data. For each case tests are repeated at least ten times for simulation, and five times for experiments. Table 3-II provides comparisons of HIM and FLB for four different simulation setups. The comparison is based on three criteria: 1) The energy per unit mass, consumed by the mobile robot in Joule/Kg. 2) The travelling time for the robot to reach the goal point in second (s). 3) The path length travelled by the robot to reach its goal point in meter (m).

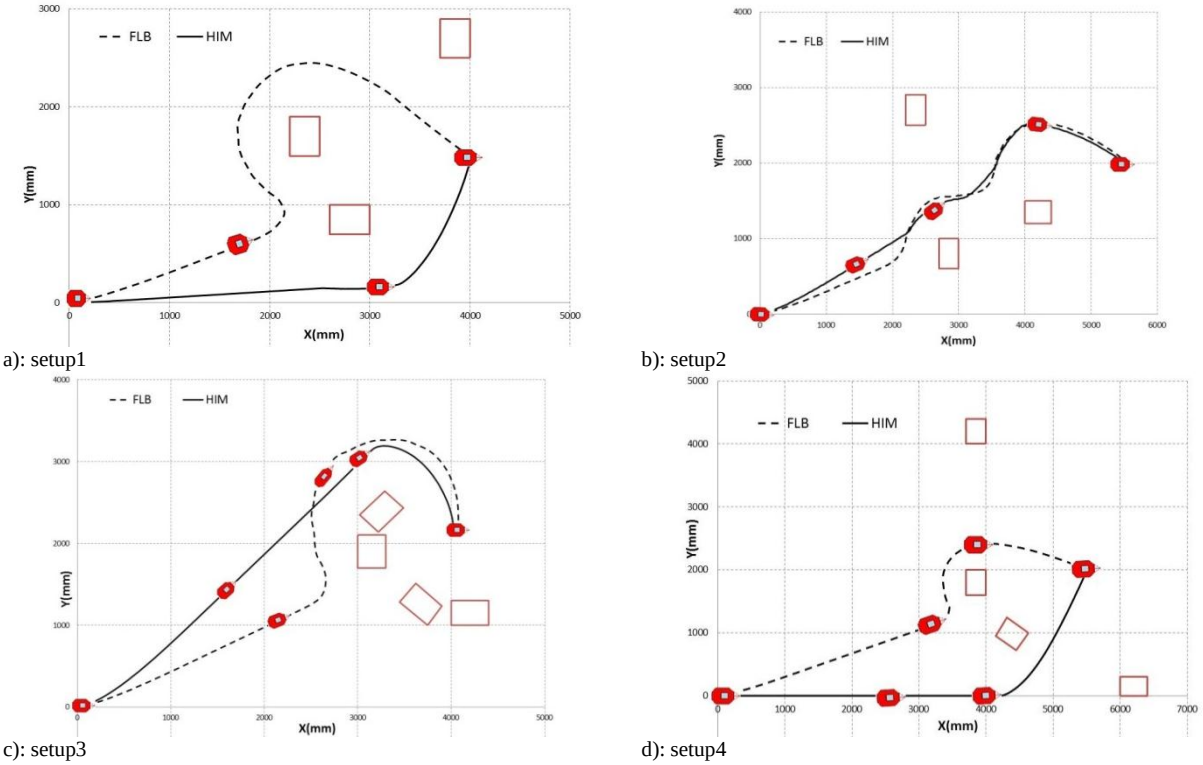


a): setup1 b): setup2

c): setup3 d): setup4

Fig. 3-13: Simulation results for verification of HIM and FLB approaches in four different setups. Navigation results for HIM are shown in solid black lines and results of the fuzzy approach are depicted in dashed black lines.

Table 3-II: Comparison of HIM and FLB in simulations

| Tests | Criterion for comparison | FLB | HIM |
|---|---|---|---|
| **setup1** | Start point (x, y) (m) | (0,0) | (0,0) |
| | Goal point (x, y) (m) | (4,1.5) | (4,1.5) |
| | Energy index (J/kg) | 474.8 | 245.6 |
| | Travelling time (s) | 29.83 | 20.26 |
| | Path length (m) | 6.288 | 4.786 |
| **Setup2** | Start point (x, y) (m) | (0,0) | (0,0) |
| | Goal point (x, y) (m) | (5.5,2) | (5.5,2) |
| | Energy index (J/kg) | 543.1 | 644.8 |
| | Travelling time (s) | 33.14 | 36.77 |
| | Path length (m) | 6.665 | 6.416 |
| **Setup3** | Start point (x, y) (m) | (0,0) | (0,0) |
| | Goal point (x, y) (m) | (4,2.1) | (4,2.1) |
| | Energy index (J/kg) | 582.7 | 334.5 |
| | Travelling time (s) | 31.90 | 20.17 |
| | Path length (m) | 6.910 | 5.959 |
| **Setup4** | Start point (x, y) (m) | (0,0) | (0,0) |
| | Goal point (x, y) (m) | (5.5,2) | (5.5,2) |
| | Energy index (J/kg) | 1173 | 381.0 |
| | Travelling time (s) | 67.41 | 20.93 |
| | Path length(m) | 6.711 | 6.551 |

The energy per unit mass consumed by the robot is computed as follows:

Work = force × displacement

=(mass × acceleration) × (velocity × time)

$$\Rightarrow E_m\left[\frac{J}{kg}\right] = a\left[\frac{m}{s^2}\right] \times v\left[\frac{m}{s}\right] \times t[s] \tag{4}$$

The path length ($P_L$) is calculated as summation of the distance between two consecutive

points in the robot's path from start point ($x_1$, $y_1$) to the goal point ($x_n$, $y_n$); where n is the number of points in path:

$$P_L[m] = \sum_{i=1}^{n} \sqrt{(x_{i+1} - x_i)^2 + (y_{i+1} - y_i)^2} \quad (5)$$

Table 3-II indicates that for all setups HIM produces shorter paths for navigation of the robot and generally it takes less time for the robot to reach goal point. This means computation time and decision making time for HIM is smaller than FLB. In addition, the energy per unit mass for HIM is less than FLB for most of the setups; which means HIM is more energy efficient compared with FLB. To validate these findings these setups were also implemented on the AGV which are presented in the next section.

### 3.4.2. Experimental results

Similar experimental setups as those of simulations were used to evaluate FLB and HIM navigation methods. The mobile robot used is equipped with a laser range finder, which gives the distance of the robot to any obstacles. In each test, the robot starts from a start point defined as (0,0) and tries to reach a given goal point, while traversing the safest path and avoiding any encountered obstacles.

Fig. 3-14 shows snapshots of the mobile robot traversing from the start point (as marked in the picture) to the goal point, using (a) fuzzy approach (b) human-inspired method.

(a)

(b)

Fig. 3-14: Snapshots of the AGV for experiments. The mobile robot traversing from start point to the goal point, using (a): FLB (b): HIM. Top-left image shows the robot at start point and bottom-right image indicates robot at the goal. Image sequence proceeds to the right and down.

The two-dimensional view of the mobile robot motion and obstacles are depicted in Fig. 3-15. The positions of the robot were recorded continuously in a file and the path of the robot was created using these data. Each scenario was carried on twice: first, implementing the fuzzy approach for navigating the robot, and then using the human-inspired method. In these figures, four different test results for both FLB and HIM are shown. In these figures, again the solid black line shows the path produced by HIM and dashed black line is the path created by FLB. In each setup, the robot avoids any obstacles and safely reaches to goal point.

As it is shown in Fig. 3-15, FLB makes the robot to go directly toward the goal point until an

obstacle is detected on the way of the robot; then it navigates the robot to avoid the encountered obstacle. Unlike FLB, HIM determines the robot's path such that, the robot does not go toward any stationary obstacles, similar to a human navigation. If a moving obstacle is detected, HIM will also change the robot's path to avoid it. This saves time and energy as it is revealed in Table 3-III.

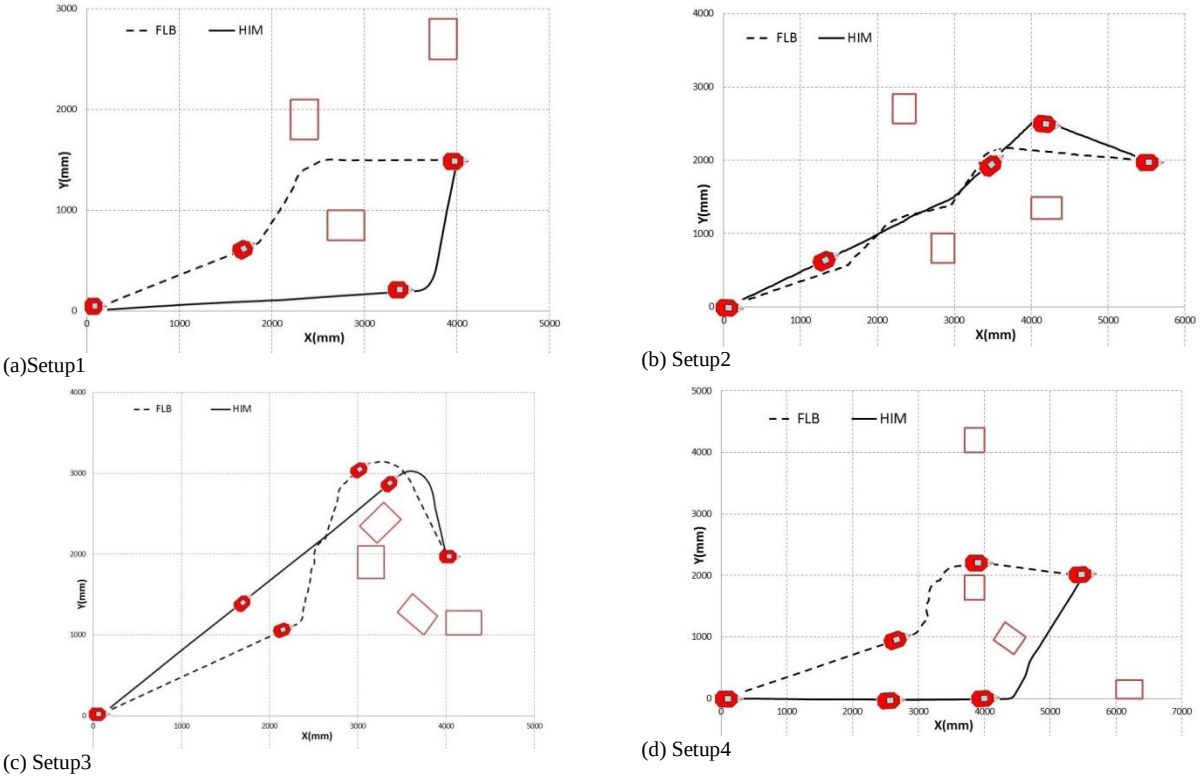


(a)Setup1 (b) Setup2

(c) Setup3 (d) Setup4

Fig. 3-15: Experimental results for validating HIM and FLB for four different setups. Navigation results for HIM are shown in solid lines and for FLB are depicted in dashed lines.

- **High speed tests**

Effectiveness of the proposed navigation strategies is also verified in high speed tests. The mobile robot was navigated in the same environment as in setup3 shown in Fig. 3-17. Both algorithms (FLB and HIM) were tested when the mobile robot was moving at a speed of 2m/sec.

As Fig. 3-16 displays, both FLB and HIM are able to navigate the robot at this high speed (2m/sec) to attain the goal point while avoiding encountered obstacles.

Fig. 3-17 demonstrates that in fuzzy approach, first the mobile robot goes directly to the goal but when obstacles are encountered the robot goes around of the wall of obstacles even though this causes the robot to move away from the goal point. In human-inspired method, the robot from the start goes directly to the edge of the wall of obstacles which is the closest scape-point to the goal point, and then moves toward the goal. This makes the total execution time for HIM, shorter than FLB and also results in less energy consumption and shorter path length.

(a)

(b)

Fig. 3-16: Snapshots of the AGV used for high speed experiments. The mobile robot movies from start point to the goal point at high speed of 2m/sec, using (a) FLB (b) HIM. Image sequence proceeds to the right and down. Top-left image shows the robot at start point and bottom-right image indicates the robot at the goal.

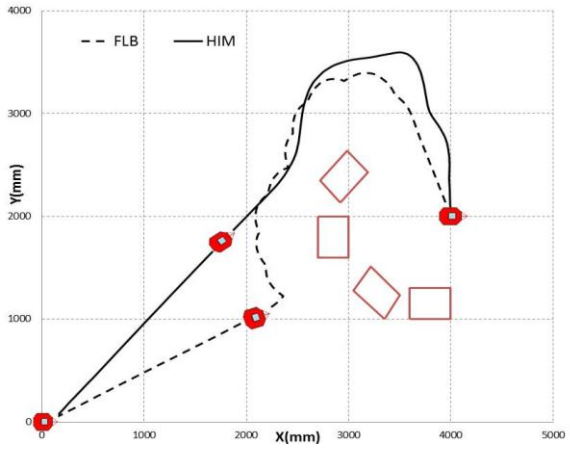


Fig. 3-17: Experimental results for testing HIM and FLB in setup3 at high speed tests (2m/sec). Robot path for HIM are shown in solid line and for FLB are depicted in dashed line.

- **Tests with moving obstacles**

The navigation strategies (FLB and HIM) were also tested for situations with moving or unforeseen obstacles. As shown in Fig. 3-18, there is a moving obstacle (guy) which blocks the robot path. Fig. 3-18 (a) shows snapshots of the navigation for FLB. From Fig. 3-19, it is revealed that the robot moves straight toward goal point until the wall of stationary obstacles keeps the robot from approaching to the goal; then the robot follows the wall and meets a moving obstacle on its way. Then, the robot changes its direction and turns away and follows the wall of stationary obstacles in opposite direction until it finds a passable way to attain goal point.

Fig. 3-18 (b) shows snapshots of the robot navigation using HIM. As it is revealed in Fig. 3-19, the robot moves straight to the edge of the wall of stationary obstacles (the best scape-point) until it encounters a moving obstacle (the moving guy); then the robot avoids the moving obstacle and finds the shortest path to reach the goal.

(a)

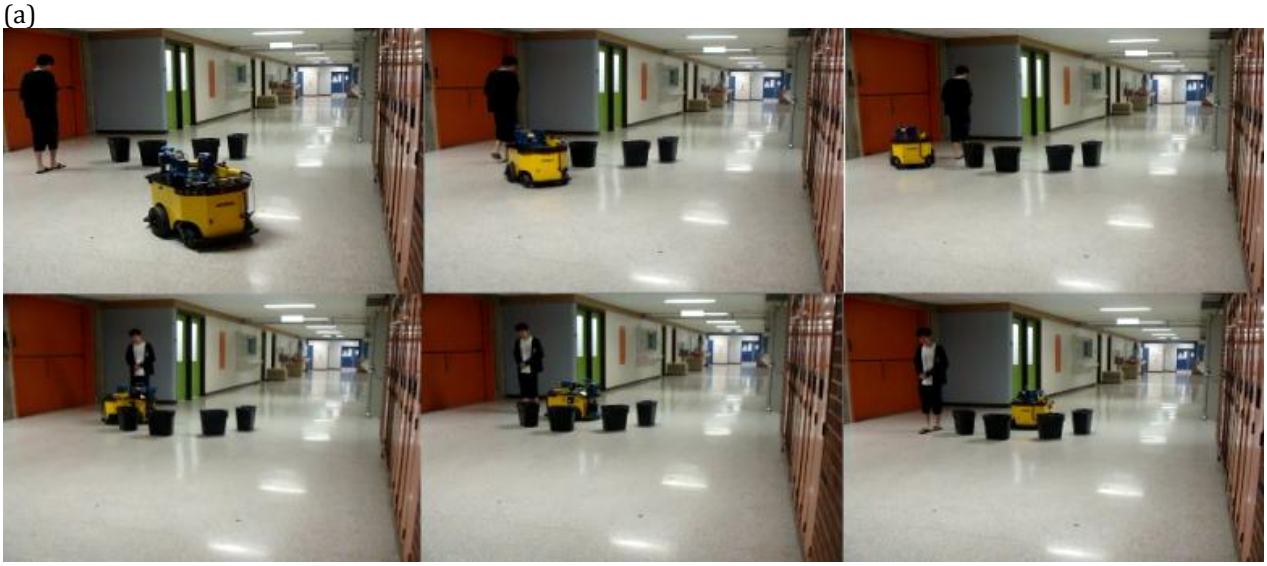

(b)

Fig. 3-18: Snapshots of the AGV used for experiments with moving obstacle. The mobile robot moves from start point to the goal point, using (a) fuzzy approach (b) human-inspired method. Image sequence proceeds to the right and down. Top-left image shows the robot at start point and bottom-right image indicates robot at the goal.

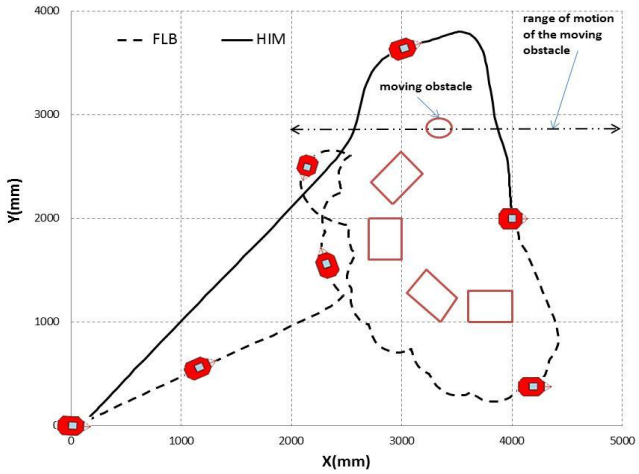


Fig. 3-19: Experimental results for HIM and FLB in setup4 at high speed (2m/s) with moving obstacle. Robot path for HIM is shown in solid line and for FLB is depicted in dashed line. Black arrow shows motion and range of the moving obstacle

Table 3-III: Comparison of HIM and FLB in experiments

| Tests | Criterion for comparison | FLB | HIM |
|---|---|---|---|
| **setup1** | Start point (x, y) (m) | (0,0) | (0,0) |
| | Goal point (x, y) (m) | (4,1.5) | (4,1.5) |
| | Energy index (J/kg) | 964.9 | 833.9 |
| | Travelling time (s) | 82.28 | 64.00 |
| | Path length(m) | 4.500 | 4.465 |
| **Setup2** | Start point (x, y) (m) | (0,0) | (0,0) |
| | Goal point (x, y) (m) | (5.5,2) | (5.5,2) |
| | Energy index (J/kg) | 1756 | 1095 |
| | Travelling time (s) | 107.2 | 65.50 |
| | Path length(m) | 6.262 | 6.150 |
| **Setup3** | Start point (x, y) (m) | (0,0) | (0,0) |
| | Goal point (x, y) (m) | (4,2) | (4,2) |
| | Energy index (J/kg) | 1573 | 896.0 |
| | Travelling time (s) | 94.89 | 57.78 |
| | Path length(m) | 6.378 | 5.863 |
| **Setup4** | Start point (x, y) (m) | (0,0) | (0,0) |
| | Goal point (x, y) (m) | (5.5,2) | (5.5,2) |
| | Energy index (J/kg) | 1151 | 1068 |
| | Travelling time (s) | 67.65 | 61.42 |
| | Path length(m) | 6.439 | 6.055 |
| **High speed (2m/sec)** | Start point (x, y) (m) | (0,0) | (0,0) |
| | Goal point (x, y) (m) | (4,2) | (4,2) |
| | Energy index (J/kg) | 1500 | 1019 |
| | Travelling time (s) | 78.75 | 55.46 |
| | Path length(m) | 7.223 | 6.866 |
| **Moving obstacle** | Start point (x, y) (m) | (0,0) | (0,0) |
| | Goal point (x, y) (m) | (4,2) | (4,2) |
| | Energy index (J/kg) | 3404 | 1024 |
| | Travelling time (s) | 125.9 | 54.56 |
| | Path length(m) | 10.35 | 7.038 |

Fig. 3-19 illustrates that HIM creates a smooth (no oscillation in path) and shorter path for the robot which is time and energy efficient compared with FLB navigation result. This test demonstrates that both FLB and HIM are able to navigate the mobile robot safely in challenging situations The other advantage of the human-inspired method is that, deadlocks can be detected and avoided. Therefore, using HIM, the robot will not be trapped in dead-ends because HIM can guide the robot to passable points like a human behavior in similar situations.

- **Effect of "Trsh" on navigation**

To consider size of obstacles and the robot, a parameter (Trsh) was defined. Changing this value (Trsh) affects behavior and outputs of the fuzzy logic approach (FLB). The (Trsh) shows the least value for control outputs to be calculated in overall outputs of the navigation system. Choosing (Trsh=0) means that the actual robot size is considered with no buffer zone. Using (Trsh=1) means that two times of robot actual size is considered (i.e. a buffer zone equal to the robot size). The smaller the (Trsh) value means the smaller the robot size, or the smaller obstacles' buffer. Consequently, smaller (Trsh) produces shorter paths.

In order to provide an insight into the effect of changing (Trsh) on navigation of the mobile robot, some test examples are simulated. The results are depicted in Fig. 3-20; in these scenarios obstacles are arranged in such a way to make narrow passages for the robot. For each example the start and final destination of the robot are given. This figure shows the robot paths. Obstacles are illustrated by bold dots. Fig. 3-20 reveals that by changing the (Trsh) value in FLB approach, the robot goes through a different path. Tuning this safety margin (Trsh) enables the robot to travel in different paths and cope with different

conditions. Thus, in cluttered environments it is recommended to use small values of the (Trsh) such as 0.3 for navigation, and (Trsh) ≥ 0.6 would be appropriate for uncomplicated situations. We tested various values of (Trsh) in FLB method performance and the results presented in the paper are the best results attained for FLB. Therefore using other values of (Trsh) does not likely improve performance of FLB.

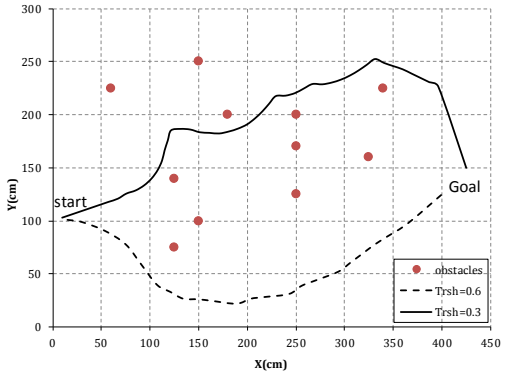


a) setup1

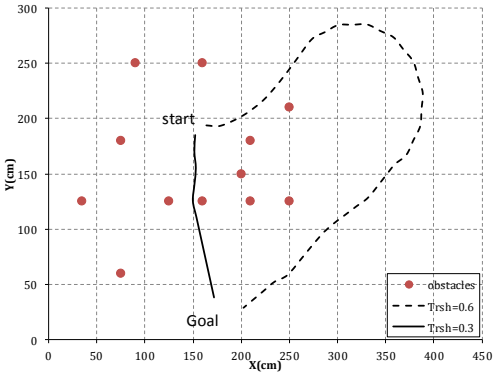


b) setup2

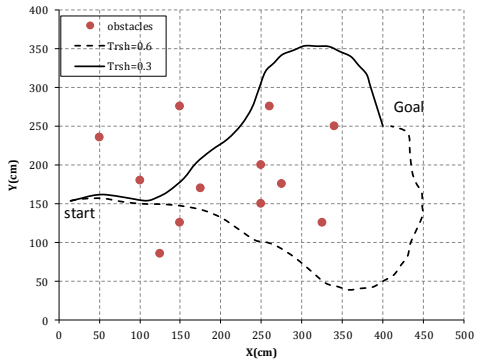


d) setup4

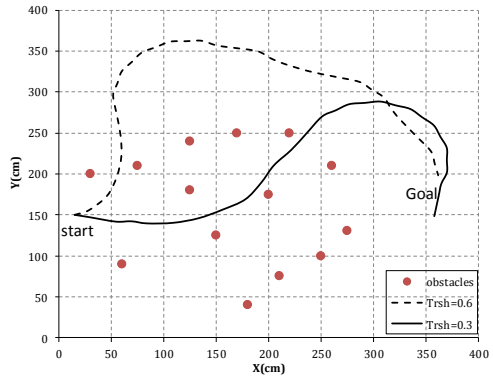


c) setup3

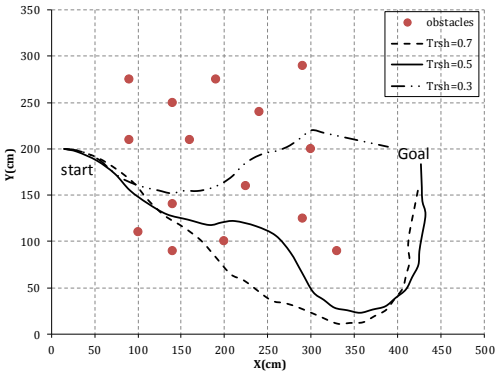


e) setup5

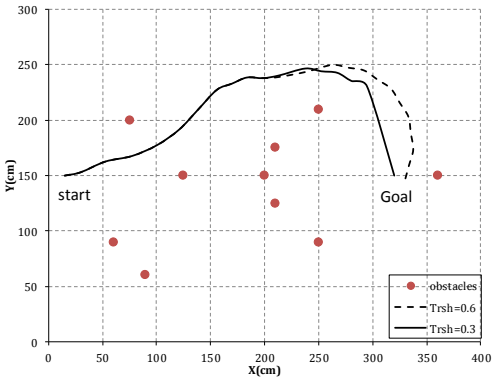


f) setup6

Fig. 3-20: Navigation results of the fuzzy approach for different values of the (Trsh) for six different examples.

## 3.5. Conclusion

Two strategies for real-time navigation of a mobile robot in outdoor settings were introduced: a Fuzzy Logic Based (FLB) approach and a Human-Inspired Method (HIM). The FLB approach is based on fuzzy logic statements and sensory data received by a laser range finder from the environment. The fuzzy logic rules used in FLB are simple and require no prior information from the environment. Tuning a safety margin (Trsh) enabled the robot to travel in different paths and cope with different conditions. In cluttered and dense environments it is recommended to use small values of the (Trsh) such as 0.3, while 0.6 could be an appropriate option for uncomplicated and unchanging situations. The FLB is a goal-oriented approach; it means that direction of the goal point is the first concern, and goal seeking will be delayed if any obstacle is detected. The FLB was compared with other methods such as vector field histogram (VFH) and preference-based fuzzy approaches in [25]. This evaluation showed that the proposed FLB method produced smoother and shorter paths in almost all of the test cases examined. Therefore this work represents a time-efficient and computationally cost-efficient approach for outdoor mobile robot navigation.

The human-inspired strategy, HIM, is designed to imitate behavior of a wise human in navigating to a goal point by finding the shortest and a safe path, while avoiding stationary and moving obstacles. The mobile robot was given a human-like ability of reasoning about the environment making the proposed strategy efficient. Test results indicated that HIM is capable of creating smooth (absence of oscillations) paths for navigating the robot. Tests were carried out indoor due to harsh (snow) weather outside, but outdoor conditions were considered during tests. HIM is capable of preventing the robot to get trapped in deadlock

and impassable conditions, which is a significant ability of this method. Compared with FLB, the navigation time, energy consumption and the path length are less in HIM. This improvement is mainly due to human-like performance of HIM which navigates the robot to take an obstacle-free path from the start point with no need to go around the obstacles during the navigation. HIM is being extended to be used in path following tasks as well.

## References


[1] C. Cariou, R. Lenain, B. Thuilot, M. Berducat, "Automatic Guidance of a Four-Wheel-Steering Mobile Robot for Accurate Field Operations," Journal of Field Robotics, v26, n 6-7, p 504-18, June 2009.

[2] A. Kulkarni, D. Tesar, "Instant Center Based Kinematic Formulation for Planar Wheeled Platforms," Journal of Mechanisms and Robotics, v 2, n 3, (12 pp.), Aug. 2010

[3] T. Zhang, Y. Zhu, J. Song, "Real-time motion planning for mobile robots by means of artificial potential field method in unknown environment," Industrial Robot, v 37, n 4, p 384-400, 2010.

[4] J. Borenstein, Y. Koren, "Real-time obstacle avoidance for fast mobile robot in cluttered environments," Proceedings of the IEEE Int. Conference on Robotics and Automation, pp. 572-577, 1990.

[5] J. Borenstein, Y. Koren, "Obstacle avoidance with ultrasonic sensors," IEEE Journal of Robotics and Automation, v4, n1, pp. 213-218, 1988.

[6] H. Noborio, T. Yoshioka, T. Hamaguchi, "On-line deadlock-free path-planning algorithms by means of a sensor-feedback tracing," Proceedings of the IEEE International Conference on System, Man and Cybernetics, pp. 1291-1296, 1995.

[7] S.M. Noorhosseini, A, S. Malowany, "GORP: a new method for mobile robot path planning problem," SPIE 183 I, Mobile Robots VII, 37-44, 1992

[8] R. Simmons, "The curvature-velocity method for local obstacle avoidance," IEEE Int. Conf. on Robotics and Automation (ICRA), pp. 3375–82, April, 1996.

[9] D. Fox, W. Burgard, and S. Thrun, "The dynamic window approach to collision avoidance," IEEE Robotics and Automation Magazine, vol. 4, March 1997.

[10] W. Li, "A hybrid neuro-fuzzy system for sensor based robot navigation in unknown environments," Proceedings of the American Control Conference, pp. 2749-2753, 1996.

[11] H. Najjaran, A. Goldenberg, "Real-time motion planning of an autonomous mobile manipulator using a fuzzy adaptive Kalman filter," Robotics and Autonomous Systems, v 55, n 2, p 96-106, 2007

[12] C. Belta, V. Kumar, "Optimal Motion Generation for Groups of Robots: A Geometric Approach," Journal of Mechanical Design, Transactions of the ASME, v 126, n 1, p 63-70, January 2004

[13] E. Akin, M. Kuis F. Alami, R.Siméon, "A human aware mobile robot motion planner Sisbot, IEEE Transactions on Robotics, v 23, n 5, p 874-883, 2007

[14] H. Teimoori, A. Savkin, " Distance-only based navigation of wheeled mobile robots with obstacle avoidance" IEEE International Conference on Robotics and Biomimetics, ROBIO 2008, p 1956-1961, 2008
[15] X. Yang, M. Moallem, R. Patel, "A layered goal-oriented fuzzy motion planning strategy for mobile robot navigation," IEEE Transactions on Systems, Man, and Cybernetics, Part B: Cybernetics, v 35, n 6, p 1214-1224, December 2005
[16] H.A. Hagras, "A hierarchical type-2 fuzzy logic control architecture for autonomous mobile robots," IEEE Transactions on Fuzzy Systems, v 12, n 4, p 524-39, Aug. 2004
[17] J. Canning, D. Edwards, M. Anderson, "Development of a Fuzzy Logic Controller for Autonomous Forest Path Navigation," Transactions of the ASAE, American Society of Agricultural Engineers ISSN 0001-2351, 2004
[18] M. Selekwa, D. Dunlap, S. Dongqing, E. Collins, "Robot navigation in very cluttered environments by preference-based fuzzy behaviors," Robotics and Autonomous Systems, v 56, n 3, p 231-46, 2008
[19] H. Hagras, M. Colley, V. Callaghan, M. Carr-West, "Online learning and adaptation of autonomous mobile robots for sustainable agriculture," Autonomous Robots, v 13, 1, 37-52, 2002
[20] S. Hrabar, "An evaluation of stereo and laser-based range sensing for rotorcraft unmanned aerial vehicle obstacle avoidance", Journal of Field Robotics, v 29, n 2, p 215-239, 2012
[21] M. Udengaard, K. Iagnemma, "Analysis, design, and control of an omnidirectional mobile robot in rough terrain," Journal of Mechanical Design, Transactions of the ASME. v 131, n 12, (11 pp.), Dec. 2009
[22] N. Chakraborty, A. Ghosal, "Dynamic modeling and simulation of a wheeled mobile robot for traversing uneven terrain without slip," Journal of Mechanical Design, Transactions of the ASME. v 127, n 5, p 901-9, Sept. 2005
[23] V. Payne, L. Isaacs, Human Motor Development: A Lifespan Approach, 8th edition, McGraw-Hill, 2012
[24] N. Pfluger, J. Yen, R. Langari, "A defuzzification strategy for a fuzzy logic controller employing prohibitive information in command formulation," IEEE Int Conf Fuzzy Syst FUZZ-IEEE, p 717-723, 1992
[25] F. Heidari, M. Vakil, R. Fotouhi, "Sensor-Based Navigation of Agricultural Autonomous Mobile Robots", ASME 2012 International Design Engineering Technical Conferences, Chicago, USA, August, 2012.
[26] C.-C. Lee. "Fuzzy logic in control systems: fuzzy logic controller. I", Systems, Man and Cybernetics, IEEE Transactions on, 20(2):404{418, 1990.
[27] C.-C. Lee. "Fuzzy logic in control systems: fuzzy logic controller. ii", Systems, Man and Cybernetics, IEEE Transactions on, 20(2):419{435, 1990.
[28] F. Fahimi, Autonomous Robots Modeling, Path Planning, and Control. Springer Science+Business Media, LLC, 233 Spring Street, New York, NY 10013, USA: Springer, 2009
[29] T. Fukao, H. Nakagawa, N. Adachi, "Adaptive tracking control of a nonholonomic mobile robot", IEEE Transactions on Robotics and Automation, v 16, n 5, p 609-15, Oct. 2000
[30] I. Waheed, R. Fotouhi, "Trajectory and temporal planning of a wheeled mobile robot on an uneven surface", Robotica, v 27, n 4, p 481-498, July 2009

# Chapter 4: A biologically inspired approach for point-to-point and path-following navigation of mobile robots

The content of this chapter is under review for publication in the ASME Journal of Mechanical Design, 2013:

**Heidari F.**, Fotouhi R., "A biologically inspired approach for point-to-point and path-following navigation of mobile robots", submitted to ASME Journal of Mechanical Design, **2013**.

## Abstract

This paper describes a fully integrated navigation strategy of a wheeled mobile robot in outdoor (farm) settings and off-road terrains. The proposed strategy is composed of four main actions which are: sensor data analysis, obstacle detection, obstacle avoidance, and goal seeking. Using these actions, the navigation approach is capable of autonomous row-detection, row-following and path planning motion in outdoor settings such as farms. In order to drive the robot in off-road terrain, it must detect holes or ground depressions (negative obstacles), that are inherent parts of these environments, in real-time at a safe distance from the robot. Key originalities of the proposed approach are its capability to accurately detect both positive (over ground) and negative obstacles, and accurately identify the end of the rows of trees/bushes in farm/orchard and enter the next row. Experimental evaluation were carried out using a differential wheeled mobile robot in different farm settings. The mobile robot, used for experiments, utilizes a tilting unit which carries a laser range finder to detect objects in the environment, and a RTK-DGPS unit for localization. The experiments demonstrate that the proposed technique is capable of successfully detecting and following rows (path following) as well as robust navigation of the robot for point-to-point motion control.

**Keywords:** Mobile robot motion control, Path following, Row-detection, Hough transform.

## 4.1. Introduction

Point-to-point mobile robot navigation is described as the process of determining a suitable and safe path between a start point and a goal point for the robot to travel between them while avoiding any encountered (static or moving) obstacles autonomously [1]. Different sensors can be used for obtaining information from the environment for the robot navigation [3, 4,5]. These sensors include cameras, sonars, laser range finders infrared, etc. There are broad areas for applications of mobile robots navigation; one of these applications is navigation of the mobile robot in farm setting for agricultural tasks. These tasks may include seeding, planting, spraying and harvesting. Autonomous row-detection and path following in farm settings are one of the most needed tasks in precision agriculture. Most of developed methods for autonomous navigations of robots in outdoor settings have been accomplished using computer vision. For example, two visual methods were designed for autonomous spraying fertilizers and planting rice in [2, 28]. Hough transform strategy was used for visual row detection and row following in agricultural setting in [29]. Work in [30] includes the computer vision technique and a laser range finder for row detection and autonomous navigation of a vehicle capable of driving in orchards. In most of the reported visual approaches for navigation of the mobile robot in outdoor settings, image processing and analyzing huge amount of data require expensive computational efforts. Also, visual methods are susceptible to variations in illumination, which can vary suddenly, thus they usually will not work at night.

Another developed technique for mobile robot navigation is a map-based method. This approach needs certain information from the environment to build a metric (grid-based) or topological map. Samples of these types of navigation systems can be found in [6] and [7];

these works solved the Simultaneous Localization and Map-building (SLAM) problem with stereo cameras and a Blackwellised particle filter. The technique included a hybrid approach of localization, and navigation. In [8], an obstacle detection technique was introduced for off-road robot navigation. They used a stereo camera, and a single axis lidar for obtaining information from the terrain. To improve navigation of mobile robot in outdoor settings overhead imagery data were used in [9]; authors introduced an online, probabilistic model to use settings' features. For using map-based navigation in outdoor settings, there are no regular landmarks or features that can be tracked. Hence, the robot explores the vicinity and moves toward a goal position while avoiding any obstacles. Therefore, map-generation and map-based navigation techniques in unstructured settings require large amounts of computational resources that make them unpopular for outdoor environments.

Several authors used laser scanners for obstacle detection and terrain modeling in off-road environments [10, 11, 12]. A method for detection and following of rut for off-road navigation of mobile robot was presented in [13]; they used laser reading and experimental offline rut models to obtain rut templates. The rut templates subsequently were used for training robot and detecting passable ruts. In pre-training navigation processes, image matching, feature detection and training algorithm need large amount of memory for storing examples as templates. Furthermore, the off-line training algorithm may not guarantee the convergence to a solution or an optimal solution [14].

While autonomous mobile robot navigation is a well-studied topic, autonomous navigation in farm fields is relatively new and not yet fully explored. One of main challenges in this

area is negative obstacle detection; such as ditches, holes, slopes and ruts. Authors of [15] reported preliminary investigation where they used stereo cameras and shadow cast for detecting negative obstacles when illuminated by two lighting sources. Authors in [16] used the fact that terrain depressions show different thermal properties than their surroundings, to detect negative obstacles.

The main contribution of this paper is proposing a new mobile robot navigation approach for outdoor terrains using 3D laser range-finder. Our approach is robust to weather conditions and time of day, as we are using an active sensor (3D laser range-finder), which does not depend on ambient illumination and can work at night time. In this paper, Hough transform algorithm was developed for row-detection in farm field using 3D laser data; the row of bushes are detected for autonomous spraying of crops. In addition, this research presents experimental evaluations of the navigation strategy in different tests such as point-to-point motion, row-detection and trajectory tracking tasks.

This paper is organized as follows: Section 2 contains the navigation structure. In Section 3, kinematics and dynamics model of the robot are described. In Section 4, the trajectory tracking control of the robot is presented. Section 5 introduces the row-detection algorithm and Hough transform method. GPS calibration and 3D laser data analysis are included in Section 6 and 7, respectively. Obstacle detection and avoidance approaches are presented in detail in Section 8 and 9, respectively. The experimental setups and results of different tests are reported in Section 10. And finally, in Section 11 conclusion and discussion of future works are presented.

## 4.2. Navigation structure

Structure of the mobile robot navigation system is depicted in Fig. 4-1. *Laser data processing*, *obstacle detection, obstacle avoidance,* and *goal seeking* are four main actions in our navigation approach. Information about the environment is provided by a 3D-laser range-finder. Laser (lidar) data are analyzed in *Laser data processing* state and a local grid map that moves with the robot is generated. The local map contains the sizes and positions of nearby obstacles. If any obstacle is identified in *obstacle detection* state then *obstacle avoidance* behavior is called in to avoid obstacles. Commands for avoiding any collision or untraversable terrain are sent to the robot control system. Then control variables, the translational speed of the robot ($v$) and the change in the heading angle of the robot ($\Delta\Phi$), are sent to the robot.

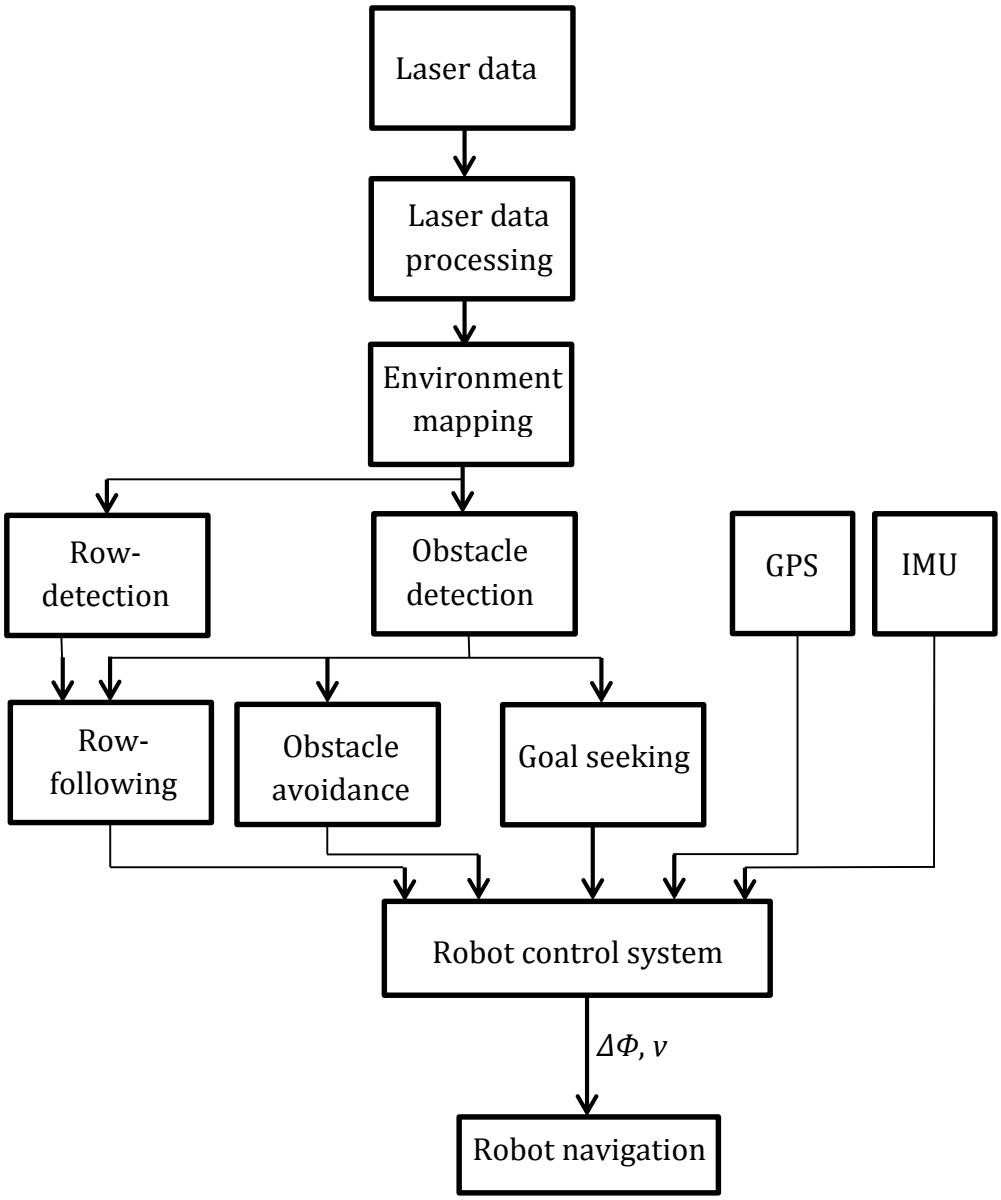


Fig. 4-1: The structure of the robot navigation algorithm

## 4.3. Robot model

Tests and evaluation of the proposed navigation strategy are conducted in two phases: computer simulations, and field experiments. In the first phase, a graphical model of a four wheeled mobile robot is developed in robots operating system (ROS). The wheeled mobile robot kinematics and on-board sensors are also modeled in the ROS. Detailed graphical

simulations are carried out for tests and are evaluated for different situations. In the second phase, the navigation strategy was implemented on the Grizzly mobile robot which is a 16.5 KW autonomous ground vehicle (AGV), shown in Fig. 4-20 (a). The AGV size is 1.8 × 1.3× 1.0 m (length× width× height). It is equipped with a nodding 3D laser range finder (LRF), mounted on the front of the robot. The LRF has a 180° horizontal sweep plane and is mounted on a tilting unit which sweeps vertically from +45° to -45° providing 3D field of view for navigation. Real-time kinematics differential global positioning system (RTK-DGPS) and an inertial measurement unit (IMU) are also installed on the vehicle for 6DOF localization designed for outdoor environment. The robot can travel to a speed of 4.4 m/s in tests. The robot's size is ideal for farm tasks and it has a trailer hitch which allows towing ground engagement tools. Therefore this robot can be used for different farm applications such as seeding, spraying and plowing.

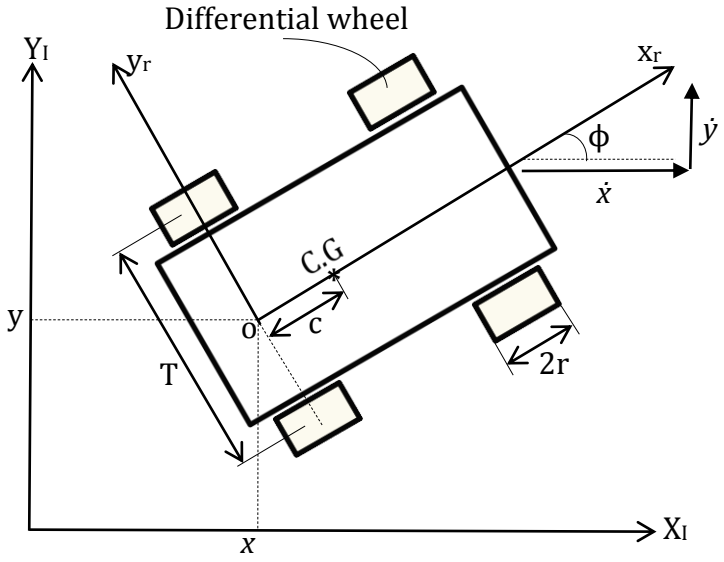


Fig. 4-2: Geometric configuration of the mobile robot

### 4.3.1. Kinematics of the robot

The AGV used for the experiments is a four-wheel-drive vehicle (having a 4x4 differential drive system) actuated by four motors, one motor drives each wheel. But for control applications, the wheels on the same side (left or right) are driven with the same velocity (meaning the wheels on the same side rotate with the same speed). The wheels are equipped with encoders. The schematic figure of the AGV is shown in Fig. 4-2. In this figure, $T$ is the width of the mobile robot and $r$ is the radius of its wheels. $X_I$ – $Y_I$ is inertial coordinate system and ϕ is the heading angle of the robot; $x_r$ - $y_r$ is the local coordinate system which is fixed to the center of the mobile robot. It is in the middle between the right and left rear wheels of the robot. The center of mass of the robot is C.G. as shown in Fig. 4-2. The distance from $x_r$ axis to the C.G. is $c$. The kinematic inputs that drive the robot and affect its speed and direction of motion are the right and the left wheels' speeds. The vector $q$ describes the configuration (position and orientation) of the robot at any time:

$$q = \begin{bmatrix} x & y & \phi \end{bmatrix}^T \tag{1}$$

$x$ , $y$ are the coordinates of the robot (point o) in the inertial frame. If the linear speed and angular velocity of the robot are $v$ and $\omega$, respectively, assuming no-slip on wheels, the velocity components can be written as:

$$\begin{aligned} \dot{x} &= v\cos\phi \\ \dot{y} &= v\sin\phi \\ \dot{\phi} &= \omega \end{aligned} \tag{2}$$

The kinematic of motion of the robot can be written as follows:

$$\dot{q} = \begin{bmatrix} \cos\phi & 0 \\ \sin\phi & 0 \\ 0 & 1 \end{bmatrix} .u \tag{3}$$

where $\dot{q}$ is time derivative of configuration $q$, and $u = \begin{bmatrix} v & \omega \end{bmatrix}^T$ is the control input given to the robot for navigation. Angular and linear velocity of the robot can be written in terms of linear velocities of the right and the left wheel centers ($v_r$, $v_l$):

$$\omega = \frac{v_r - v_l}{T} \qquad v = \frac{v_r + v_l}{2} \tag{4}$$

### 4.3.2. Dynamics of the mobile robot

The dynamics equations of the motion of the robot (Fig. 4-2) are presented as [17]:

$$\overline{M}(q).\dot{u} + \overline{C}(q,\dot{q})u = \overline{B}(q).\tau \tag{5}$$

Where matrices are defined as following:

$$\overline{M}(q) = \begin{bmatrix} \frac{r.m}{2} + \frac{I_w}{r} & \frac{r.I}{T} + \frac{T.I_w}{2.r} \\ \frac{r.m}{2} + \frac{I_w}{r} & \frac{-r.I}{T} - \frac{T.I_w}{2.r} \end{bmatrix}$$

$$\overline{C}(q,\dot{q}) = \begin{bmatrix} \frac{r}{T} m_c.c.\dot{\phi} & -\frac{r}{2} m_c.c.\dot{\phi} \\ -\frac{r}{T} m_c.c.\dot{\phi} & -\frac{r}{2} m_c.c.\dot{\phi} \end{bmatrix} \tag{6}$$

$$\overline{B}(q) = \begin{bmatrix} 1 & 0 \\ 0 & 1 \end{bmatrix} \qquad \tau = \begin{bmatrix} \tau_r \\ \tau_l \end{bmatrix} \qquad u = \begin{bmatrix} v \\ \omega \end{bmatrix} \tag{7}$$

which $\tau_r$ and $\tau_l$ are torques applied at the right and the left wheels of the robot, respectively. We let $m = m_c + 2m_w$. and $I = m_c c^2 + m_w \frac{T}{2}^2 + I_c + 2I_m$. where, $m_c$ is the mass of the robot body, $m_w$ is mass of each wheel including its motor, $I_c$ is the mass moment of inertia of the robot body about the vertical axis passing through C.G., $I_w$, is for each wheel about its horizontal rotational axis, and $I_m$ is for each wheel about a vertical axis passing through its center. A trajectory tracking controller is designed for the kinematic model of mobile robot.

## 4.4. Path planning control of the robot

This section describes in detail the path following controller designed for row tracking navigation system. The robot and the paths are modeled as illustrated in Fig. 4-3. The desired trajectory for the robot in the inertial coordinate system is defined as following:

$$\begin{aligned} x^d &= x^d(t) \\ y^d &= y^d(t) \\ v^d &= v^d(t) \end{aligned} \tag{8}$$

The lateral no-slip condition states that the lateral component of the velocity of midpoint of front axle is zero and also, interaction forces between tires and the floor do not exceed maximum allowable static friction. This condition is described as follows:

$$\dot{x}^{(d)} \sin\phi - \dot{y}^{(d)} \cos\phi = 0 \tag{9}$$

$$\Rightarrow \begin{cases} \phi^d(t) = \text{atan2}\left(\dot{y}^d(t), \dot{x}^d(t)\right) \\ \omega^d(t) = \dot{\phi}^d(t) \end{cases} \tag{10}$$

The change in the heading angle of the robot is determined using the following equation:

$$\Delta\phi = \text{atan2}\left(\left(y(t_2) - y(t_1)\right), \left(x(t_2) - x(t_1)\right)\right) \tag{11}$$

$$\phi(t_2) = \phi(t_1) + \Delta\phi \tag{12}$$

where $(x(t_1), y(t_1), \phi(t_1))$ and $(x(t_2), y(t_2), \phi(t_2))$ are the pose (position and orientation) of the robot at time $t_1$ and $t_2$, respectively. The goal is to control the robot to follow the desired trajectory given in Eq. (8). The error equations are defined as the difference between the desired and the actual values:

$$e = \sqrt{\left(x - x^d\right)^2 + \left(y - y^d\right)^2 + \left(z - z^d\right)^2}$$
$$\theta = \phi^d - \phi \tag{13}$$

The term $e$ is indicating the position error, and $\theta$ is the error in heading angle of the robot. Our goal is to control the heading angle of the robot, $\phi$, in a way to minimize $\theta$ (given in Eq. (13)).

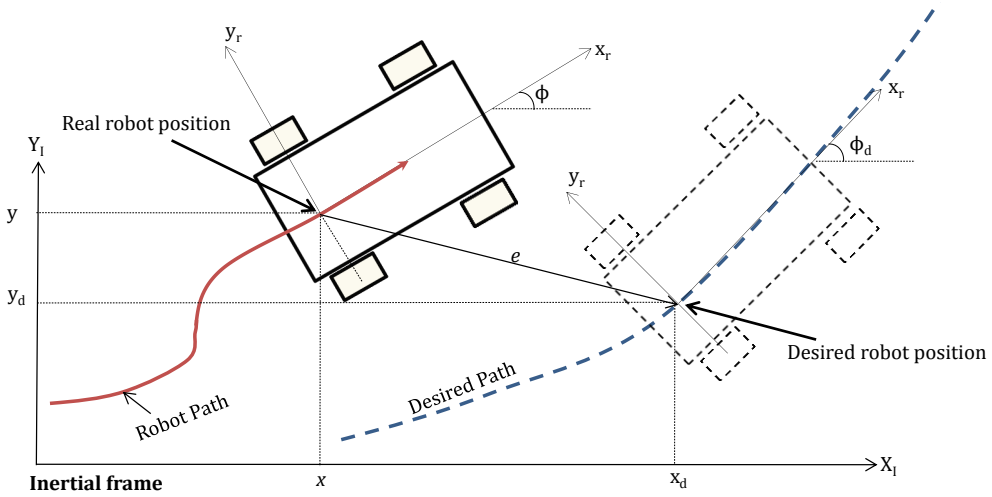


Fig. 4-3: General model of the robot for path following

The next step is to find control inputs to minimize the tracking errors in Eq. (13). The kinematics control laws used in this research were developed using techniques described in [24]. The developed controller is capable of solving the position stabilization, and path following, problems simultaneously. As a result the robot is asymptotically driven to an arbitrarily small neighborhood of the desired position, path, or trajectory. Control

parameters are then tuned to assure that physical constraints are satisfied. The linear velocity of the robot is chosen as:

$$v = \frac{k_1.e.k_e.\tanh\left(e - k_2\sqrt{2}\right) + v^d.e.k_e.\cos(\theta) + v^d.k_r.\left(\sin(\theta) + \omega^d.e/v^d\right)}{e.k_e + k_r.\sin(\alpha)} \quad (14)$$

where $k_1$ and $k_2$ are the controller parameters which control the response; $k_e$ and $k_r$ are defined as:

$$k_e = \sqrt{\zeta - \cos(2\theta)} \quad (15)$$

$$k_r = k_2\sqrt{2}\sin(2\theta) \quad (16)$$

$$\zeta = 1 - \varepsilon \quad (17)$$

where $\varepsilon$ is a small perturbance to avoid a discontinuity in the response. The optimized control law governing rotational velocity is given by:

$$\omega = k_3.\tanh(\theta) + 2\dot{\theta} + \dot{\phi}^d \quad (18)$$

where $k_3$ is a positive scalar gain to control the angular response of the controller.

Initial values of $v$ and ω obtained from equations (14) and (18) are rarely performing well for the row following system. To solve these problems the dynamic extensions [25] are defined as follow:

$$\dot{v}^r = -k_v.(v_a - v) + \dot{v} \quad (19)$$

$$\dot{\omega}^r = -k_\omega.(\omega_a - \omega) + \dot{\omega} \quad (20)$$

The values $v_a$ and $\omega_a$ are the measured velocity states of the robot. The states $\dot{v}^r$ and $\dot{\omega}^r$ are the control commands sent to the robot. These new states are introduced to decline steady state error and improve boundedness. The extensions perform as low pass filters, which improve the controller response in the presence of noisy state feedback. The gains $k_v$ and $k_\omega$ are used to control the response of the dynamic extension. The variables $v$ and $\omega$ are the

outputs from equations (14) and (18). By modeling the system as a discrete one, the control commands $\dot{v}^r$ and $\dot{\omega}^r$ are calculated from following equations:

$$\dot{v}^r = \frac{v^r(t_2) - v^r(t_1)}{t_2 - t_1} \tag{21}$$

$$\dot{\omega}^r = \frac{\omega^r(t_2) - \omega^r(t_1)}{t_2 - t_1} \tag{22}$$

All tests (in both simulations and experiments) are performed with assumption of zero initial conditions. After various simulations and testing of the controller system, the controller parameters are chosen. The controller parameters are properly tuned, after several tests, for the navigation system in order to follow the desired path to achieve the desired performance. The experiments are performed with the following values chosen for the controller parameters: $k_2$= 0.02 m, ε= 0.003 m, $k_1$= 0.85, $k_3$= 0.3, and $k_v$= $k_\omega$= 3.0. The maximum reference velocity of the robot is 4m/s, and the maximum robot acceleration is 1m/s$^2$. Initial and final velocities of the AGV are zero, with a linear ramp function to a constant velocity.

## 4.5. Row-detection and Hough transform

In this paper, for detecting rows of trees in a farm field, data from the laser range finder were used. The algorithm developed here, for row detection is Hough transform, which was originally patented by Hough [23]. This approach is a curve fitting technique to a group of data points. It is used for line or any circular shape detection. Since in farm field, rows of trees may not be exactly in one line therefore using a Hough transform is a superior method compared with alternative approaches such as least-squared for curve fitting of laser data. Hough transform is used here to generate a path (equation of a line) for the

robot to follow. The data detected by LRF produce equation of a line using Hough transform. The approach is briefly described here.

A line in the image space can be expressed in Cartesian coordinate system as follows:

$$y = m.x + c \tag{23}$$

where m is the slope of the line and c is the y-intercept. The line equation can also be expressed in a ($r_i$–θ) Polar coordinate system as follows (see Fig. 4-4):

$$y = -\frac{\cos\theta}{\sin\theta}.x + \frac{r_i}{\sin\theta} \tag{24}$$

Hence, the line equation can be written as:

$$r_i = x.\cos\theta + y.\sin\theta \tag{25}$$

The representation of the straight line in Cartesian and polar coordinate system is shown in Fig. 4-4.

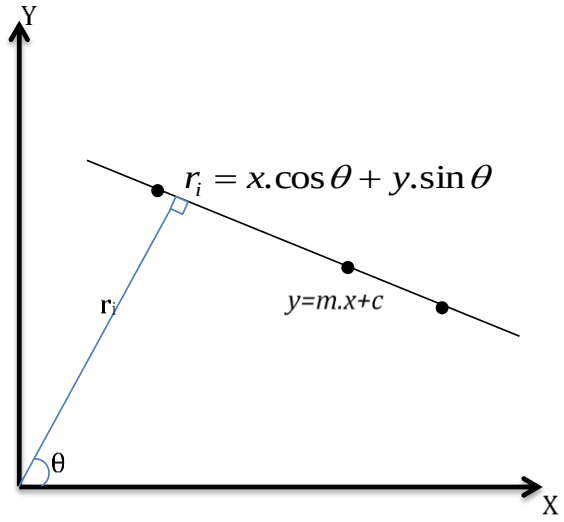


Fig. 4-4: Polar ($r_i$–θ) representation of a line

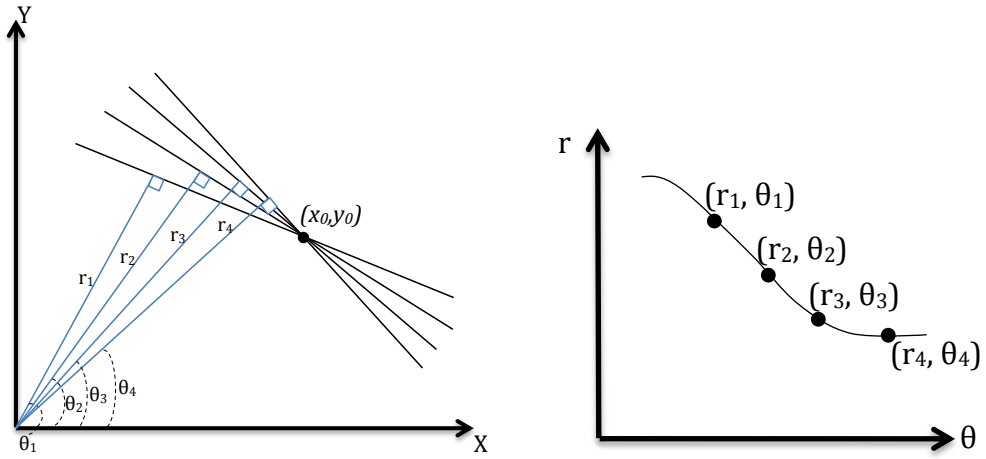


Fig. 4-5: a) a group of lines passing through a point ($x_0$, $y_0$); b) each line can be represented by a pair of ($r_i$, $\theta_i$ ) that becomes a sinusoidal curve at the $r_i$–$\theta_i$ plane.

In general, for each point ($x_0$, $y_0$), a group of lines passing through that point can be parameterized by a pair of ($r_i$, $\theta_i$) as following:

$$r_i = x_0.\cos\theta_i + y_0.\sin\theta_i \tag{26}$$

Therefore each pair of ($r_i$, $\theta_i$) represents a line that passes through point ($x_0$, $y_0$) (Fig. 4-5a). For a given point ($x_0$, $y_0$), the family of lines that passes through it in polar coordinate system represents a sinusoidal wave. This sinusoidal representation is shown in Fig. 4-5b. Thus each line can be represented with a pair of ($r_i$, $\theta_i$).

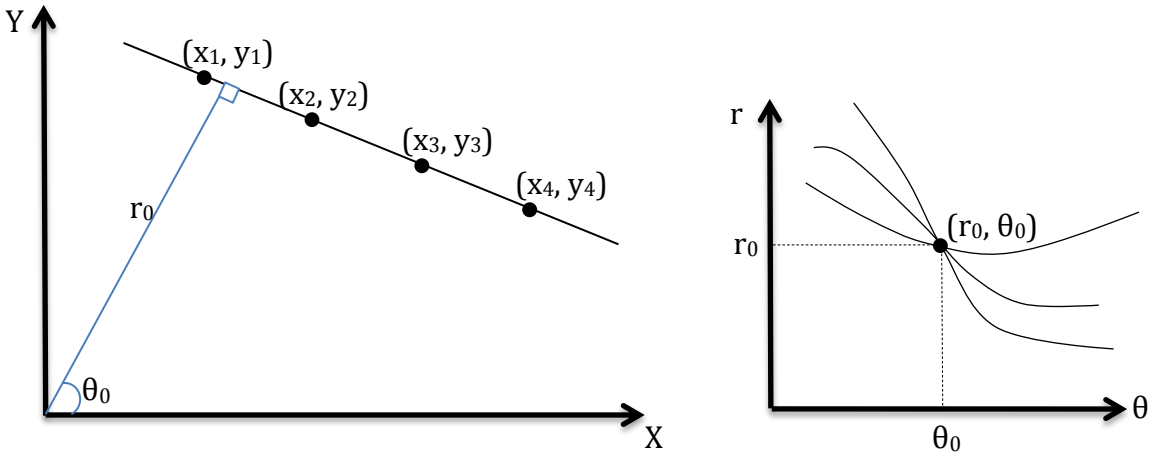


Fig. 4-6: a) Collinear points with normal parameterization of ($r_0$, $\theta_0$). b) Collinear points are transformed into curves that intersect in a single point in the r-θ plane.

The Hough transform method uses this transformation of points to sinusoidal curves to find a line passing through a group of points; this is based on the premise that points that belong to the same line in the X-Y plane will be transformed into curves with an intersection point in the $(r_i, \theta_i)$ plane (see Fig. 4-6b). Thus, to find the line passing through a group of points, such as $(x_1,y_1)$, …, $(x_4,y_4)$, one can find the point where the majority of these sinusoidal waves intersect in corresponding domain $(r_i, \theta_i)$; this gives the equation of the line passing through group of the points using Eq. 24.

In general, in Hough transform, a line can be identified by finding the number of intersections between curves in $(r_i, \theta_i)$ domain. This is the basic of the Hough transform for identifying lines.

The purpose of using Hough transform here is to automatically detect the lines of the row of bushes or trees in a farm field and to provide lateral offset and heading measurements sent to the mobile robot controller. Then the robot moves beside the rows of bushes while keeping proximity with them for spraying as an example of a given task. Again the result of implementing Hough transform algorithm on a sample of laser point clouds is depicted in Fig. 4-7; it is observed that detected lines (light blue lines) are matched real lines (dark blue).

The path generated by the navigation system for the robot to follow is shown in Fig. 4-8; two parallel lines (1), (3) generated by Hough transform are also depicted in this figure. These parallel lines indicate the rows of bushes; the robot is programmed to follow a line between the two rows of bushes shown here as line (2).

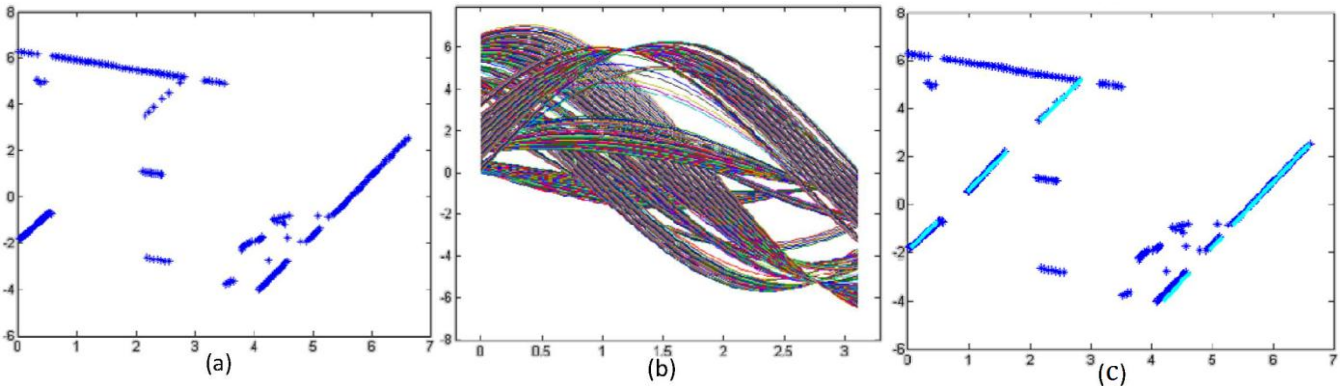


Fig. 4-7: (a) Original laser point clouds. (b) Hough transform of the points. (c) Line detection using Hough transform algorithm. Detected lines are shown in light blue.

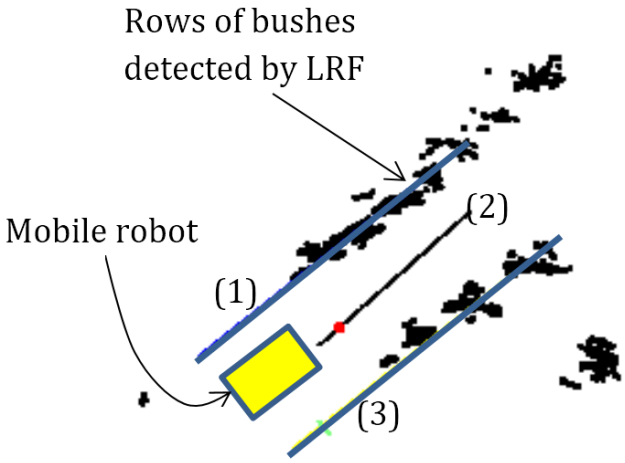


Fig. 4-8: Row of bushes detected by LRF, and lines (1), (3) generated by Hough transform.

## 4.6. GPS calibration and data analysis

Localization of the robot is necessary for navigation and control. Using dead-reckoning and robot's wheel encoders data are not very accurate for outdoor localizations, particularly when the robot is going to travel in an uneven terrain or on loose soils such as agricultural farm fields. The encoders' calculations may have large errors because of wheel slippage and wheel imperfection which cause quick accumulation of the position errors. Therefore for accurate localization of the robot a real-time kinematics differential global positioning system (RTK-DGPS) is used. Here, we used a set of rover-and-fix Novatel GPS system.

Differential GPS (DGPS) uses a fixed GPS receiver at a position whose coordinate is known with accuracy of less than 1 meter. The position of the base station itself is configured by a correction supplied by the service of some companies for example, Canadian Satellite Station in Calgary. The fixed receiver collects data from all visible satellites to the base GPS and computes predicted satellite ranges. The difference is the satellite range error, which is then converted to correction signals sent via radio transmission to the rover GPS using Pacific Crest radio antenna. Using RTK-DGPS accuracy of localization is improved down to 2 cm, which is quite satisfactory for our purpose.

RTK-DGPS provides latitude ($\psi$) and longitude ($\lambda$) of positions on Earth at each time step. Therefore Mercator projection is used to convert geographical data ($\psi$, $\lambda$) to the Cartesian coordinate ($x$, $y$) measured on the Earth surface. The Mercator projection includes parallel equally spaced lines of longitude, and parallel but increasingly spaced lines of latitude. The GPS data is converted to Cartesian coordinates using following equations:

$$y = a_1 \ln\left[ \tan\left(\frac{\pi}{4} + \frac{\psi}{2}\right) \cdot \left(\frac{1 - a_2 \sin\psi}{1 + a_2 \sin\psi}\right)^{a_2/2} \right] \quad (27)$$

$$x = a_1(\lambda - \lambda_0) \quad (28)$$

where ($a_1$ = 6378206.4) is the equatorial radius of Earth ellipsoid in meters, and ($a_2$= 8.227185 E-2) is Earth ellipsoid eccentricity. Start point of the tests is assumed as origin for the Cartesian coordinate system (x=0, y=0, z=0). Then the Cartesian coordinates x and y obtained from Eqs 27 and 28 are sent to the *robot control* action module.

## 4.7. 3D Laser data analysis

A 2D laser scanner detects objects facing its planar field of view. Thus, it cannot recognize ground-level obstacles, negative obstacles (such as holes), and above the robot level's

objects. In order to provide a 3D-scan of the environment, a rotating laser range finder (LRF) is used for navigation. The LRF consists of a 2D-laser scanner (SICK 511 for outdoor), to scan a horizontal plane, installed on a tilting unit with a stepper motor that mechanically sweeps the scan-plane continuously up and down. The 3D LRF provides a horizontal view of $\alpha = 180°$ (yaw angle) with an angular resolution of down to $\Delta\alpha = 0.25°$ (rotating mirror device). A relatively low resolution ($\Delta\alpha = 1°$) and horizontal range of view of $\alpha = 160°$ are adequate for safe obstacle avoidance. These setting dramatically decreases operation time of real-time navigation and obstacle avoidance. In this operating mode a single 2D laser scan of 181 distance-measurements is read approximately in 13.32 ms (with about 75 Hz frequency). The tilting LRF system allows to pitch the scanner over a vertical angular range of up to $\theta = 120°$ with a maximum resolution of $\Delta\theta = 0.25°$. By controlling pitch angle ($\theta$) of the laser a 3D-scan of the front of the robot is obtained. The pitch angle resolution is set to one degree ($\Delta\theta = 1°$) and range of change of $\theta$ is set to $-45° < \theta < +45°$ are adequate for safe obstacle avoidance. Therefore, the tilting LRF provides necessary scans of the farm setting for avoiding obstacles and also for accurately detecting nontravelable paths in the terrain. As shown in Fig. 4-20, the scanner system is mounted on front-top of the robot. Fig. 4-9 clarifies the operating range of the tilting LRF.

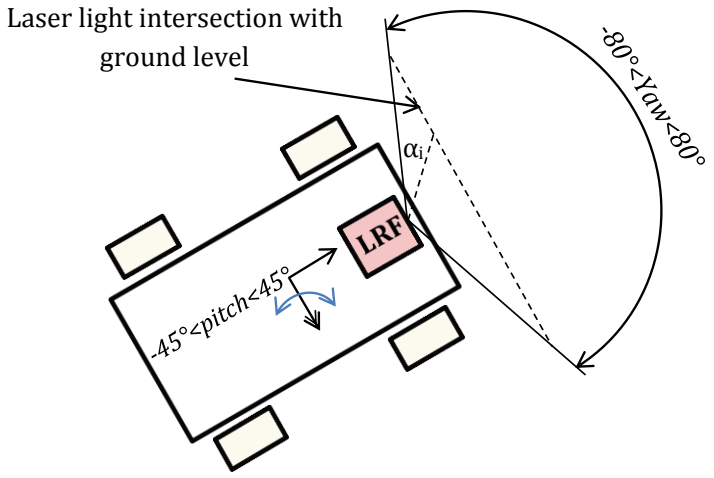


Fig. 4-9: Laser range finder position

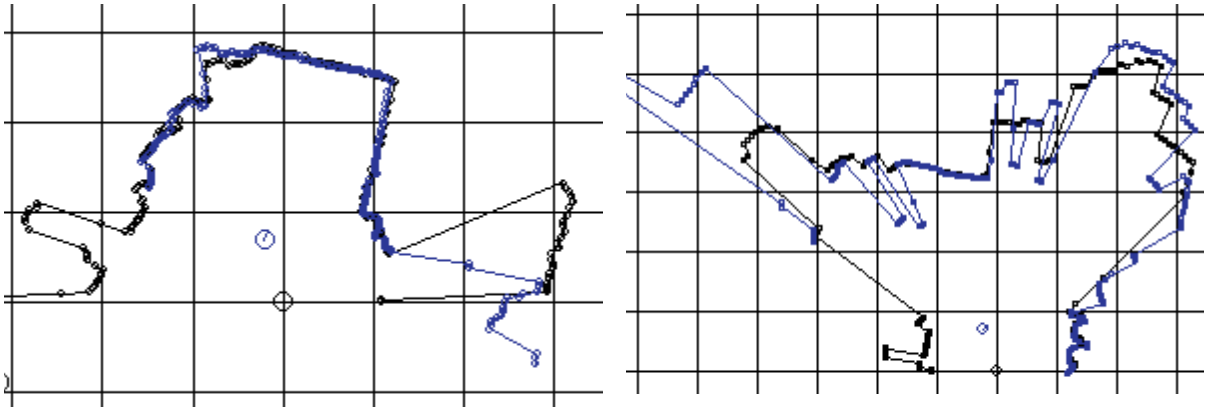

Fig. 4-10: 3D point clouds acquired by the laser range finder in two example scenes: a) titling angle θ= 10°; b) θ= -15°. The point clouds are analyzed for path planning and obstacle avoidance algorithms.

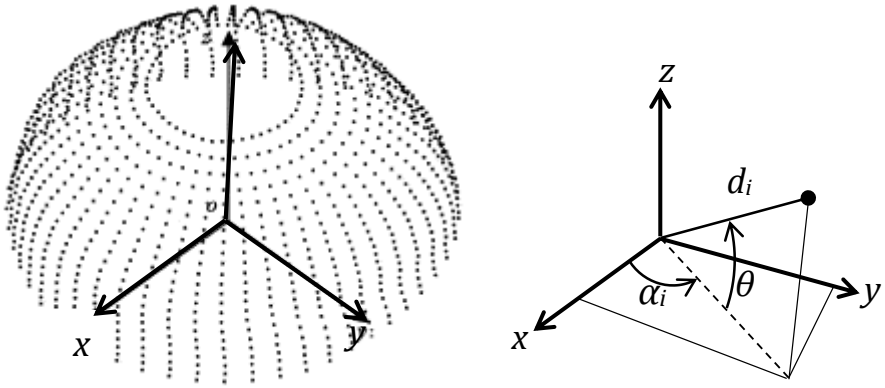


Fig. 4-11: Spherical mapping for laser point clouds.

In this work, 3D-scans of the setting for obstacle avoidance while robot is moving is provided by adjusting tilting range of the tilting unit from +45° to -45° downward. Each laser scan generates a vector of 181 distance-measurements spaced 1° apart. Projecting

these scans into the global coordinate frame according, to the pose of the robot, results in a 3D point cloud. Fig. 4-11 shows an example of the point clouds acquired by the laser range finder. Each point from the point cloud is represented by the tuple ($d_i$, θ, $\alpha_i$) which $d_i$ is ith distance-measurement along the line-of-sight of the laser ray in the current scan-plane tilted θ°); where θ and $\alpha_i$ are the current pitch angle and the yaw angle of that measurement. The corresponding Cartesian coordinates of the scan-point, (x, y, z), can be expressed using an image transformation. Based on the sensor geometry, a spherical mapping exists from ($d_i$, θ, $\alpha_i$) to (x, y, z), as shown in Fig. 4-11. The laser plane view rotates about the Y-axis. The transformation of point from point cloud to the Cartesian frame is as follows:

$$\begin{bmatrix} x \\ y \\ z \end{bmatrix} = \begin{bmatrix} d_i.\cos\theta.\sin\alpha_i \\ d_i.\cos\theta.\cos\alpha_i \\ d_i.\sin\theta \end{bmatrix} \tag{29}$$

By tilting the laser plane (changing θ), the operating range of the laser can be adjusted to detect both positive and negative obstacles in real-time in the environment.

## 4.8. Obstacle detection algorithm

The laser range finder, described in section 6, continuously delivers 3D measurements of the robot surrounding. The data is interpreted in a way that allows real-time obstacle detection and avoidance for navigation of the robot. A real-time local map, containing obstacles in front of the robot (see Fig. 4-9) is obtained. An example of this map is depicted in Fig. 4-12b for the scene shown in Fig. 4-12a.

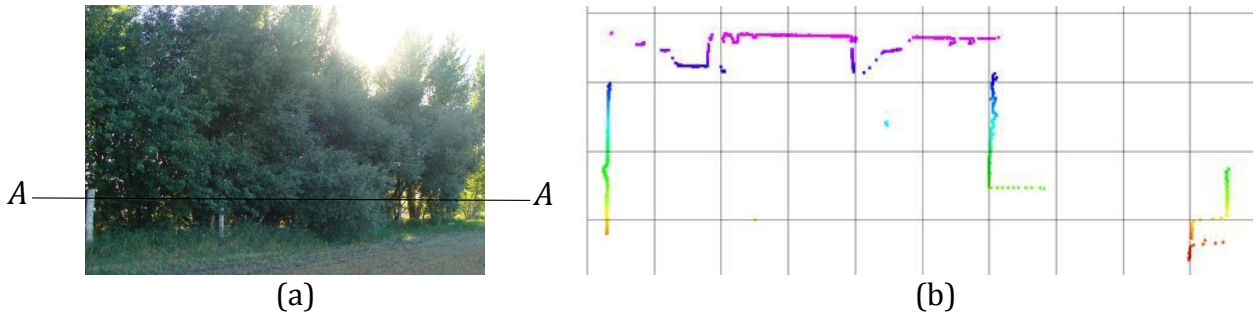


Fig. 4-12: (a) A sample scene. (b) Section A-A view of the obstacle map generated using the laser data (point cloud) for scene in (a)

3D Cartesian coordinates of laser point cloud (e. g. shown in Fig. 4-12b) are indicated by $\left(X_{i,j}, Y_{i,j}, Z_{i,j}\right)$; where *i* is for the yaw angle, and *j* is for the pitch angle of the laser beam (see Fig. 4-9). Obstacle detection algorithm is based on measured distances of the robot to obstacles. Laser point clouds are used for determination of obstacles' location in the local map of the surroundings. The terrain local map is updated from the latest laser scans. A sample raw terrain local map generated from a laser point clouds is shown in Fig. 4-13. This map was created from laser data shown in Fig. 4-12 in a farm setting. The rows of trees and uneven ground surface are visible in this figure.

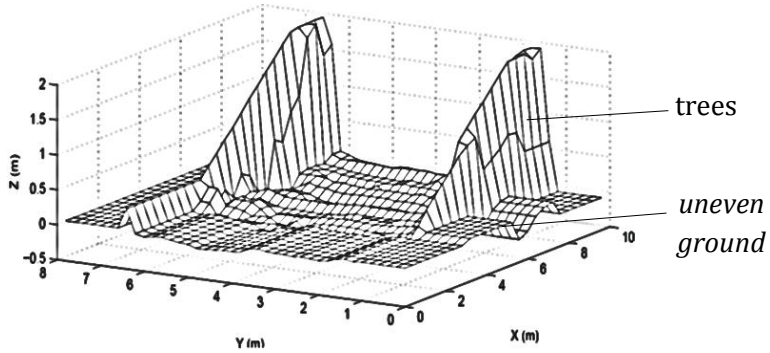


Fig. 4-13: A local map of the environment generated using laser data from Fig. 4-12

If two nearby points (e. g. (1) and (2)) whose vertical difference $\left|Z_{i,j}^{(1)} - Z_{i,j}^{(2)}\right|$ exceeds a critical vertical value *L,* (which is a threshold for detecting positive or negative obstacles) can be found in the local map, then an obstacle is identified:

$$\left| Z_{i,j}^{(1)} - Z_{i,j}^{(2)} \right| > L \tag{30}$$

The threshold value for the farm setting was chosen as L= 0.2 m.

Beside obstacle detection, traversability of the terrain is also extracted from 3D laser data. Terrain slopes and inclinations are used to divides the environment into regions that are crossable or non-crossable for the robot. The surface inclination or slope can be defined as the angle between surface normal vector $\vec{N}$ and the vector $\vec{K} = (0,0,1)$ which is perpendicular to the horizontal surface, as shown in Fig. 4-14. The slope angle is calculated using definition of dot products:

$$\zeta = \cos^{-1} \frac{\vec{N}.\vec{K}}{(|\vec{N}|)(|\vec{K}|)} \tag{31}$$

At a point *P* in 3D space, normal unit vector $n_p$ (shown in Fig. 4-15), is obtained as cross product of the vectors $P_\beta$ and $P_\gamma$, which are tangent to curves β–scan and γ–scan respectively, as follows:

$$\vec{n}_P(\beta,\gamma) = \frac{\vec{P_\gamma} \times \vec{P_\beta}}{\left|\vec{P_\gamma} \times \vec{P_\beta}\right|} \tag{32}$$

$$\vec{P_\gamma} = \begin{pmatrix} \frac{\partial x}{\partial \gamma} & \frac{\partial y}{\partial \gamma} & \frac{\partial z}{\partial \gamma} \end{pmatrix}^T \qquad \vec{P_\beta} = \begin{pmatrix} \frac{\partial x}{\partial \beta} & \frac{\partial y}{\partial \beta} & \frac{\partial z}{\partial \beta} \end{pmatrix}^T \tag{33}$$

Using image processing techniques derivative vectors $P_\beta$ and $P_\gamma$ are calculated numerically. Roughness of the terrain, *R,* with normal vector $\vec{n}_i = (n_x, n_y, n_z)_i$ can be calculated from following equation:

$$R = \sqrt{\left(\sum_{i=1}^{np}(n_x)_i\right)^2 + \left(\sum_{i=1}^{np}(n_y)_i\right)^2 + \left(\sum_{i=1}^{np}(n_z)_i\right)^2} \quad (34)$$

Where *np* is the number of points to be considered in the terrain. If the roughness, R, of the terrain exceeds a threshold value, R> 0.2m, the terrain will be considered as impassable. Therefore, in addition to obstacles such as rocks, terrain's depression, slope and unevenness are considered in this stage of navigation. In the slope analysis, a path is considered as crossable due to their low depression. Then traversable region model is built based on the sensor data in the real-time. This model represents the free space for the robot to navigate through. A sample of the traversable region modeling is shown in Fig. 4-16, where the horizontal axis is the beam yaw angle and the vertical axis is the range values (obstacles' distances to the robot). This 2D-graph is used for safe path planning. Obstacle-free paths available to the robot are depicted in dashed lines. The widths of these obstacle-free paths are determined according to the size of the AGV (also shown in Fig. 4-16). Then the robot is navigated to the goal point using these safe paths.

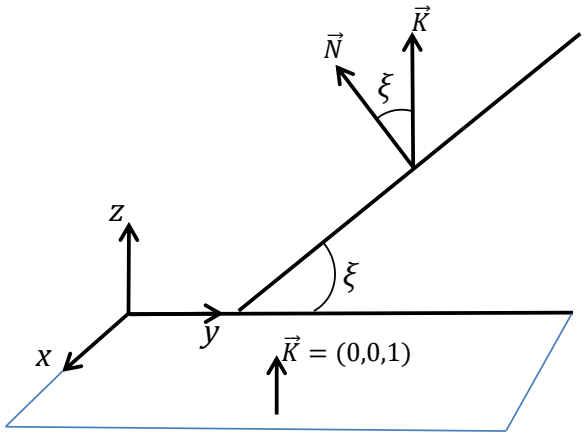


Fig. 4-14: Terrain slope definition

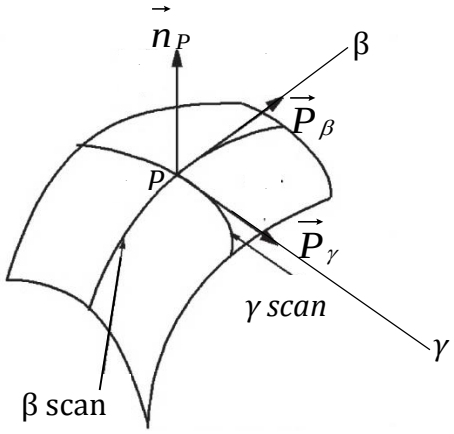

Fig. 4-15: estimating normal vector at point P

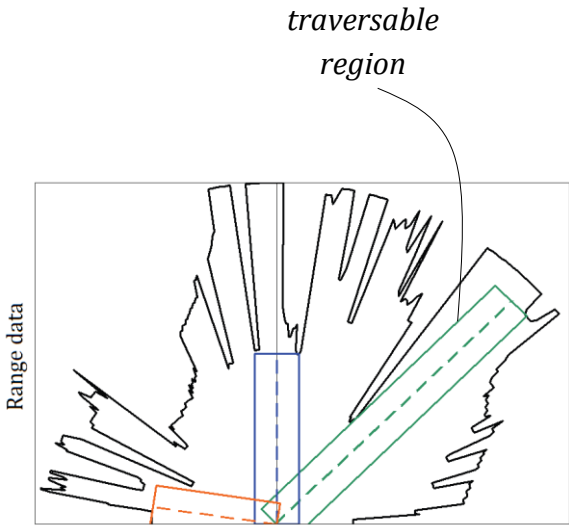

Fig. 4-16: A sample of the traversable region modeling from the laser scanner data: traversable paths are depicted in dashed lines, width of the AGV is also shown along these paths.

## 4.9. Obstacle avoidance algorithm

In the case that any obstacle is detected in *obstacle detection* module, the navigation technique invokes *obstacle avoidance* action and a collision free path is generated. Two approaches were developed for obstacle avoidance in [19]: Fuzzy Logic Based (FLB) and Human Inspired Method (HIM). These two approaches (FLB and HIM) are applied to prevent collision with obstacles and also to plan safe paths for the robot.

### 4.9.1. Fuzzy logic based (FLB)

Fuzzy logic controller has been suggested for navigation of mobile robots in some research [26, 27]. This navigation strategy is composed of sets of fuzzy-logic rule statements designed for achieving appropriate values for control parameters ($\Delta\Phi$ and $v$). The control variables of the mobile robot are the translational speed of the robot ($v$) and the change in the heading angle of the robot ($\Delta\Phi$). Inputs for the *obstacle avoidance* blocks are sensor reading information: obstacles' distances to the robot. Laser measurements in right, front and left sectors are used to determine the distances to the obstacles in each sector according to Eq. (31).

$$\begin{aligned} &\text{dR= min \{distance data reading for } -90 \le \text{angle} \le -30\} \\ &\text{dF= min \{distance data reading for } -30 \le \text{angle} \le +30\} \\ &\text{dL= min \{distance data reading for } +30 \le \text{angle} \le +90\} \end{aligned} \tag{35}$$

Where dR, dF, and dL are the distances to the objects detected by LRF in right, front, and left sectors respectively. These distances are mapped in to fuzzy membership functions {Far, Medium, Close} as shown in Fig. 4-17. Then according to the defined fuzzy rules, control outputs ($\Delta\Phi_j$ and $v_j$) for each rule are produced. The final control output $\Delta\Phi$ and v are obtained using centroid defuzzification method:

The change in the robot heading angle is represented using five linguistic fuzzy sets {NB, NS, ZE, PS, PB}; these membership functions are illustrated in Fig. 4-18. NB is negative-big, NS: negative-small, ZE: zero, PS: positive-small and PB: positive-big. The positive and negative terms mean counter-clock wise and clock wise rotation of the robot, respectively.

$$\Delta\Phi = \frac{\sum_{j=1}^{n} \alpha_j(\Phi_j).\Delta\Phi_j}{\sum_{j=1}^{n} \alpha_j(\Phi_j)} \tag{36}$$

$$v = \frac{\sum_{j=1}^{n} \alpha_j(v_j).v_j}{\sum_{j=1}^{n} \alpha_j(v_j)} \tag{37}$$

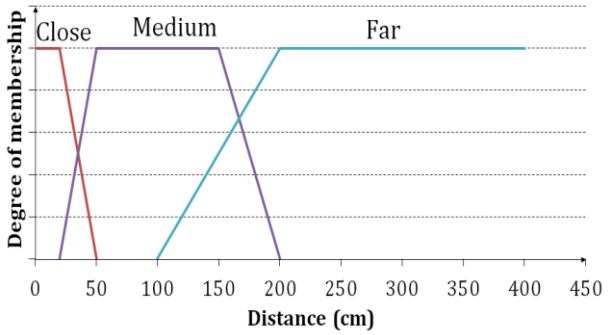


Fig. 4-17: fuzzy membership functions for measured distance

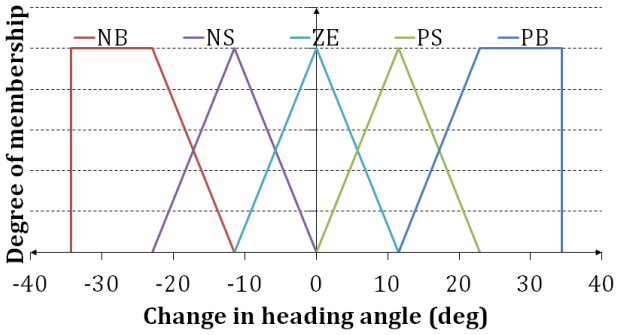


Fig. 4-18: fuzzy membership functions for change in the robot heading angle

### 4.9.2. Human inspired method (HIM)

The other method applied for *obstacle avoidance* action is HIM [19]. This method is designed to imitate a wise adult human behavior in dynamic environments to reach a goal point [20]. Laser data and data from obstacle detection state are used to find the closest traversable scape-points to the goal point. Scape-points are defined as points that are passable by the AGV according to the predefined safety factor and the actual size of the robot. HIM uses obstacles boundaries to detect the scape-points and the best collision-free path for the robot navigation. HIM finds passable ways ahead and avoids very narrow passages therefore it avoids local minima or local traps. Fig. 4-19 summarizes the basic structure of HIM.

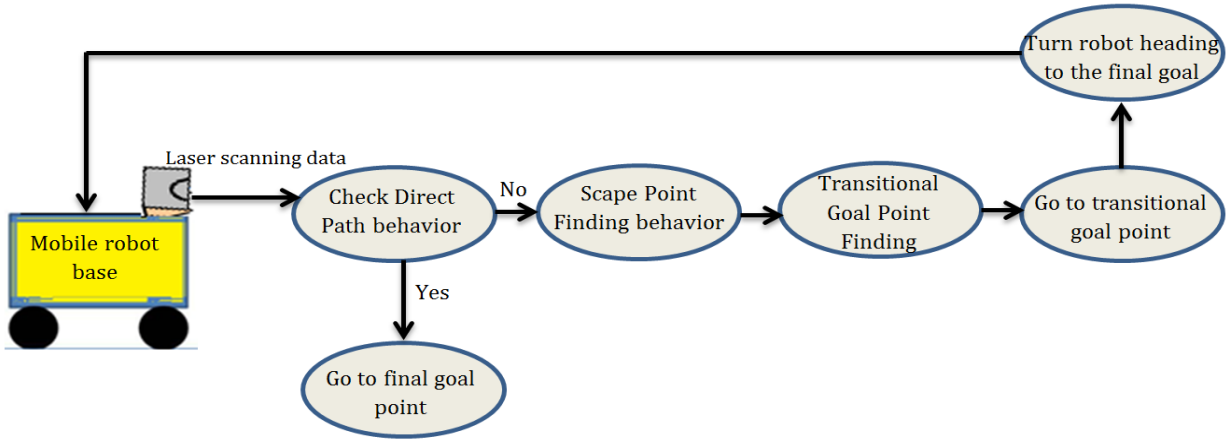


Fig. 4-19: obstacle avoidance behavior of HIM

## 4.10. Evaluation and experimental results

The proposed navigation strategy was tested on a custom-build mobile robot (the AGV) as illustrated in Fig. 4-20 in farm fields for different setups. Each test scenario was repeated at least ten times**.** Fig. 4-22 shows the robot paths for eight different setups of point-to-point motion experiments. In each experimental scenario, the results of both FLB and HIM for obstacle avoidance are depicted; in these figures, solid black lines show the paths produced by HIM and dashed lines are the routes created by FLB approach. The robot was set at a specific start point for each test, and position of the goal point and final heading of the robot were also specified. Pose of the robot during motion was recorded; and is also shown in Fig. 4-22 for eight different test setups. In each case, the robot avoided all obstacles and reached the final goal point safely and successfully. The navigation approach was tested with different obstacle densities and sizes over 100 times for both positive and negative obstacles. Both FLB and HIM navigated the AGV in almost all test situations successfully with no failure. In each case, if there was at least one feasible way for the AGV to reach its goal position, then the robot normally found the best possible route to its destination. Different actions in navigation strategy such as obstacle-detection, obstacle-avoidance and

goal-seeking behaviors were fully performed in each test and the AGV finished all tests successfully. In the experimental evaluation of the proposed navigation approach, first, path planning navigation, obstacle detection and avoidance actions for both negative and positive obstacles under different conditions were evaluated. Finally, row-detection and path following experiments were performed in farm fields. All experimental evaluations were accomplished on soft soil in farm fields. The robot average speed in most tests was 1 m/s.

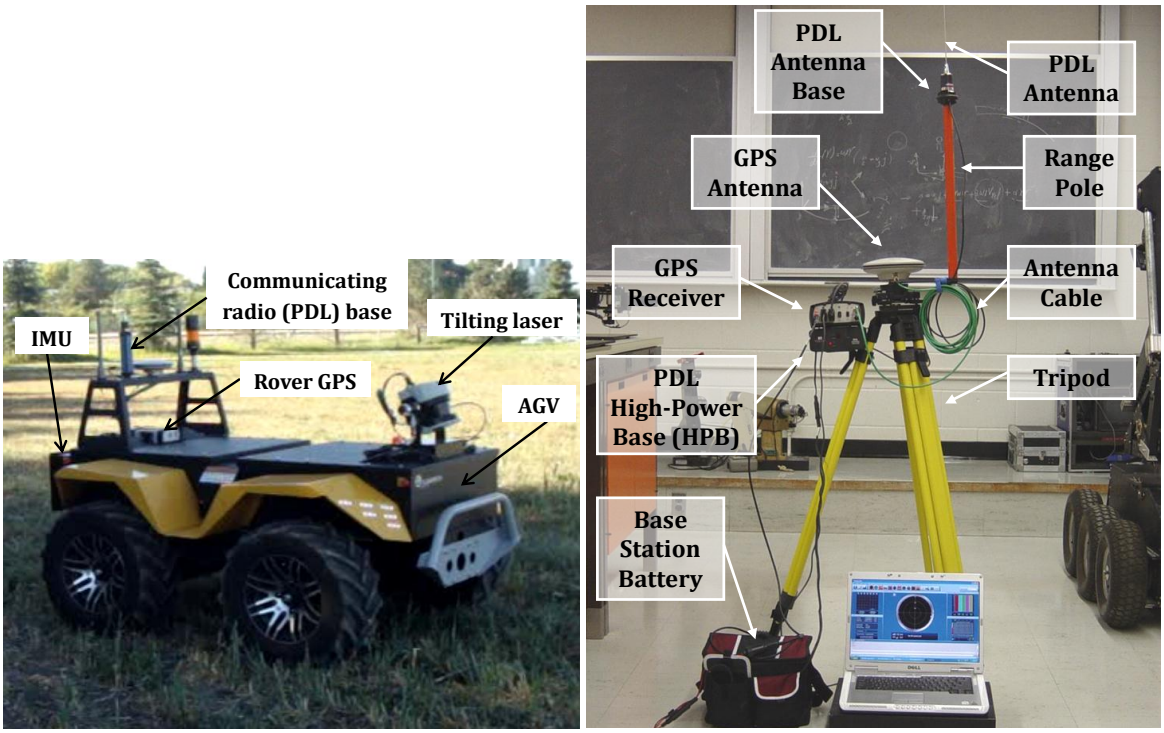

Fig. 4-20: Experimental outline: 4×4 differential drive Grizzly mobile robot (AGV), tilting laser range finder for obstacle detection and base RTK-DGPS for localization

### 4.10.1. Point-to-point motion navigation

First, the ability of the proposed navigation approach for path planning (point-to-point motion) is evaluated. In these experimental setups, the configurations of obstacles are chosen in a way that there is at least one traversable path for the robot. In each test, the

robot starts from a start point defined as (0,0,0) and reaches its user-specified goal point, while traversing a safe path and avoiding any encountered positive or negative obstacles. Figs. 4-21 and 4-23 show snapshots of the actual robot run travelling from the start point to the goal point while avoiding obstacles.


Fig. 4-21: Snapshots of the robot for a typical experiment: The robot is travelling from "start point" to the "goal point", using HIM for obstacle avoidance. Left: robot at start point, middle: robot at mid-point, right: robot at the goal point in [21]

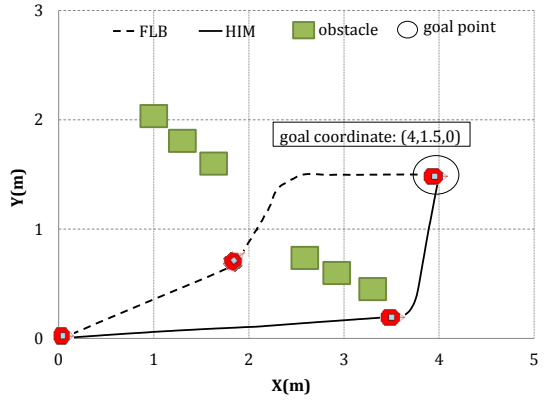


a): setup1

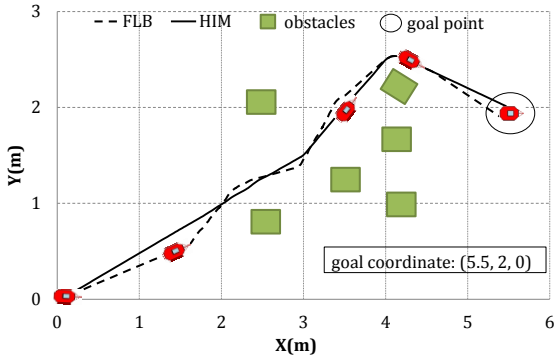


b): setup2

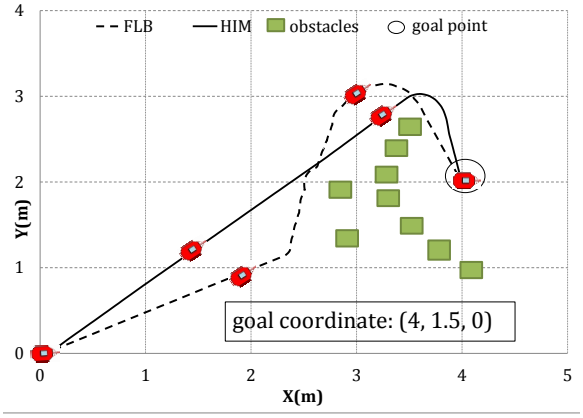


c): setup3

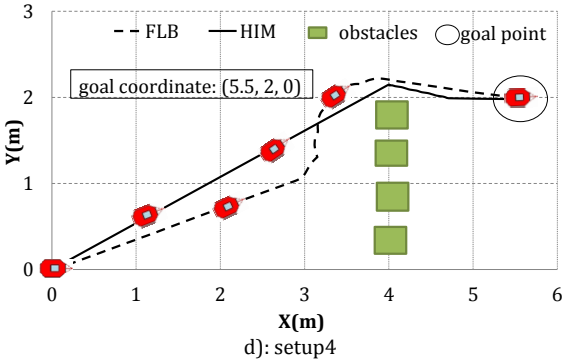


d): setup4

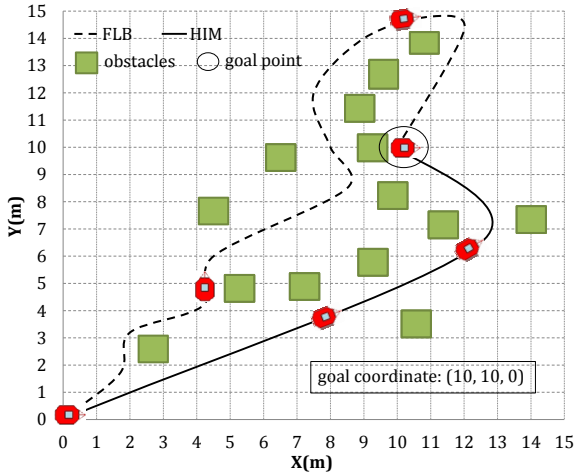


e): setup5

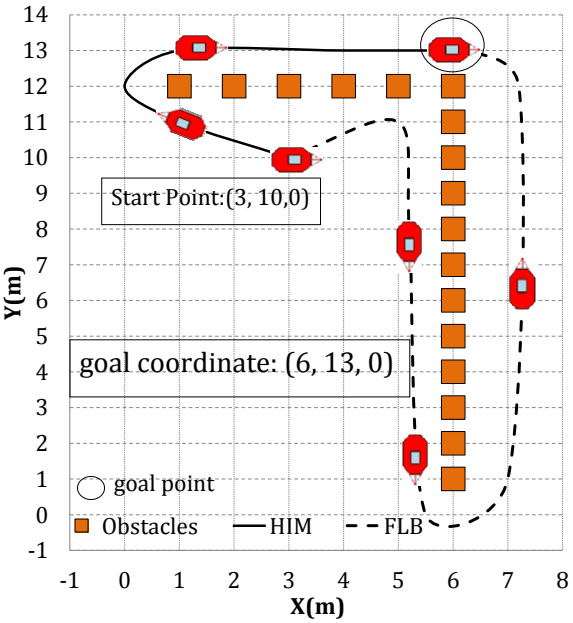


f): setup6

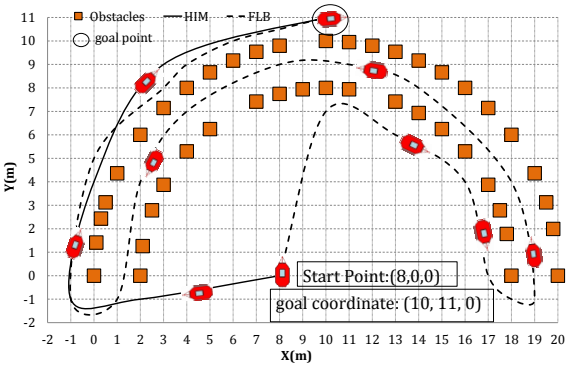


g): setup7

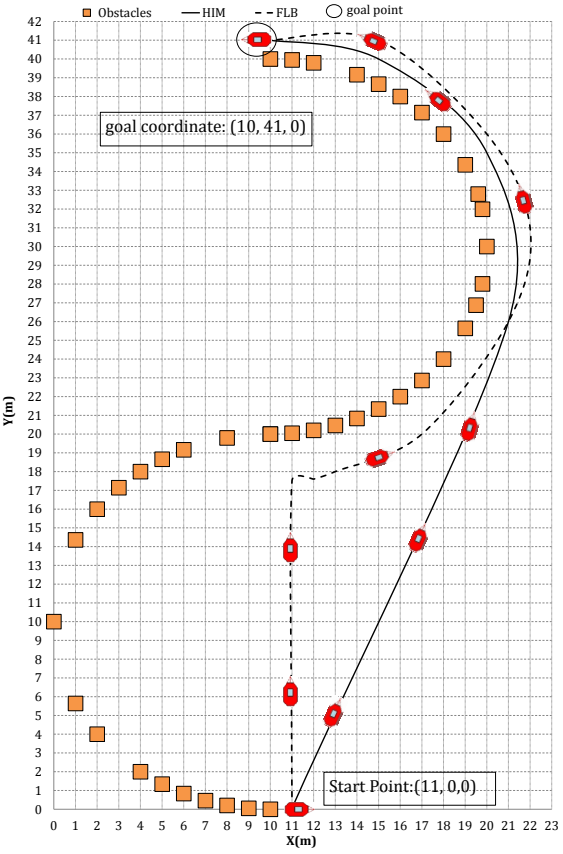


h): setup8

Fig. 4-22: Experimental results for validating navigation strategy for eight different setups (a) to (h). Solid line: robot's path using HIM, dashed line: robot's path using FLB.

Fig. 4-23: Snapshots of the robot run for experiment in setup8: The robot is traversing from start point to the goal point, using HIM for obstacle avoidance. Top-left: the robot at start point, and bottom-right: the robot at the goal. Image sequence proceeds to the right and down. [22]

The two-dimensional top view of the test results (robot path and obstacles) are depicted in Fig. 4-22. The paths of the AGV are created using data from LRF and RTK-DGPS. Both fuzzy (FLB) approach and human-inspired method (HIM) are implemented for obstacle-avoidance behavior in each scenario. Setups 1 and 3, represent simple walls of obstacles that require the robot to go between walls of obstacles and find the passable space. Setups 2 and 4 illustrate more complex situations and the ability of the robot to navigate very small gaps and reach the goal point successfully. Setup 5 shows a very crowded situation that obstacles surrounded the goal point. The robot needed to travel through small gaps and avoid all obstacles to reach the goal position. In setups 6 to 8 different shapes of obstacle walls (S-shape, L-shape and semi-circular) were constructed between the start point and the goal position; the robot needs to follow the walls and find a way around the obstacles to reach the goal.

It can be observed from Fig. 4-22 that FLB directs the robot to go straight toward the goal point until an obstacle is detected on its way; then the robot avoids the encountered obstacles. However, HIM determines the robot's path such that, the robot does not go

toward any stationary obstacles, as a human would do during navigation. If an unforeseen obstacle is detected, HIM will also change the robot's path to avoid colliding with the obstacle. This saves time and energy during the navigation. The performance of the navigation approach for path planning motion is summarized in Table 4-I; the proposed navigation method proved to be robust for point-to-point motion in outdoor settings (such as farm fields).

Table 4-II provides comparisons of HIM and FLB for eight different experimental results in point-to-point motion. The comparison is based on three criteria: 1) The energy per unit mass, consumed by the mobile robot in Joule/Kg. 2) The travelling time for the robot to reach the goal point in second (s). 3) The path length travelled by the robot to reach its goal position in meter (m). The energy per unit mass consumed by the robot is computed as follows:

Work = force × displacement =(mass × acceleration) × (velocity × time)

$$E_m\left[\frac{J}{kg}\right] = a\left[\frac{m}{s^2}\right] \times v\left[\frac{m}{s}\right] \times t[s] \tag{38}$$

The path length ($P_L$) is calculated as summation of the distance between two consecutive points in the robot's path from start point ($x_1$, $y_1$, $z_1$) to the goal position ($x_n$, $y_n$, $z_n$); where n is the number of points in path:

$$P_L = \sum_{i=1}^{n} \sqrt{(x_{i+1} - x_i)^2 + (y_{i+1} - y_i)^2 + (z_{i+1} - z_i)^2} \tag{39}$$

Table 4-II indicates that for all tests, HIM produces shorter paths for navigation of the robot and generally it takes less time for the robot to reach the goal position. This means computation time and decision making time for HIM is smaller than FLB. In addition, the

energy per unit mass for HIM is less than FLB for most of the setups; which means HIM is more energy efficient compared with FLB.

Table 4-I: summary of the path-planning navigation (point-to-point motion) experimental results in a farm field. Robot navigation was tested for eight different setups.

| Tests | Number of trials per setup | Failed tests | Success rate (%) |
|---|---|---|---|
| **Setups 1 to 7** | 10 | 0 | 100 |
| **Setup8** | 8 | 0 | 100 |

Table 4-II: Comparison of HIM and FLB in experiments

| Tests | Criterion for comparison | FLB | HIM |
|---|---|---|---|
| **setup1** | Start point (x, y) (m) | (0,0,0) | (0,0,0) |
| | Goal point (x, y) (m) | (4,1.5,0) | (4,1.5,0) |
| | Energy index (J/kg) | 1500 | 1200 |
| | Travelling time (s) | 71.20 | 61.00 |
| | Path length(m) | 4.500 | 4.235 |
| **Setup2** | Start point (x, y) (m) | (0,0,0) | (0,0,0) |
| | Goal point (x, y) (m) | (5.5,2,0) | (5.5,2,0) |
| | Energy index (J/kg) | 1826 | 1082 |
| | Travelling time (s) | 80.2 | 55.50 |
| | Path length(m) | 6.357 | 6.010 |
| **Setup3** | Start point (x, y) (m) | (0,0,0) | (0,0,0) |
| | Goal point (x, y) (m) | (4,2,0) | (4,2,0) |
| | Energy index (J/kg) | 1473 | 856.0 |
| | Travelling time (s) | 75.71 | 38.38 |
| | Path length(m) | 6.621 | 5.963 |
| **Setup4** | Start point (x, y) (m) | (0,0,0) | (0,0,0) |
| | Goal point (x, y) (m) | (5.5,2,0) | (5.5,2,0) |
| | Energy index (J/kg) | 1120 | 904.0 |

| | | | |
|---|---|---|---|
| | Travelling time (s) | 57.65 | 49.42 |
| | Path length(m) | 6.539 | 5.842 |
| **Setup5** | Start point (x, y) (m) | (0,0,0) | (0,0,0) |
| | Goal point (x, y) (m) | (10,10,0) | (10,10,0) |
| | Energy index (J/kg) | 2800 | 2009 |
| | Travelling time (s) | 200.1 | 101.1 |
| | Path length(m) | 15.22 | 11.86 |
| **Setup6** | Start point (x, y) (m) | (3,10,0) | (3,10,0) |
| | Goal point (x, y) (m) | (6,13,0) | (6,13,0) |
| | Energy index (J/kg) | 1512 | 851.2 |
| | Travelling time (s) | 100.0 | 45.12 |
| | Path length(m) | 20.11 | 10.86 |
| **Setup7** | Start point (x, y) (m) | (8,0,0) | (8,0,0) |
| | Goal point (x, y) (m) | (10,11,0) | (10,11,0) |
| | Energy index (J/kg) | 1500 | 1019 |
| | Travelling time (s) | 248.7 | 65.46 |
| | Path length(m) | 60.22 | 15.20 |
| **Setup8** | Start point (x, y) (m) | (11,0,0) | (11,0,0) |
| | Goal point (x, y) (m) | (10,41,0) | (10,41,0) |
| | Energy index (J/kg) | 4512 | 3501 |
| | Travelling time (s) | 300.0 | 255.1 |
| | Path length(m) | 57.11 | 46.86 |

### 4.10.2. Row-detection and path following

This section documents the performance of the navigation strategy to detect plant rows and follow them. These scenarios contain different shapes of rows on hilly and uneven grounds. This strategy can be used for spraying rows of bushes and/or trees in a farm setting. Fig. 4-24 shows a snapshot from the actual robot run in the row-detection and path following. In one case, three rows of pylons were set; the length of each path was 8m thus

the total length of the path that the robot traversed was 24m. Hough transform algorithm was used to detect the lines passing through the rows. Then the robot followed the detected rows. The novelty of this *row-detection* algorithm is that this state is able to detect the end of the rows and directs the robot to turn around at the end of row and go to the next row. Long gaps in detected lines were considered as signal for end of rows and were defined as potential end-points. These gaps are analyzed more specifically to identify exact end-points. Then the robot is guided to the next row. Fig. 4-25 shows the desired and actual paths for the robot in a typical row-detection and path following test performed.

For path following tests, positions and heading angles of the robot, as explained in detail in Section 4, are controlled. At each time, control commands, which are the linear velocities of the right and left wheels of the robot ($v_r$, $v_l$), are sent to the program. The performances of the path following tests are represented in terms of errors indices (e, θ) which are given in Eq. (13).

Figures 26– 31 illustrate the performance of the navigation approach in path following tests; the desired and actual paths of the robot in row-following test for scenarios 1 to 5 are depicted in these figures. Error indices (e, θ) for these scenarios are also depicted in these figures. These results show that the distance error index, *e*, is less than 0.1 m for all cases. Further, it is important to mention that all error indices almost converge to zero, which means that the robot followed the reference paths reasonably accurate. These results verify that the row-detection and row-following algorithms perform efficiently in the farm fields. Hence, the robustness of the proposed method under different conditions is demonstrated.

In scenario 5, as depicted in Fig. 4-30, the terrain contains a highly sloped hill; this scenario shows the ability of the navigation system to handle situations on hilly and rough terrains. Figure 30 displays a set of snapshots obtained from the actual robot run on hills, and Fig. 4-31 shows the desired and actual paths of the robot. The error terms (e, θ) obtained from the system response are shown in Fig. 4-31 (b) and (c); it is shown that error indices go to zero eventually, which means that AGV is following the desired path.

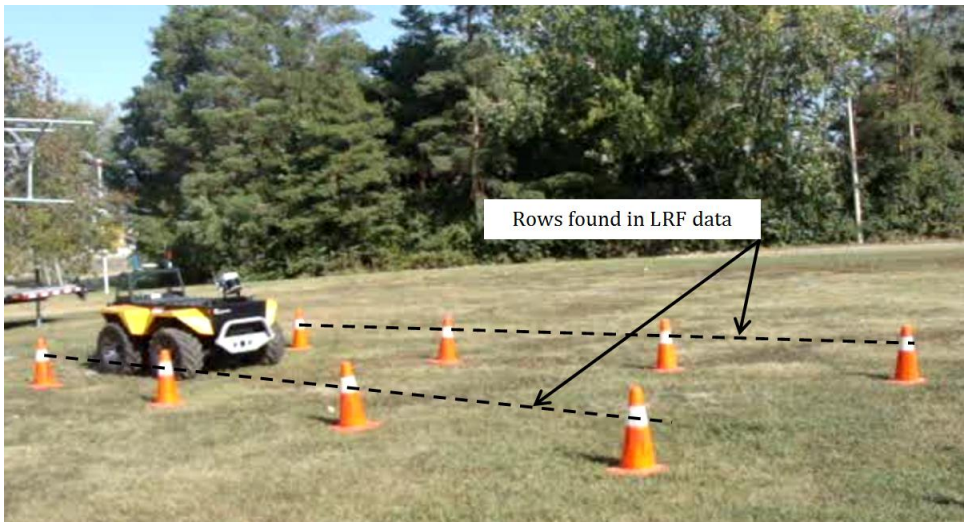


Fig. 4-24: Lines corresponding to the rows detected by the navigation method using Hough transform in [22]

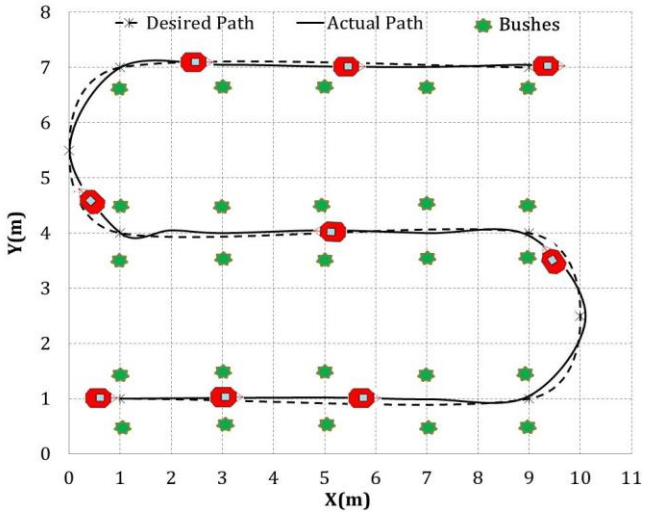


Fig. 4-25: A typical experimental result for row-detection and path following scenario: desired and actual paths of the robot are depicted by dashed line and solid line; bushes are shown by stars.

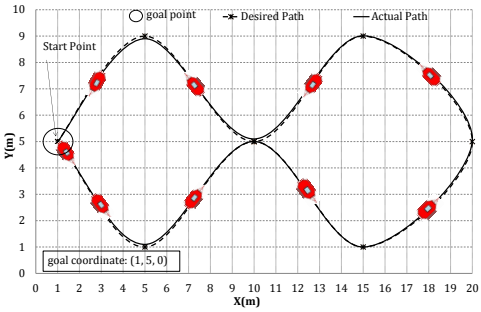


(a) Desired and actual paths of the robot

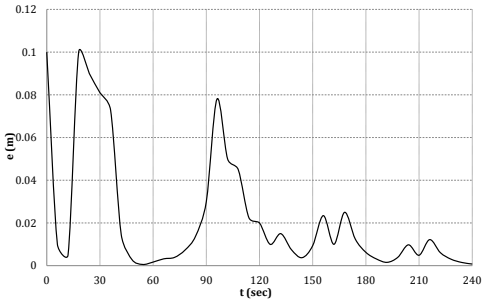


(b) Position error

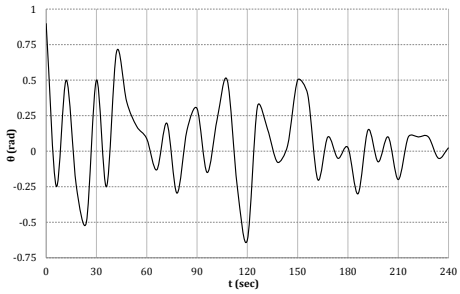


(c) Heading angle error

Fig. 4-26: Experimental results obtained for scenario 1 (path following test)

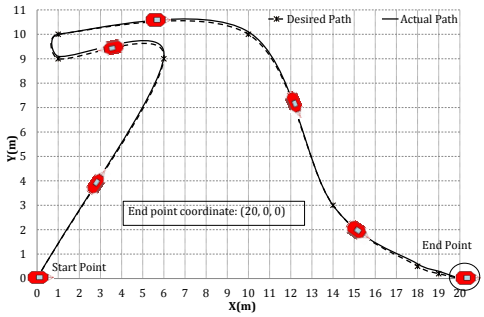


(a) Desired and actual paths of the robot

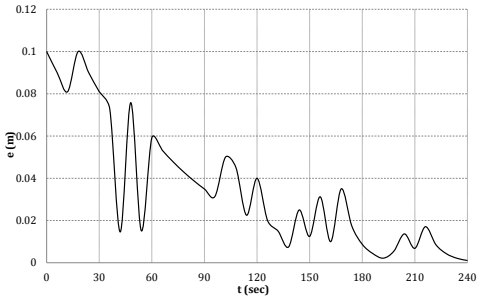


(b) Position error

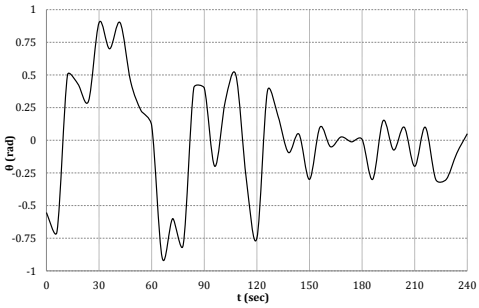


(c) Heading angle error

Fig. 4-27: Experimental results obtained for scenario 2 (path following test)

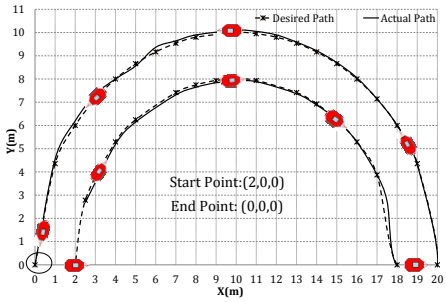


(a) Desired and actual paths of the robot

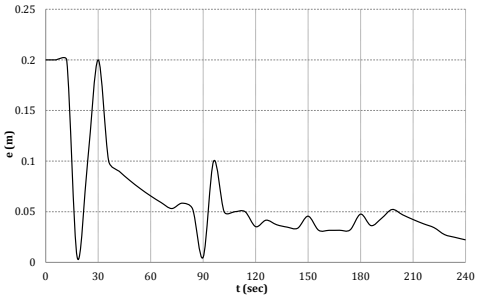


(b) Position error

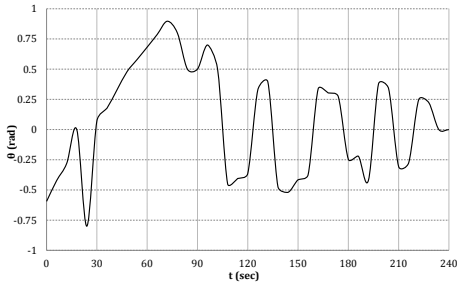


(c) Heading angle error

Fig. 4-28: Experimental results obtained for scenario 3 (path following test)

Table 4-III provides summary of experimental results in path following tests. The maximum, minimum, and average of the error (e, θ) for all five scenarios are calculated in this table.

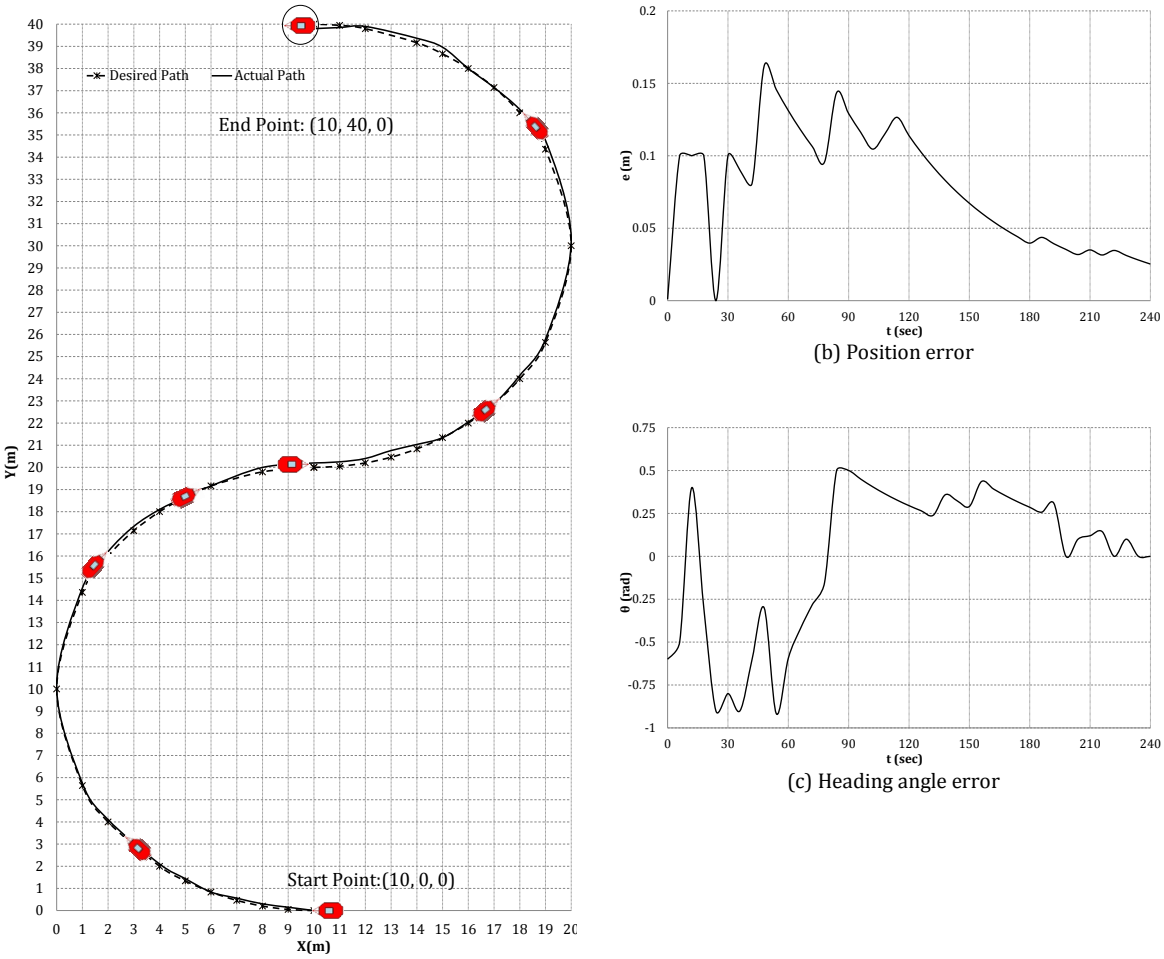


(a) Desired and actual paths of the robot

(b) Position error

(c) Heading angle error

Fig. 4-29: Experimental results obtained for scenario 4 (path following test)

Fig. 4-30: Snapshots of the robot following a path on a hill in [21]. Top-left: the robot at start point, and bottom-right: the robot at the end-point. Image sequence proceeds to the right and down.

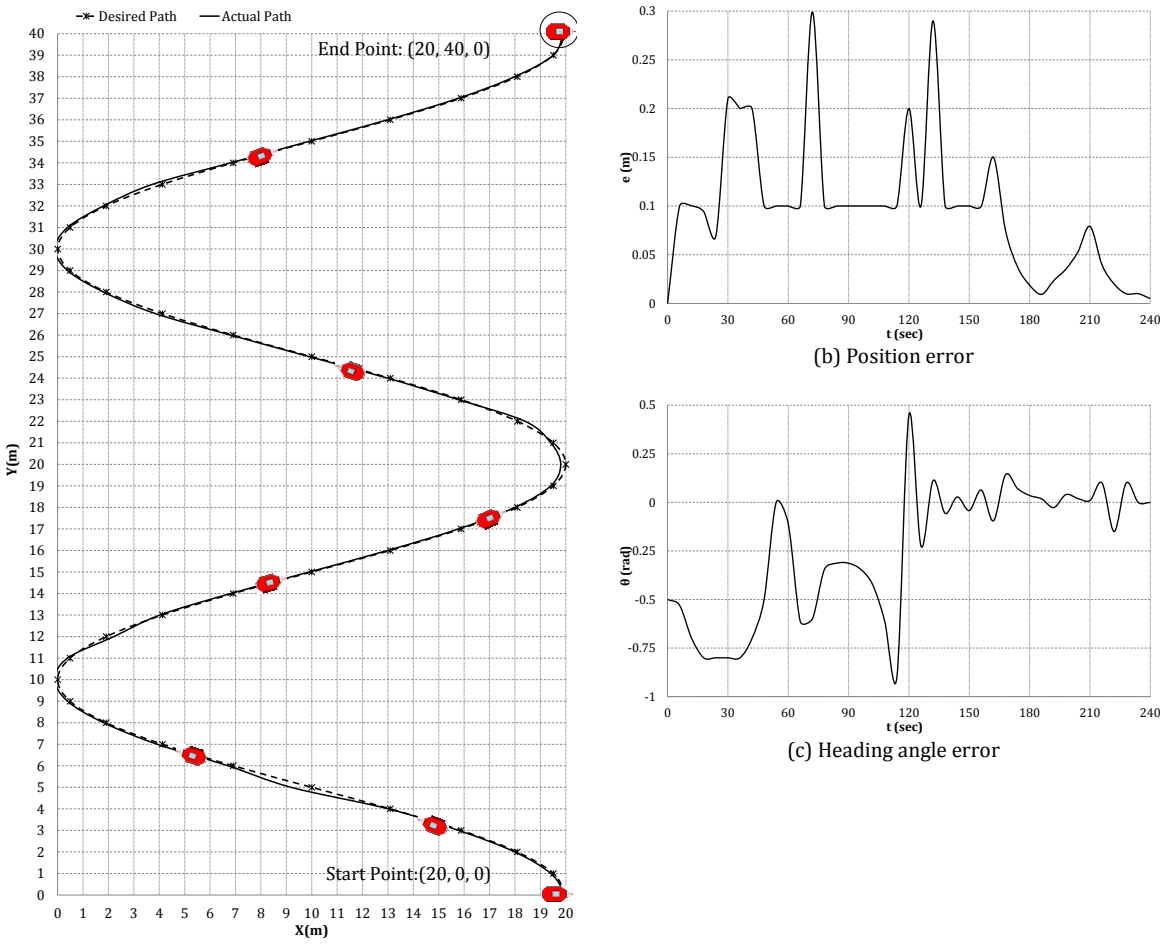


(a) Desired and actual paths of the robot

(b) Position error

(c) Heading angle error

Fig. 4-31: Experimental results obtained for scenario 5 (path following test)

Table 4-III: summary of the path following navigation experimental results in a farm field. Maximum, minimum and average of the errors (e, θ) are presented.

| **Path following tests** | **error: e (m)** | | | **error: θ (rad)** | | |
|---|---|---|---|---|---|---|
| | **max** | **min** | **average** | **max** | **min** | **average** |
| **Scenario 1** | 1.00 | 0.00 | 0.21 | 0.90 | -0.62 | 0.07 |
| **Scenario 2** | 1.00 | 0.00 | 0.34 | 0.90 | -0.90 | 0.01 |
| **Scenario 3** | 2.00 | 0.05 | 0.6 | 0.89 | -0.80 | 0.08 |
| **Scenario 4** | 1.62 | 0.00 | 0.76 | 0.50 | -0.91 | 0.00 |
| **Scenario 5** | 2.99 | 0.00 | 0.93 | 0.45 | -0.90 | -0.24 |

### 4.10.3. Obstacle detection and avoidance

Negative obstacles such as holes, gaps and ground depression are inherent parts of off-road terrains and farm fields. Therefore the performance of the proposed navigation strategy was tested in cases with negative obstacles. This scenario contained both positive and negative obstacles. Negative obstacle was a hole with depth and diameter of 50cm on the ground. The results of this experiment are shown in Fig. 4-33. Fig. 4-32 shows a set of snapshots obtained from the actual robot run; and in Fig. 4-33 the desired and actual paths of the robot while avoiding both positive and negative obstacles are depicted. The robustness of the proposed navigation module in hole-detection and avoidance are proved experimentally.

Fig. 4-32: Snapshots of the robot following a path while avoiding obstacles in [22]

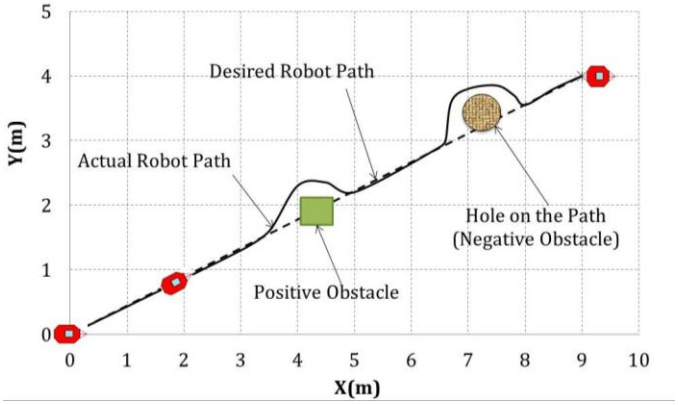


Fig. 4-33: Experimental results for path following scenario in the presence of both positive and negative obstacles on the way of the robot. The size of positive obstacle was 50×50×40 cm (length× width× height) and the hole depth and diameter was 50 cm.

## 4.11. Conclusion and future work

In this paper, we presented a navigation strategy which is composed of different actions for coping with diverse situations; sensors data processing, environment mapping, obstacle detection, obstacle avoidance, and goal seeking are the main behaviors in the navigation strategy. All of these behaviors are evaluated in different scenarios for point-to-point motion, path following, row-detection, and row-following. A tilting laser range finder was used for row-detection and following and also for obstacle avoidance. One major advantage of the proposed strategy over existing methods is that negative obstacles (such as holes, ditches and ground depressions) which are inherent part of off-road terrains, are detected and avoided in real-time. It was demonstrated that the algorithms presented in this paper analyze 3D laser data and detect both positive and negative obstacles accurately for high-speed navigation of a wheeled mobile robot in outdoor (such as farm settings). The other novelty of the suggested navigation strategy is that in row-detection approach, the end of the rows of trees can be identified. Therefore the proposed algorithm is capable of autonomously traversing entire farm for spraying, mowing and seeding which results in increasing efficiency with no need of having prior information about the setting. By adjusting vertical angular resolution of the laser, the obstacle detection algorithm was improved to detect negative obstacles at long ranges continuously. The proposed strategy was experimentally evaluated in different settings. The navigation method was validated in eight different setups for point-to-point motion control successfully. Six different paths (S-shape, curvy, etc.) were tested to evaluate the proposed path following strategy. In all of these experiments, the displacement error, $e$, was less than 0.2 m; the error in heading angle of the robot, $\theta$, approached to zero as well.

Future work will involve development of the navigation approach for proximity-following actions. This will be used for sparing rows of bushes and crops in farm fields. In addition, the proposed strategy is going to be applied for rut detection and rut following algorithms. Finally, we would like to expand the application of the proposed navigation strategy for towing and plowing tasks in a farm setting. It is planned to develop the current system to consider effect of interaction forces of ground engagement tools for seeding on robot navigation as well.

## References


1- F. Bonin, A. Ortiz, G. Oliver, "Visual Navigation for Mobile Robots: A Survey" Journal of Intelligent and Robotic Systems: Theory and Applications, v 53, n 3, p 263-296, November 2008

2- G., R. Belforte, P. Deboli, P. Piccarolo, "Robot design and testing for greenhouse applications" Biosystems Engineering, v 95, n 3, pp. 309-321, 2006

3- Y. Kobayashi, E. Kurita, M. Gouko, "Integration of multiple sensor spaces with limited sensing range and redundancy" International Journal of Robotics and Automation, v 28, n 1, p 31-41, 2013.

4- D. Nguyen, L. Kuhnert, K. Kuhnert, "General vegetation detection using an integrated vision system" International Journal of Robotics and Automation, v 28, n 2, p 170-179, 2013.

5- L. Su, C. Luo, F. Zhu, "Obtaining obstacle information by an omnidirectional stereo vision system" International Journal of Robotics and Automation, v 24, n 3, p 222-7, 2009.

6- R. Sim, P. Elinas, M. Griffin, A. Shyr, J.J. Little, "Design and analysis of a framework for realtime vision-Based SLAM using Rao-Blackwellised particle filters". In: Proc. of the 3rd Canadian Conference on Computer and Robotic Vision, 2006

7- R. Sim, J.J. Little, "Autonomous vision-based exploration and mapping using hybrid maps and Rao-Blackwellised particle filters", In: Proc. of IEEE Int'l Conf. on Intelligent Robots and Systems (IROS), 2006

8- R. Manduchi, A. Castano, A. Talukder, L. Matthies, "Obstacle detection and terrain classification for autonomous off-road navigation" Autonomous Robots, v 18, n 1, p 81-102, Jan. 2005

9- S. Boris, E. Lin, J. Bagnell,J. Cole, N. Vandapel, A. Stentz "Improving robot navigation through self-supervised online learning" Journal of Field Robotics, v 23, n 11-12, p 1059-1075, November 2006

10- C. A. Wellington, Courville, A. Stentz, "A Generative Model of Terrain for Autonomous Navigation in Vegetation" International Journal of Robotics Research. v 25, n 12, p 1287-1304, 2006

11- B. Hamner, S. Singh, S. Roth, T. Takahashi, "An efficient system for combined route traversal and collision avoidance" Autonomous Robots. v 24, n 4, p 365-385, 2008

12- T. Peynot, J. Underwood, S. Scheding, "Towards reliable perception for unmanned ground vehicles in challenging conditions" In Proceedings of the

2009 IEEE/RSJ International Conference on Intelligent Robots and Systems. 1170-1176, 2009

13- C. Ordonez, O.Y. Chuy, E.G. Collins, L. Xiuwen, "Laser-Based Rut Detection and Following System for Autonomous Ground Vehicles", Journal of Field Robotics 28(2), 158–179, April 2011

14- A. M. Zou, Z. G. Hou, S. Y. Fu, M. Tan "Neural Networks for Mobile Robot Navigation: A Survey" Advances in Neural Networks-ISNN 2006. Third International Symposium on Neural Networks. Proceedings (Lecture Notes in Computer Science Vol.3972), p 1218-26, 2006

15- G. Witus, R. Karlsen, D. Gorsich, G. Gerhart, "Preliminary investigation into the use of stereo illumination to enhance mobile robot terrain perception" Proceedings of the SPIE, the International Society for Optical Engineering, v 4364, p 290-301, 2001

16- L. Matthies, "Negative obstacle detection by thermal signature," Proceedings IEEE/RSJ International Conference on Intelligent Robots and Systems (IROS 2003) (Cat. No.03CH37453), p 906-13 vol.1, 2003

17- T. Fukao, H. Nakagawa, N. Adachi, "Adaptive tracking control of a nonholonomic mobile robot", IEEE Transactions on Robotics and Automation, v 16, n 5, p 609-15, Oct. 2000

18- F. Fahimi, Autonomous Robots Modeling, Path Planning, and Control. Springer Science+Business Media, LLC, 233 Spring Street, New York, NY 10013, USA: Springer, 2009

19- F. Heidari, R. Fotouhi, and M. Vakil, "Two New Approaches for Navigation of Wheeled Mobile Robots", ASME Journal of Mechanisms and Robotics, 2013, in 2nd review

20- V. Payne, L. Isaacs, Human Motor Development: A Lifespan Approach, 8th edition, McGraw-Hill, 2012

21- CNH farm field north of Saskatoon, Saskatchewan, Canada.

22- Campus farm field, University of Saskatchewan, Saskatchewan, Canada.

23- O. Barawid, A. Mizushima, K. Ishii, N. Noguchi, "Development of an Autonomous Navigation System using a Two-dimensional Laser Scanner in an Orchard Application", Biosystems Engineering, v 96, n 2, p 139-149, 2007.

24- K. Youngshik, M.A. Minor, "Path manifold-based kinematic control of wheeled mobile robots considering physical constraints" International Journal of Robotics Research, v 26, n 9, p 955-75, 2007.

25- D.M. Flickinger, M.A. Minor, "Remote low frequency state feedback kinematic motion control for mobile robot trajectory tracking" IEEE International Conference on Robotics and Automation, 6 pp., 2007.

26- M. Amoozgar, H. Sadati, K. Alipour, “Trajectory tracking of wheeled mobile robots using a kinematical fuzzy controller” International Journal of Robotics and Automation, v 27, n 1, p 49-59, 2012.

27- T. Suo, S. Yang, Z. Anmin, “A novel ga-based fuzzy controller for mobile robots in dynamic environments with moving obstacles” International Journal of Robotics and Automation, v 26, n 2, p 212-28, 2011.

28- T. Torii, “Research in autonomous agriculture vehicles in Japan” Computers and electronics in agriculture, v 25, n(1-2),pp. 133-153, 2000

29- B. Astrand, A. Baerveldt, “A vision based row-following system for agricultural field machinery” Mechatronics. v 15, n 2, p 251-269, 2005

30- B. Hamner, S. Singh, M. Bergerman, “Improving orchard efficiency with autonomous utility vehicles” American Society of Agricultural and Biological Engineers Annual International Meeting, v 6, p 4670-4685, 2010

# Chapter 5: A New 3D Laser-Based Method for Proximity-Following in Orchard Rows

The content of this chapter is under review for publication in Journal of Robotica, 2013:

**Heidari F.**, Fotouhi R., Bitner D., "A new 3D laser-based method for proximity-following in orchard rows", submitted to Journal of Robotica, **2013**.

## Abstract

This article presents an original strategy for autonomous navigation of a mobile robot in farm fields to perform precision farming. The proposed navigation approach in this paper involves a novel method for recognition and following of rows of crops. The introduced approach generates piecewise smooth path for the mobile robot to follow in a farm field. This technique is applicable for different shape and size of rows of bushes and is able to detect and identify two or more rows, simultaneously. The accuracy of the proposed method is verified using field experiments, such as proximity-following and rut following tests. The other originality of this research is introducing a new technique for real-time detecting and avoiding negative obstacles such as holes, ground depressions and ditches in off-road terrains. The presented algorithm analyzes the terrain using data generated by a 3D-laser range finder (LRF) to perceive the environment and utilizes a geometry-based tactic to detect both positive (over ground) and negative (below ground level) obstacles in real-time at a safe distance from the robot. The navigation system is implemented on a 4x4 differential drive autonomous ground vehicle (AGV) in a variety of field setups. The experimental evaluation showed the accuracy and robustness of the proposed system in rut detection and tracking, proximity-following, and negative obstacle detection and avoidance tests.

**Keywords:** Negative obstacle avoidance, Path planning, Trajectory tracking control, Row detection.

## 5.1. Introduction

Although considerable progress has been made on autonomous navigation of mobile robots in unstructured and off-road terrains, up to now, there are still several open problems remaining unsolved for implementations as well. In particular, existing navigation methods generally do not adapt to different types of environment such as farm fields and may not be reliable for these situations. Moreover, many existing approaches are limited to near-field sensing and consequently show myopic performance [1]. Since agricultural fields are very complex and mostly unknown, navigation of robots involve difficulties such as: operation of the robot in continuously changing tracks, targets which are difficult to detect and reach. Therefore to design an autonomous navigation system for agricultural machines that can robustly operate in all conditions is really difficult. In outdoor settings there are no regular landmarks or features that can be tracked for navigation. Hence, the robot explores the vicinity and moves toward a goal position while avoiding any encountered moving or stationary obstacles. In these cases, two kinds of methods can be used: Map-based or Map-Less Navigation Techniques.

Most of the developed methods for robot navigation in orchards were map-based techniques wherein the autonomous vehicle may only be used in some specific orchard sites. Map-based navigation techniques explore the environment and automatically build a metric or topological map, thus they need certain information from the environment. Examples of this system can be found in [2, 3, 4]; they used a stereo camera, and a single axis lidar for obtaining information from the terrain. Color-based technique was used for analysis of camera data and terrain classification to distinguish between grass and ground. In [5], authors introduced an online, probabilistic model to use settings' features by taking

advantage of other features. Their approach was self-supervised learning method that extracted color features and predicted traversal costs over large areas from overhead camera data. Performance of the color-based terrain detection deeply depends on environment light and grass color which vary with seasons and day or night time. Also, these techniques have short-range view; to improve short-range view of sensors for robot navigation, [1] presented an adaptable path planning strategy that used look-ahead sensing of possible obstacle configurations. This navigation strategy was based on a "what-if" analysis of hypothetical future configurations of the environment. Hough transform algorithm combined with vision-based method was used for crop row detection in farm field by [6]. An enhanced topological map fused with sensors' data such as wheel odometer, global positioning system (GPS), and mono-camera was presented in [7]. A stereovision based crop row detection method for navigation of an autonomous ground vehicle (AGV) was described in [8]; stereo-image processing, elevation map creation and navigation point determination for crop row detection were different functions of the presented algorithm. Applying map-based navigation approaches in a farm field requires path planning before the vehicle can perform its tasks. The navigation phase starts only if the map of the environment has been built. This task of surveying and map generation is time consuming for the farmer and requires expensive computational resources and storage capacity.

The other type of robot navigation technique, map-less, does not need prior knowledge of the setting. The movements of the robot depend only on sensory data as it perceives them. Vision-based navigation methods have been used for map-less techniques. Two main methods were developed for vision-based navigation approaches: optical-flow-based and appearance-based. Optical-flow-based methods estimate the motion of objects or features

within a sequence of data. Appearance-based techniques are based on the storage of images in previous recording phase. These images are used as templates. The robot self-localizes and navigates in the environment by matching the current viewed frame with the stored templates. Talukder et al. [9] applied an optical flow-based technique to detect moving obstacles within the camera field of view. The procedure assumed that moving objects caused a discontinuity in optical flow orientation and magnitude with respect to the background pixels. Talukder et al. [10] enhanced the approach in [9] by combining the stereo disparity field and optical flow to estimate depth, to model the robot motion and to detect moving obstacles in the scene. In [11], stereo data were combined with the optical flow from one of the stereo images, to build an occupancy grid and perform a real-time navigation technique. Another example of the appearance-based techniques is proposed in [12]; authors presented a color-based image segmentation approach for object detection, and grayscale image processing for detecting the opponent robots. The fuzzy logic concept was combined with visual navigation approaches by several authors. One example of these techniques is [13].

A developed method to detect weed using machine vision and geometrical measurements such as shape factor, aspect ratio, and length is presented in [14]. Color based image processing was successfully used to detect weeds [15, 16, 17]. Real-time differential images obtained from a set of three digital cameras were used to detect small weed in different crops. Later, [18] developed a vision based approach for differential spraying of farm fields; their method determined the quantity and distribution of weeds in the row of crop and decided, based on information from images, whether to undertake selective spraying to control the weeds. The main problems of appearance-based strategies are finding an

appropriate algorithm to create the environment representation and defining the on-line matching criteria. Also, extraction of qualitative information and feature detection from sequences of images may be a time consuming process that causes these approaches to fail. Most of the developed techniques for precision agriculture use machine vision sensors for navigation [18]. Therefore one issue which affects the robustness of these approaches is ambient light conditions that vary a great deal in outdoors.

The goal of this research is to present a new approach for robust recognition of plant rows based on the modified Hough transform. The novelty of the paper is in proposing a new curve fitting technique for row detection and following. The proposed method generates piecewise smooth path for the robot to follow and it does not have the shortages of Hough transform in line recognition. To demonstrate the capabilities of the suggested method in row detection and row following, it was evaluated in different test situations in farm fields. Another contribution of this paper is to use a 3D lidar for row detection and following in farm fields. This paper is organized as follows: Section 2 contains the research components. In Section 3, the proposed approach is described in detail. In Section 4, the trajectory tracking control of the robot is presented. Section 5 introduces the negative obstacle detection approach. The experimental setups and results from different tests are reported in Section 6. And finally, in Section 7 conclusion and discussion of future works are presented.

## 5.2. Test robot

In this research a four wheeled autonomous ground vehicle (AGV) is used for tests and evaluation of the proposed navigation strategy. The AGV is a 16.5 KW robot (shown in Fig.

5-10) with size: 1.8 × 1.3× 1.0 m (length× width× height). It is equipped with a nodding 3D laser range finder (LRF), mounted on the front of the robot. The LRF has a 180° horizontal sweep plane and is mounted on a tilting unit which sweeps vertically from +45° to -45° providing 3D field of view for navigation. Real-time kinematics differential global positioning system (RTK-DGPS) and an inertial measurement unit (IMU) are also installed on the vehicle for 6DOF localization designed for outdoor environment. The robot can travel up to a speed of 4.4 m/s. The robot's size is ideal for farm tasks and it has a trailer hitch which allows towing ground engagement tools. Therefore this robot can be used for different farm applications such as seeding, spraying and plowing.

## 5.3. The proposed approach for path following algorithm

Existing algorithms for row detection were not found to be sufficient for application in farm fields due to following reasons: (1) Most of these techniques are vision-based and their performance deeply depends on environment light and grass color which vary with seasons and day or night time. (2) Using Hough transform for image data or even 3D laser data has two main drawbacks: large memory requirement and slowness. (3) Another weakness of the Hough transform algorithm is that it often recognizes many similar lines instead of the main one. Then the algorithm returns a lot of lines without starting and ending points. Hence, current methods cannot produce a smooth and robust continuous path for the robot to follow in farm field for doing its task such as spraying or weed control. Therefore a new row detection algorithm was developed to use 3D laser to detect rows of plants. A curve fitting technique is applied to Hough transform results to produce robust piecewise smooth paths for the robot to follow in farm fields.

### 5.3.1. Hough transform for line recognition

In this paper, for detecting rows of trees in a farm field, data from the laser range finder were used. The algorithm developed here, for row detection is Hough transform, which was originally patented by Hough [23]. This approach is a curve fitting technique to a group of data points. It is used for line or any circular shape detection. Since in farm field, rows of trees may not be exactly in one line therefore using a Hough transform is a superior method compared with alternative approaches such as least-squared for curve fitting of laser data. Hough transform is used here to generate a path (equation of a line) for the robot to follow. The data detected by LRF produce equation of a line using Hough transform. The approach is briefly described here.

A line in the image space can be expressed in Cartesian coordinate system as follows:

$$y = m.x + c \tag{1}$$

where m is the slope of the line and c is the y-intercept. The line equation can also be expressed in a ($r_i$–θ) Polar coordinate system as follows (see Fig. 5-1a):

$$y = -\frac{\cos\theta}{\sin\theta}.x + \frac{r_i}{\sin\theta} \tag{2}$$

Hence, the line equation can be written as:

$$r_i = x.\cos\theta + y.\sin\theta \tag{3}$$

The representation of the straight line in Cartesian and polar coordinate system is shown in Fig. 5-4.

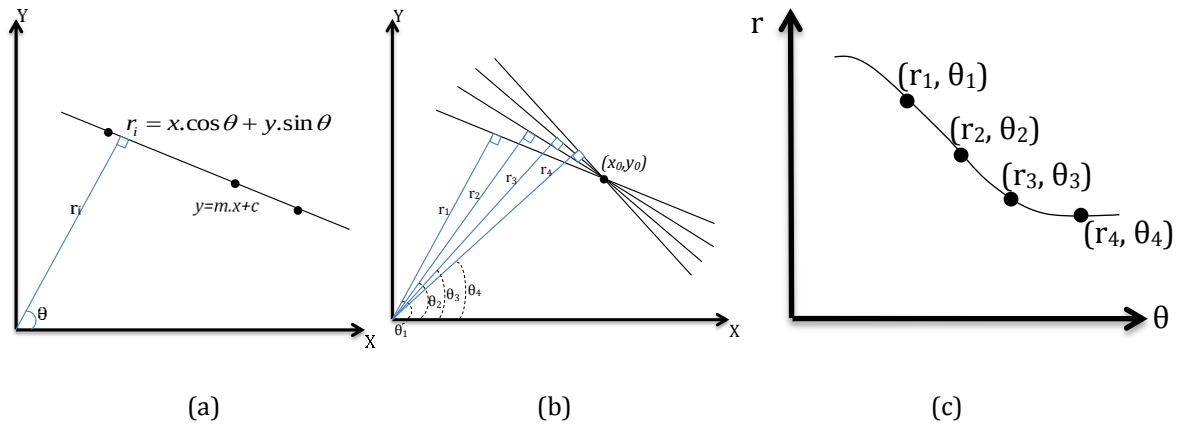


Fig. 5-1: a) Polar ($r_i$–θ) representation of a line; b) a group of lines passing through a point ($x_0$, $y_0$); c) each line can be represented by a pair of ($r_i$, $\theta_i$ ) that becomes a sinusoidal curve at the r–θ plane.

In general, for each point ($x_0$, $y_0$), a group of lines passing through that point can be parameterized by a pair of ($r_i$, $\theta_i$) as following:

$$r_i = x_0.\cos\theta_i + y_0.\sin\theta_i \tag{4}$$

Therefore each pair of ($r_i$, $\theta_i$) represents a line that passes through point ($x_0$, $y_0$) (Fig. 5-1b). For a given point ($x_0$, $y_0$), the family of lines that passes through it in polar coordinate system represents a sinusoidal wave. This sinusoidal representation is shown in Fig. 5-1c. Thus each line can be represented with a pair of ($r_i$, $\theta_i$).

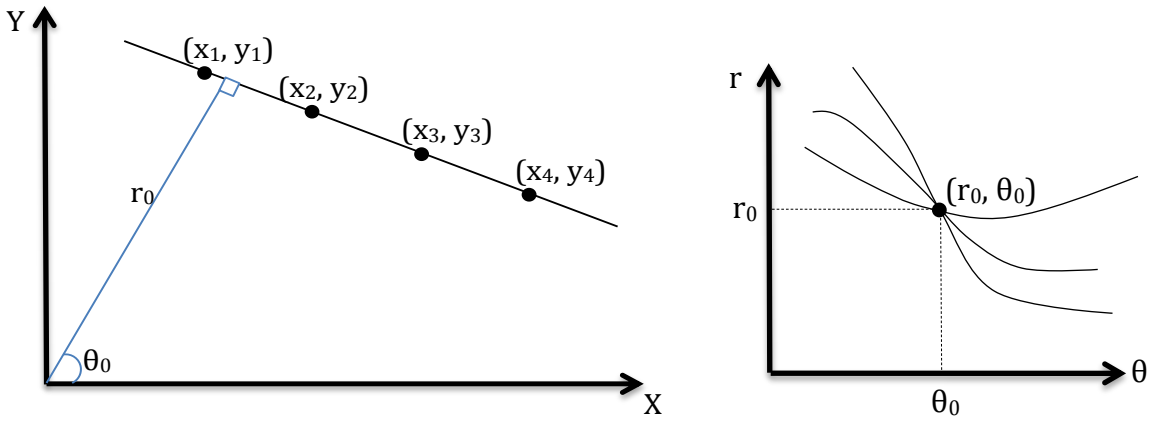


Fig. 5-2: a) Collinear points with normal parameterization of ($r_0$, $\theta_0$). b) Collinear points are transformed into curves that intersect in a single point in the r-θ plane.

The Hough transform method uses this transformation of points to sinusoidal curves to find a line passing through a group of points; this is based on the premise that points that belong to the same line in the X-Y plane will be transformed into curves with an intersection point in the $(r_i, \theta_i)$ plane (see Fig. 5-6b). Thus, to find the line passing through a group of points, such as $(x_1,y_1)$, …, $(x_4,y_4)$, one can find the point where the majority of these sinusoidal waves intersect in corresponding domain $(r_i, \theta_i)$; this gives the equation of the line passing through group of the points using Eq. 2.

In general, in Hough transform, a line can be identified by finding the number of intersections between curves in $(r_i, \theta_i)$ domain. This is the basic of the Hough transform for identifying lines.

The purpose of using Hough transform here is to automatically detect the lines of the row of bushes or trees in a farm field and to provide lateral offset and heading measurements sent to the mobile robot controller. Then the robot moves beside the rows of bushes while keeping proximity with them for spraying as an example of a given task. Result of implementing Hough transform algorithm on a sample of laser point clouds is depicted in Fig. 5-3; it is observed that several lines (black lines) are identified using Hough transform for a crop row.

Fig. 5-3: (a) Original crop rows in farm field [19]. (b) Hough transform of the points. Lines recognized using Hough transform are shown in black lines in (a).

Therefore the path generated by navigation algorithm would not be a particular smooth one. To obtain a smooth path which fits the crop row, the exponential curve fitting technique is applied to the Hough-recognized lines. This is a novelty of this algorithm. Employing the proposed curve fitting technique on Hough-identified lines generates a piecewise smooth model of the row of bushes and as a result smooth paths for the robot to follow.

### 5.3.2. Curve fitting technique to generate smooth paths

A curve fitting approach is introduced for processing generated lines from Hough transform. The method uses different lines for estimation and is adjustable according to each set of collected data by LRF. This technique estimates piecewise smooth curve with specified accuracy and an overall approximation model of the data is generated. Sets of coefficients that describe a profile shape within each piece of the model are calculated; then the final model is fitted to the measured data points.

The generated lines by Hough transform are used as reference lines for producing curve in this model. The goal is to make the estimated curve tangent to the reference lines in as much points as possible (Fig. 5-4).

Model construction and curve generation involves specification of the parameters of the model and determination of the coefficients of data. In order to produce a smooth curve from the reference lines, (reference lines that are recognized by Hough transform) various curve fitting techniques were studied and tested here. In many cases, the generated curves, which are the paths for the robot to follow, are either too simple to fully describe the real rows of bushes, or too complex with many parameters that need long computations and

cannot be used for online row detection or row following. More importantly, these curve fitting techniques are only useful for some particular shape of crop rows and inapplicable to other shapes of rows. In this paper, a general flexible path creation method is proposed. This approach is tested and applied for different crop rows in farm fields.

Let's y(x) be a smooth curve for the robot path. This curve is developed from Hough transform reference lines. The inclinations of the i-th reference line is indicated by $\lambda_i$. The goal is to make the tangent of the curve at any point vary from the tangent of the initial reference line $\lambda_0$ to the tangent of the final reference $\lambda_f$ as x increases. Thus, the tangent of the curve is defined with an exponential expression described as:

$$\lambda(x) = \lambda_f + (\lambda_0 - \lambda_f)e^{-Kx} \tag{5}$$

where parameter K is a positive number adjusted for different paths. Then we can have:

$$\frac{dy(x)}{dx} = \lambda(x) \tag{6}$$

$$y(x) = \lambda_f x - \frac{(\lambda_0 - \lambda_f)}{K} e^{-Kx} + const \tag{7}$$

where *const* is a constant, which can be calculated using the reference inclinations and initial positions as follows:

$$c = y_0 - \lambda_f x_0 + \frac{(\lambda_0 - \lambda_f)}{K} e^{-Kx_0} \tag{8a}$$

$$\Rightarrow y(x) = \lambda_f (x - x_0) + \frac{(\lambda_0 - \lambda_f)}{K} (e^{-Kx_0} - e^{-Kx}) + y_0 \tag{8b}$$

The equation of the whole curve is sum of all piecewise curves of y(x). The curves y(x) are computed from laser data at each time for online path planning. The proposed path provides smooth transition from initial to final conditions without any abrupt changes in

the heading angle of the robot. Several experimental results from row following and rut following tests are used in order to verify the equations and evaluate the value of the parameter K.

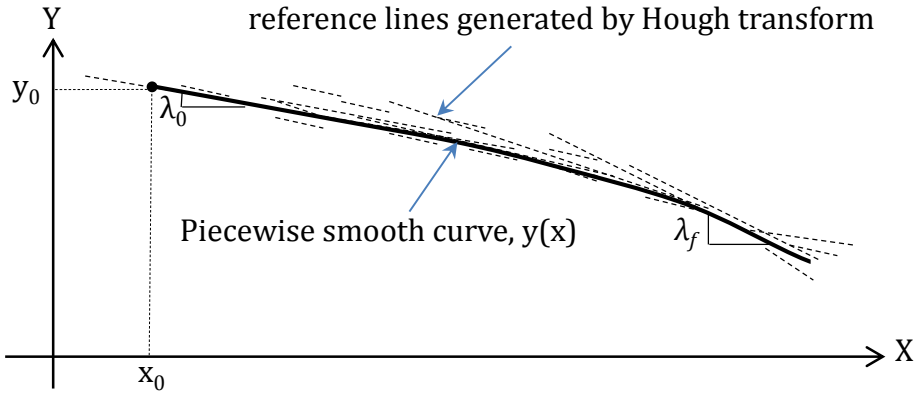


Fig. 5-4: Lines generated by Hough transform (dash lines) are used as reference lines for generating smooth curve (solid curve) for the robot to track. Initial position: ($x_0$, $y_0$).

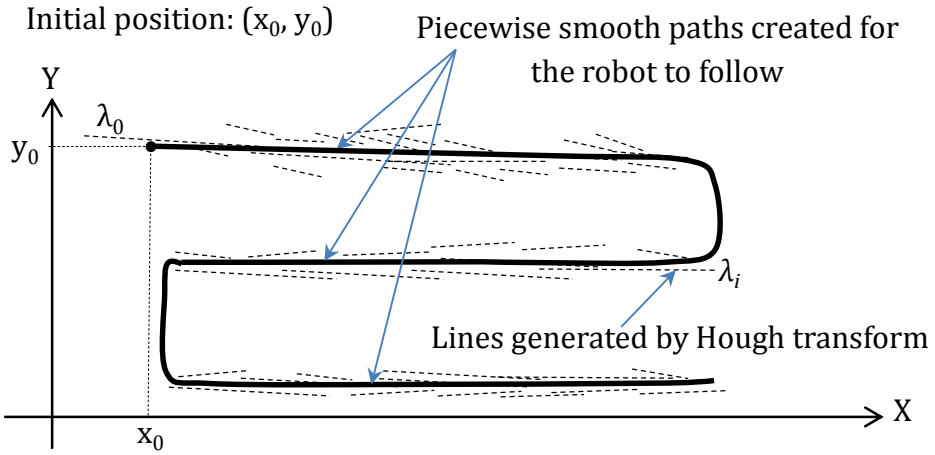


Fig. 5-5: Application of the curve fitting technique for path planning. Lines generated by Hough transform (dash lines) are used to create piecewise smooth path for the robot to follow.

One sample of a curve generated for path planning and row following is illustrated in Fig. 5-5.

## 5.4. Path following control of the robot

This section describes in detail our proposed method for path following control of the robot for rut and proximity-following actions. First, general kinematic model of the four wheel drive AGV is giving then a control law applied for the rut following and the proximity-following is presented.

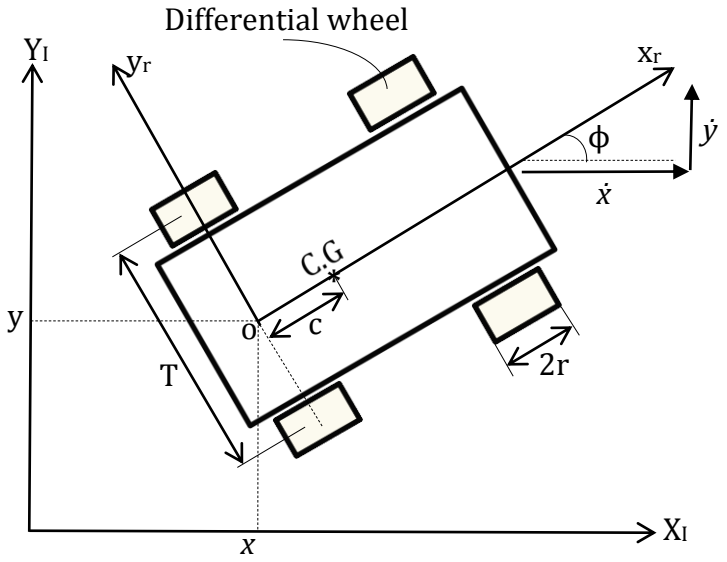


Fig. 5-6: Geometric configuration of the mobile robot

### 5.4.1. Kinematics of the robot

The AGV used for the experiments is a four-wheel-drive vehicle (having a 4x4 differential drive system) actuated by four motors, one motor drives each wheel. But for control applications, the wheels on the same side (left or right) are driven with the same velocity (meaning the wheels on the same side rotate with the same speed). The wheels are equipped with encoders. The schematic figure of the AGV is shown in Fig. 5-6. In this figure, $T$ is the width of the mobile robot and $r$ is the radius of its wheels. $X_I$ – $Y_I$ is inertial coordinate system and $\phi$ is the heading angle of the robot; $x_r$ - $y_r$ is the local coordinate system which is fixed to the center of the mobile robot. It is in the middle between the right

and left rear wheels of the robot. The center of mass of the robot is C.G. as shown in Fig. 5-6. The distance from $x_r$ axis to the C.G. is $c$. The kinematic inputs that drive the robot and affect its speed and direction of motion are the right and the left wheels' speeds. The vector $q$ describes the configuration (position and orientation) of the robot at any time:

$$q = \begin{bmatrix} x & y & \phi \end{bmatrix}^T \tag{9}$$

$x$ , $y$ are the coordinates of the robot (point o) in the inertial frame. If the linear speed and angular velocity of the robot are v and ω, respectively, assuming no-slip on wheels, the velocity components can be written as:

$$\begin{aligned} \dot{x} &= v\cos\phi \\ \dot{y} &= v\sin\phi \\ \dot{\phi} &= \omega \end{aligned} \tag{10}$$

The kinematic model of the robot can be written as follows:

$$\dot{q} = \begin{bmatrix} \cos\phi & 0 \\ \sin\phi & 0 \\ 0 & 1 \end{bmatrix} .u \tag{11}$$

where $\dot{q}$ is time derivative of configuration $q$, and $u = \begin{bmatrix} v & \omega \end{bmatrix}^T$ is the control input given to the robot for navigation. Angular and linear velocity of the robot can be written in terms of linear velocities of the right and the left wheel centers ($v_r$, $v_l$):

$$\omega = \frac{v_r - v_l}{T} \quad , \qquad v = \frac{v_r + v_l}{2} \tag{12}$$

### 5.4.2. Path following control

This section describes in detail the path following controller designed for row following and proximity-following systems. The robot and the paths are modeled as illustrated in Fig.

5-7. The desired trajectory for the robot in the inertial coordinate system is defined as following:

$$\begin{aligned} x^d &= x^d(t) \\ y^d &= y^d(t) \\ v^d &= v^d(t) \end{aligned} \tag{13}$$

The lateral no-slip condition states that the lateral component of the velocity of midpoint of front axle is zero and also, interaction forces between tires and the floor do not exceed maximum allowable static friction. This condition is described as follows:

$$\dot{x}^{(d)} \sin\phi - \dot{y}^{(d)} \cos\phi = 0 \tag{14}$$

$$\Rightarrow \begin{cases} \phi^d(t) = \arctan\left(\dfrac{\dot{y}^d(t)}{\dot{x}^d(t)}\right) \\ \omega^d(t) = \dot{\phi}^d(t) \end{cases} \tag{15}$$

The change in the heading angle of the robot is determined using following equation:

$$\Delta\phi = \phi_2 - \phi_1 = \arctan\left((y_2 - y_1), (x_2 - x_1)\right) \tag{16}$$

$$\Rightarrow \quad \phi_2 = \phi_1 + \Delta\phi \tag{17}$$

where $(x_1, y_1, \phi_1)$ and $(x_2, y_2, \phi_2)$ are the pose (position and orientation) of the robot at time $t_1$ and $t_2$, respectively. The goal is to control the robot to follow the desired trajectory given in Eq. (13). The error equations are defined as the difference between the desired and the actual values:

$$\begin{aligned} e &= \sqrt{\left(x - x^d\right)^2 + \left(y - y^d\right)^2 + \left(z - z^d\right)^2} \\ \theta &= \phi^d - \phi \end{aligned} \tag{18}$$

The term $e$ is indicating the position error, and $\theta$ is the error in heading angle of the robot. Our goal is to control the heading angle of the robot, $\phi$, in a way to minimize $\theta$ (given in Eq. (18)).

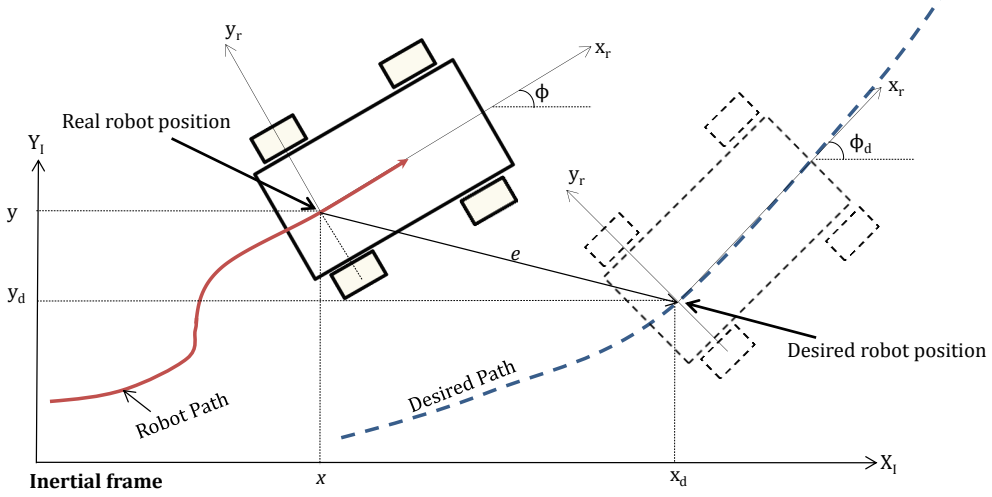


Fig. 5-7: General model of the robot for path following

The next step is to find control inputs to minimize the tracking errors in Eq. (18). The kinematics control laws used in this research were developed using techniques described in [21]. The developed controller is capable of solving the position stabilization, and path following, problems simultaneously. As a result the robot is asymptotically driven to an arbitrarily small neighborhood of the desired position, path, or trajectory. Control parameters are then tuned to assure that physical constraints are satisfied. The linear velocity of the robot is chosen as:

$$v = \frac{k_1.e.k_e.\tanh\left(e - k_2\sqrt{2}\right) + v^d.e.k_e.\cos(\theta) + v^d.k_r.\left(\sin(\theta) + \omega^d.e/v^d\right)}{e.k_e + k_r.\sin(\alpha)} \tag{19}$$

where $k_1$ and $k_2$ are the controller parameters which control the response; $k_e$ and $k_r$ are defined as:

$$k_e = \sqrt{\zeta - \cos(2\theta)} \tag{20}$$

$$k_r = k_2\sqrt{2}\sin(2\theta) \tag{21}$$

$$\zeta = 1 - \varepsilon \tag{22}$$

where $\varepsilon$ is a small perturbance to avoid a discontinuity in the response. The optimized control law governing rotational velocity is given by:

$$\omega = k_3.\tanh(\theta) + 2\dot{\theta} + \dot{\phi}^d \quad (23)$$

where $k_3$ is a positive scalar gain to control the angular response of the controller.

Initial values of $v$ and ω obtained from equations (19) and (23) are rarely performing well for the row following system. To solve these problems the dynamic extensions [22] are defined as follow:

$$\dot{v}^r = -k_v.(v_a - v) + \dot{v} \quad (24)$$

$$\dot{\omega}^r = -k_\omega.(\omega_a - \omega) + \dot{\omega} \quad (25)$$

The values $v_a$ and $\omega_a$ are the measured velocity states of the robot. The states $\dot{v}^r$ and $\dot{\omega}^r$ are the control commands sent to the robot. These new states are introduced to decline steady state error and improve boundedness. The extensions perform as low pass filters, which improve the controller response in the presence of noisy state feedback. The gains $k_v$ and $k_\omega$ are used to control the response of the dynamic extension. The variables $v$ and $\omega$ are the outputs from equations (19) and (23). By modeling the system as a discrete one, the control commands $\dot{v}^r$ and $\dot{\omega}^r$ are calculated from following equations:

$$\dot{v}^r = \frac{v^r(t_2) - v^r(t_1)}{t_2 - t_1} \quad (26)$$

$$\dot{\omega}^r = \frac{\omega^r(t_2) - \omega^r(t_1)}{t_2 - t_1} \quad (27)$$

All tests (in both simulations and experiments) are performed with assumption of zero initial conditions. After various simulations and testing of the controller system, the controller parameters are chosen. The controller parameters are properly tuned for the navigation system in order to follow the desired path to achieve the desired performance. The experiments are performed with the following values chosen for the controller

parameters: $k_2$= 0.02 m, ε= 0.003 m, $k_1$= 0.85, $k_3$= 0.3, and $k_v$= $k_\omega$= 3.0. The maximum reference velocity of the robot is 4m/s, and the maximum robot acceleration is 1m/s$^2$. Initial and final velocities of the AGV are zero, with a linear ramp function to a constant velocity.

## 5.5. Negative obstacle detection behavior

One of challenges in autonomous navigation of the robot in farm field is existence of negative obstacles (depression of the ground as shown in Fig. 5-8) that if traversed by the robot, would be a danger to the robot because they could cause roll-over, tip-over, or high-centering. Usually ditches that are larger than the diameter of the wheel of the robot can cause damage to the robot. Hence, we introduced a new robust method for negative obstacle detection using 3D laser data.

Fig. 5-8: Sample of negative obstacles in off-road terrain

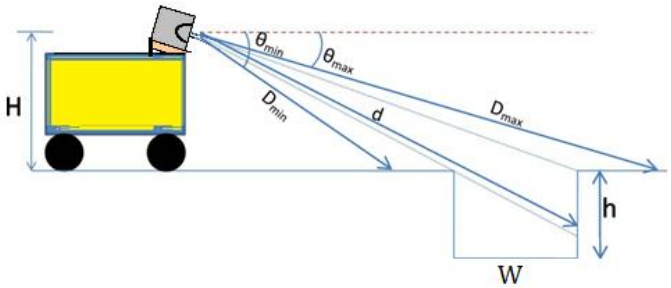


Fig. 5-9: Geometry of negative obstacle (ditch) detection

Schematic of a negative obstacle is shown in Fig. 5-9. The width and the height of the obstacle are "W" and "h", respectively; "H" is the height of LRF from the ground. The 3D laser range finder has α=180 degree of horizontal view (yaw angle) and vertical range of view (pitch angle $\theta_{min} \leq \theta \leq \theta_{max}$). $D_{min}$, $D_{max}$ and *d* are laser readings at angles $\theta_{min}$, $\theta_{max}$ , and θ respectively. Laser readings over flat ground level (when there is no positive or negative obstacle) will be computed as following:

$$D_{\min} = \frac{H}{\sin\theta_{\min}} . \frac{1}{\sin\alpha} \tag{28}$$

$$D_{\max} = \frac{H}{\sin\theta_{\max}} . \frac{1}{\sin\alpha} \tag{29}$$

$$D_{\theta} = \frac{H}{\sin\theta} . \frac{1}{\sin\alpha} \tag{30}$$

where "$D_\theta$" is laser reading on ground level at pitch angle θ, and α is the azimuth (yaw) angle in the plane view of LRF. By using the following equations, both positive and negative obstacles can be detected:

$$at \quad \theta = \theta_{\min} : \begin{cases} if \quad d \leq D_{\min} - L \Rightarrow positive \quad obstacle \\ if \quad d \geq D_{\min} + L \Rightarrow negative \quad obstacle \end{cases} \tag{31}$$

$$at \quad \theta = \theta_{\max} : \begin{cases} if \quad d \leq D_{\max} - L \Rightarrow positive \quad obstacle \\ if \quad d \geq D_{\max} + L \Rightarrow negative \quad obstacle \end{cases} \tag{32}$$

$$for \quad \theta_{\min} \leq \theta \leq \theta_{\max} \quad and \quad \alpha_{\min} \leq \alpha \leq \alpha_{\max} : \begin{cases} if \quad d_\theta \leq D_\theta - L \Rightarrow positive \quad obstacle \\ if \quad d_\theta \geq D_\theta + L \Rightarrow negative \quad obstacle \end{cases} \tag{33}$$

where "$d_\theta$" is the laser reading at angle θ, and *L* is the size of passable (small) obstacles (*L* is threshold length for *obstacle detection* action to kick in).

## 5.6. Experiments and results

In this section, the experimental evaluations of the proposed navigation system in various setups are presented. All experiments are conducted on the four wheel drive AGV in farm fields in different trials. The AGV, the tilting laser range finder (LRF), and the global positioning system, RTK-DGPS, used as experimental platform are depicted in Fig. 5-10. First, the navigation algorithm was evaluated to recognize and avoid different holes appeared on the way of the robot. Then proximity-following tests, which included the rows with undefined shapes were conducted. Also, the performance of the new navigation technique was tested to detect and follow different ruts (S-shape ruts, broken ruts, and shallow ruts). Finally, some tests were performed to validate the hole detection, hole avoidance and proximity-following algorithms altogether.

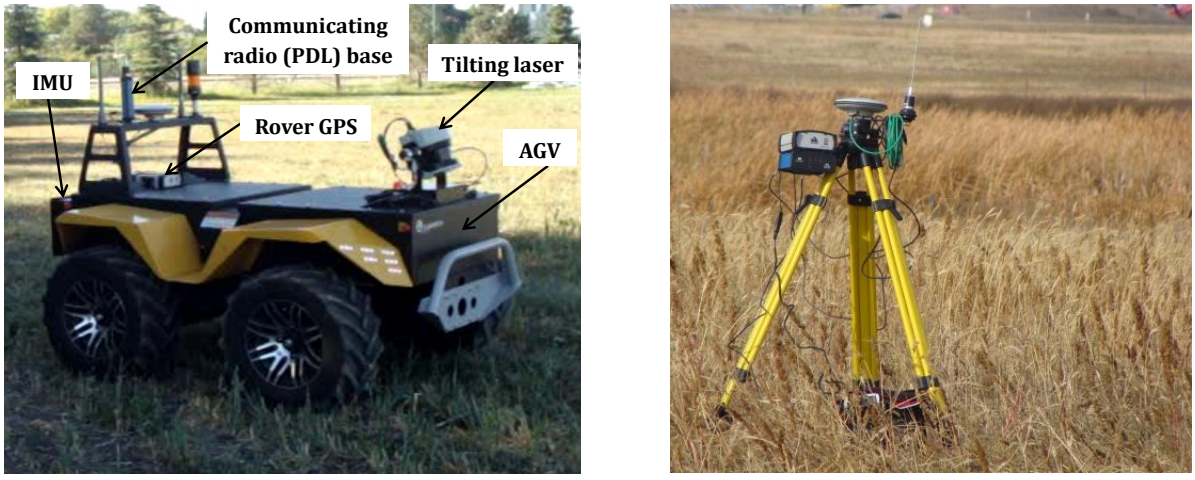


(a) (b)

Fig. 5-10: Experimental platform: (a): 4x4 differential drive AGV, tilting laser range finder for obstacle detection, and (b): global positioning system RTK-DGPS for localization

### 5.6.1. Negative obstacle detection and avoidance

Negative obstacles such as holes, gaps and ground depression are inherent parts of off-road terrains and farm fields. Therefore the performance of the proposed navigation strategy was tested in these cases. We conducted experiments on various types of holes which were placed on the path of AGV. Results of hole detection and avoidance tests are displayed in Figs. 5-11 to 5-20. Tests were conducted on holes with different shapes and sizes. The results of all these experiments showed that the robot managed to accurately avoid and pass all holes appeared on its way.

In the first scenario, the navigation strategy is utilized for guiding the robot from a start position to a user-specified goal point, while avoiding encountered negative or positive obstacles. The goal position is chosen approximately 11 meters in front of the robot, measured on a straight line. Directly in between the start and goal position, there is a hole with length, width and depth of 0.5m ×2m ×0.8 m respectively as seen in Fig. 5-11. The robot begins from the start point moving toward the goal point until it detects the hole; then the robot turns to follow the hole's boundaries and avoid entering the hole. Once AGV passes the hole, it travels toward the goal position. Fig. 5-11 demonstrates snapshots of the actual robot navigation in point-to-point motion (moving directly from start point (*) to goal point (⍟)) while avoiding a hole in the first scenario. Fig. 5-12 shows the path traversed by the robot (AGV) from its start position until it has autonomously reached the specified goal point, using the proposed navigation strategy.


Fig. 5-11: Scenario 1: Snapshots of the robot navigation in point-to-point motion, moving directly from the start point (*), left image, to the goal point (⊛) while avoiding a hole. The actual path of the robot is shown in black dash-dotted line and the direct path from (*) to the (⊛) is depicted in white dash line. Right image shows close up view of the hole.

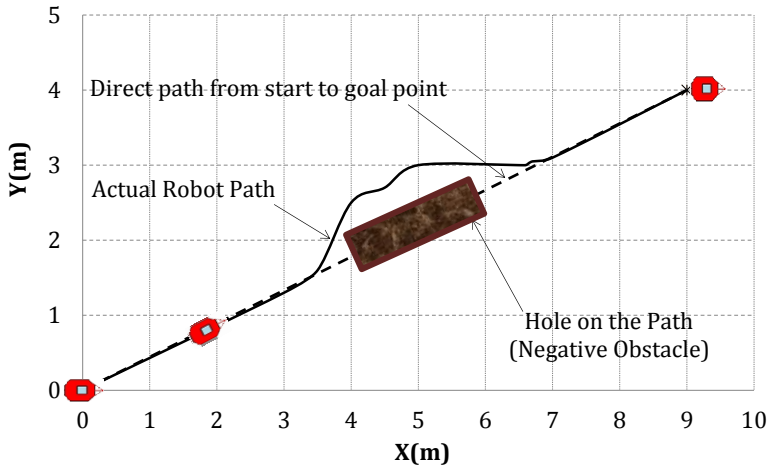


Fig. 5-12: Scenario 1: Performance of the navigation strategy in the presence of a narrow hole on the way of the robot

In the second scenario, the same hole as in scenario 1 is used but the robot is approached in different direction with respect to the hole, as seen in Fig. 5-13. In this case, the goal position is chosen approximately 7 meters in front of the robot, measured on a straight line from start point. As the robot navigated toward the goal, it detected the hole and followed the hole's boundaries and continued its way toward goal point on a straight path. Snapshots of the actual robot run in point-to-point motion while avoiding the hole in scenario 2 is depicted in Fig. 5-13 and Fig. 5-14.


Fig. 5-13: Scenario 2: Snapshots of the robot navigation in point-to-point motion, from the start point (*), left image, to the goal point (⊛) while avoiding a hole. The actual path of the robot is shown in black dash-dotted line and the direct path from (*) to the (⊛) is depicted in white dash line. Right image shows close up view of the hole.

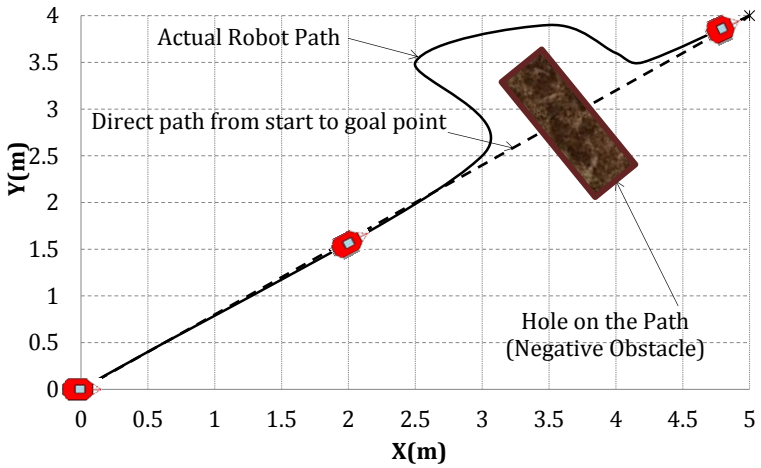


Fig. 5-14: Scenario 2: Performance of the navigation strategy in the presence of a wide hole on the way of the robot

The third scenario demonstrates the performance of the proposed strategy to navigate the robot in passing a deep rectangular hole. Directly in between the start and goal position, there is a hole with length, width and depth of 0.6 m × 0.5 m × 0.6 m respectively. Snapshots of the actual robot run in point-to-point motion while avoiding the hole in scenario 3 is depicted in Fig. 5-15. The robot reached the goal position successfully as its path is depicted in Fig. 5-16.

In the next two scenarios, two very wide natural ground depressions, which are unsafe for the robot to traverse them, are used to verify the performance of the proposed navigation method to guide the robot when confronting big holes. In these two situations, there are big and relatively deep holes between the start and specified goal positions on the specified

path of the robot. Theses cavities have unspecified shapes with approximate length, width and depth of 7 m ×2.5 m ×1 m and 3 m ×4 m ×1 m for scenarios 4 and 5, respectively, as seen in Figs. 5-17 and 5-19. As illustrated in Figs. 5-18 and 5-20, the robot reached the goal position successfully avoiding entry into the very wide holes.


Fig. 5-15: Scenario 3Snapshots of the robot navigation in point-to-point motion, going in a straight line from the start point (*), left image, to the goal point (✪) while avoiding a hole. The actual path of the robot is shown in dash-dotted line and the direct path from (*) to the (✪) is depicted in dash line. Right image shows more detail of the hole.

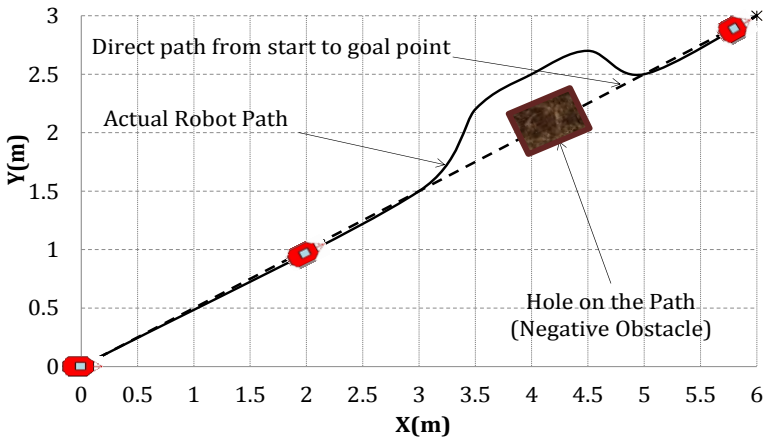


Fig. 5-16: Scenario 3: Performance of the navigation strategy in the presence of a deep hole on the way of the robot


Fig. 5-17: Scenario 4: Snapshots of the robot navigation in point-to-point motion, when moving directly from the start point (*), left image, to the goal point (✪) while avoiding a very wide hole. The actual path of the robot is shown in black dash-dotted line and the straight path from (*) to the (✪) is depicted in white dash line.

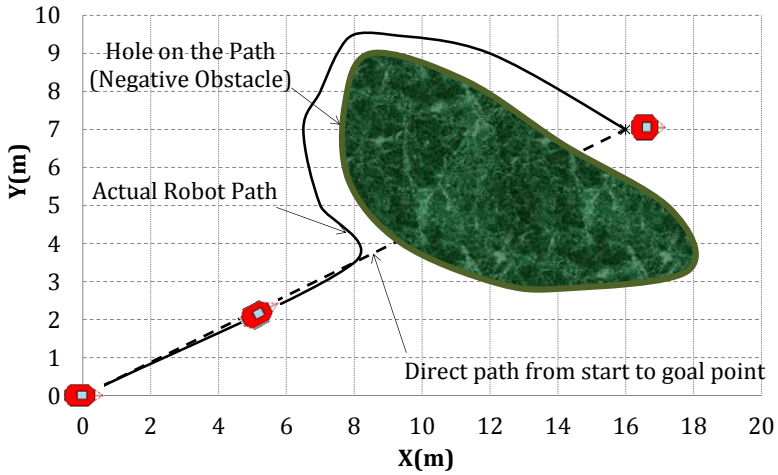


Fig. 5-18: Scenario 4: Performance of the navigation strategy in the presence of a very wide hole on the way of the robot

Fig. 5-19: Scenario 5: Snapshots of the robot navigation in point-to-point motion, moving in a straight line from the start point (*), left image, to the goal point (⍟) while avoiding a very big hole. The actual path of the robot is shown in black dash-dotted line and the straight path from (*) to the (⍟) is depicted in white dash line.

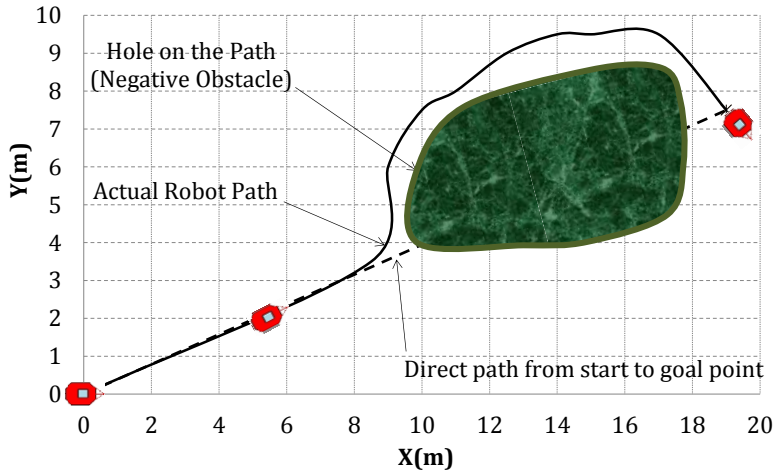


Fig. 5-20: Scenario 5: Performance of the navigation strategy in the presence of a very big hole on the way of AGV

The results of hole detection and avoidance tests are summarized in Table 5-I.

Table 5-I: Hole detection and avoidance experimental results in outdoor setting. Approximate dimensions of holes are: length× width× depth measured in meter.

| Tests | Hole dimension in meters: (L× W× D) | Number of trials | Success rate (%) |
|---|---|---|---|
| **Scenario 1** | 2×0.5×0.8 | 3 | 100 |
| **Scenario 2** | 0.5×2×0.8 | 3 | 100 |
| **Scenario 3** | 0.6× 0.5×0.6 | 2 | 100 |
| **Scenario 4** | 7 ×2.5 ×1 | 2 | 100 |
| **Scenario 5** | 3 ×4 ×1 | 2 | 100 |

### 5.6.2. Rut detection and following

A rut is a long deep track formed by the repeated passage of wheeled vehicles in soft terrains such as mud, sand, and snow. Fig. 5-23 shows a typical rut made by the passage of manned vehicles in a farm field. In this section, capabilities of the proposed navigation system to follow different shapes of ruts including very shallow and curvy ones are verified. In addition these tests confirm that the navigation method works well regardless of initial posture (position and heading angle) of the robot with respect to the ruts. The snapshots from the actual run of the robot tracking a curvy rut is depicted in Fig. 5-21. Both the actual and the desired paths of the robot are presented in Fig. 5-22; this figure shows that the proposed method is able to detect and track curvy ruts.


Fig. 5-21: Scenario 6: Snapshots of the robot following a curvy rut in the farm field [19].

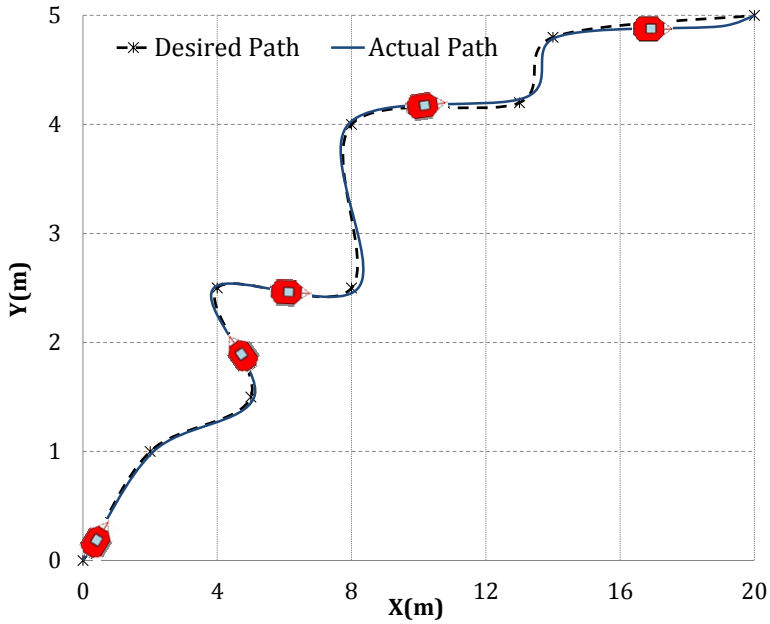


Fig. 5-22: Scenario 6: Rut following scenario with a curvy rut: rut (desired path) and actual path traveled by the robot.

Fig. 5-23: Scenario 7: Snapshots of the robot following a shallow rut in the farm field [19].

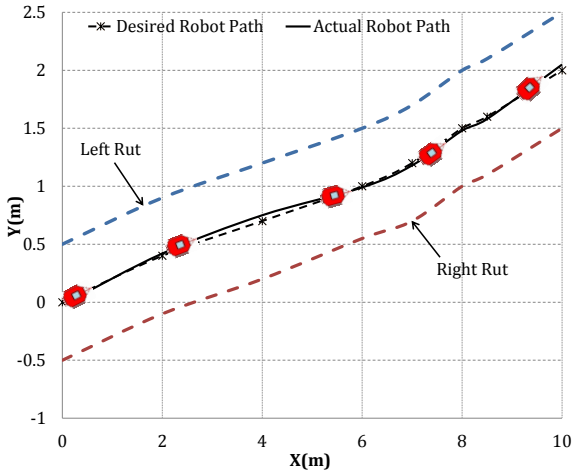


Fig. 5-24: Scenario 7: Rut following scenario of shallow ruts: desired path is middle of the left and right ends of the ruts and actual path is solid line.

### 5.6.3. Proximity-following

In the next set of experiments, we investigated the ability of the navigation algorithm to detect rows of bushes and follow them while keeping a constant proximity distance (about f=1m) from the rows. This process can be used for spraying the rows of crops. Fig. 5-25 shows a set of snapshots from actual robot run in a proximity-following test. In this scenario, the row of bushes has a curvy shape and a length of about 50 m. The robot started

from the beginning of the row; it detected and tracked the row while retained an offset distance of equal to 1m from the row. The desired and actual paths of the robot are depicted in Fig. 5-26. The performance and accuracy of the navigation strategy in proximity-following test is displayed in Fig. 5-27; it is seen that the distance from the row of bush was not constant. This distance changed from a min 0.8 m and max 1.17 m with an average of 0.97 m. This test demonstrates that the proposed navigation strategy is able to effectively detect and track the crop rows and at the same time maintaining a given distance from the row.

Fig. 5-25: Scenario 8: Snapshots of the robot in a proximity-following test in the farm field [19].

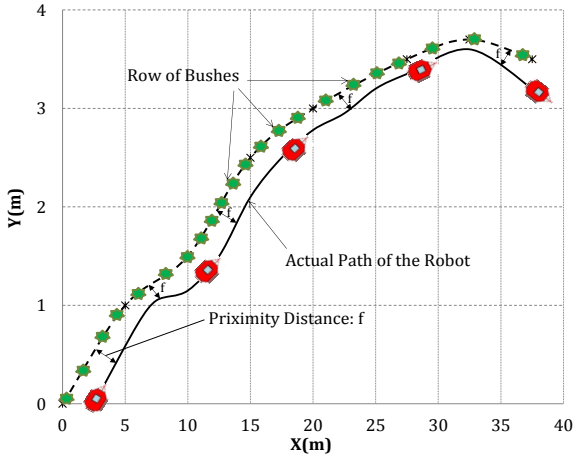


Fig. 5-26: Scenario 8: Proximity-following scenario: the row of bushes and the actual path traveled by the robot are shown in dashed * and solid lines respectively. The robot was to keep a distance of 1m from the row.

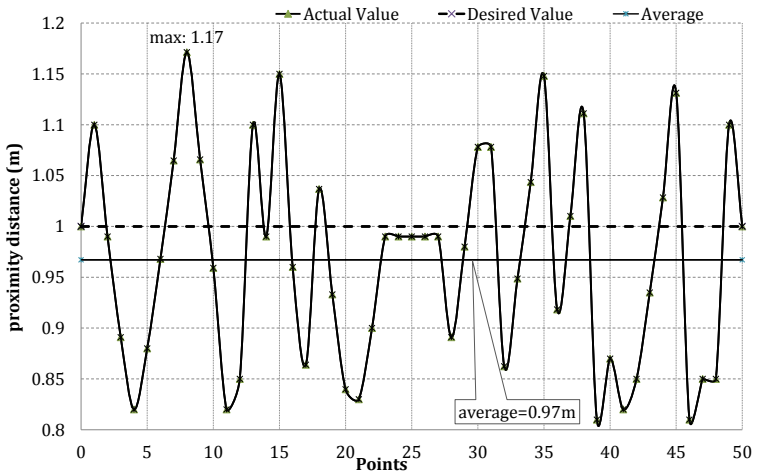


Fig. 5-27: Scenario 8: Performance of navigation strategy in proximity-following experiment

### 5.6.4. Proximity-following and hole avoidance

These experiments serve two purposes: first, they are performed to show that the system is capable of detecting and tracking row of bushes while retaining the desired proximity distance (f =1m) from the row. The second, these tests are used to verify the performance of the navigation strategy to recognize and avoid any holes and ground depressions that appear on the way of the robot simultaneously. The results of these experiments are shown in Figs. 5-28 to 5-30. Fig. 5-28 displays a set of snapshots from the actual robot run in scenario 9. There were two holes with approximate length, width and depth of 0.5m× 0.6m× 0.5m respectively on the planned path of the robot. The desired and actual paths of the robot following the row of bushes while avoiding holes are depicted in Fig. 5-29.


Fig. 5-28: Scenario 9: Snapshots of the robot in proximity-following and hole avoidance test in a farm field [19].

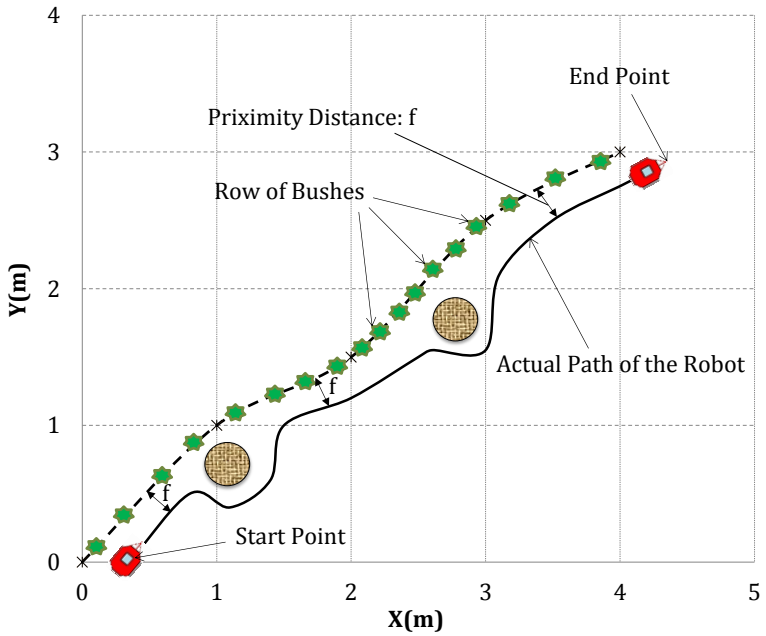

Fig. 5-29: Scenario 9: Experimental results for proximity-following in the presence of two holes on the path of robot: desired and actual paths of the robot are depicted as dashed * and solid lines respectively; holes are shown as solid circles.

Performance of the navigation strategy in scenario 10 is depicted in Fig. 5-30; there were two given holes with approximate length, width and depth of 0.7m× 0.7m× 0.7m respectively on the way of the robot. The desired and actual paths of the robot tracking the rows of bushes while avoiding holes are depicted here. As illustrated in this test, the robot is capable of following two parallel rows of bushes and avoiding encountered obstacles (holes here).

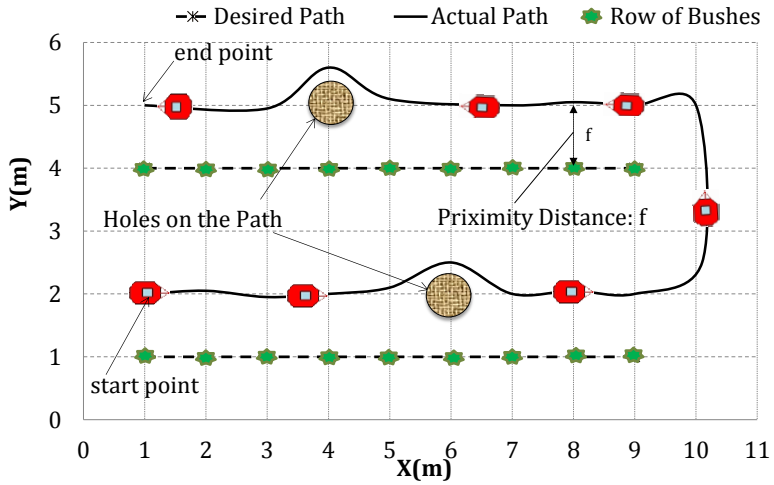


Fig. 5-30: Scenario 10: Experimental results for proximity-following of two parallel rows of bushes in the presence of two negative obstacles on the path of robot: desired and actual paths of the robot are depicted in dashed * and solid lines respectively.

## 5.7. Conclusion and future work

In this article a navigation strategy for mobile robots in outdoor settings was proposed. The main advantages of this technique are: (i) accurately identifies negative (below ground holes) and positive obstacles (over ground level); (ii) creates a flexible and smooth path using a proposed curve fitting technique for path planning, row following and rut following in outdoor settings such as farm fields; (iii) precisely detects and follows rows of crops or bushes. The proposed approach was experimentally evaluated in different outdoor terrains and in diverse situations. The navigation system is not restricted to a specific crop or row of bushes and it was tested on diverse scenarios. A 3D laser range finder was employed to perceive the environment, detect the rows of bushes, and ruts and also guided the robot to its desired goal points.

One major advantage of the proposed strategy over existing methods is that negative obstacles such as holes, ditches and ground depressions, which are inherent part of the off-

road terrains, are detected and avoided in real-time. By adjusting vertical angular resolution of the laser, the obstacle detection algorithm was improved to detect negative obstacles at long ranges continuously. It means that the laser data were analyzed in both downward and upward tilting of the laser scanner for detecting negative obstacles at a safe distance from the robot.

The other novelty of the suggested navigation technique is that in rut and proximity-following approaches, a curve fitting method is applied to the identified lines from Hough transform to create a smooth model of the ruts/plant rows for the robot to follow. Using Hough transform for row detection using laser data yields in many scattered short lines. If the robot follows these Hough lines, there would be abrupt changes in the heading angle of the robot which results in waste of energy and time. Thus, employing the proposed curve fitting algorithm generates a smooth model of the crop rows and consequently smooth paths for the robot to follow, hence both the power consumption of the robot and time of execution will reduce substantially.

The field tests reported in this paper demonstrated that the designed navigation strategy is capable of autonomously traversing an entire farm field for spraying, mowing and seeding with no need of prior information from the settings which results in increasing farming efficiency in the future. The performance of the navigation strategy in proximity-following test showed that the distance from the row of bush was not constant. This distance changed from a min 0.8 m and max 1.17 m with an average of 0.97 m. The ability of the proposed navigation strategy to effectively detect and track the crop rows and at the same time maintaining a given distance from the row was validated.

Future work may involve improvement of the navigation strategy in handling holes and negative obstacles to navigate faster and more efficient. For example, if the width of a hole is less than a threshold value then the robot can pass over the hole safely without trying to avoid it.

Furthermore, as a possible extension, the applications of the proposed navigation strategy is planned to be used in towing, seeding, and plowing tasks in farm fields. It is planned to develop the current system to consider effect of interaction forces of towing till and soil on robot navigation in seeding as well.

Acknowledgment: of CNH and University of Saskatchewan department of soil science for providing fields for tests; CFI and government of Saskatchewan (science fund) for equipment, NSERC for research funding.

## References


1- B. Nabbe, M. Hebert, “Extending the path-planning horizon” International Journal of Robotics Research v 26, n 10 , pp. 997-1024, 2007.

2- R. Sim, P. Elinas, M. Griffin, A. Shyr, J.J. Little, “Design and analysis of a framework for realtime vision-Based SLAM using Rao-Blackwellised particle filters” In: Proc. of the 3rd Canadian Conference on Computer and Robotic Vision, 2006.

3- R. Sim, J.J. Little, “Autonomous vision-based exploration and mapping using hybrid maps and Rao-Blackwellised particle filters” In: Proc. of IEEE Int’l Conf. on Intelligent Robots and Systems (IROS), 2006.

4- R. Manduchi, A. Castano, A. Talukder, L. Matthies, “Obstacle detection and terrain classification for autonomous off-road navigation” Autonomous Robots, v 18, n 1, p 81-102, Jan. 2005.

5- S. Boris, E. Lin, J. Bagnell,J. Cole, N. Vandapel, A. Stentz, “Improving robot navigation through self-supervised online learning” Journal of Field Robotics, v 23, n 11-12, p 1059-1075, November 2006

6- F. Rovira-Mas, Q. Zhang, J. F. Reid, J. D. Will, “Hough transform-based vision algorithm for crop row detection of an automated agricultural vehicle” Journal of Automobile Engineering, 219(8), 999–1010, 2005.

7- Y. C. Lee, W. Yu, J. Cho, “Adaptive localization for mobile robots in urban environments using low-cost sensors and enhanced topological map” 15th International Conference on Advanced Robotics, p 569-75, 2011.

8- M. Kise, Q. Zhang, F. Rovira-Mas, “A stereovision-based crop row detection method for tractor-automated guidance” Biosystems Engineering, 90(4), 357–367, 2005.

9- A. Talukder, S. Goldberg, L. Matties, A. Ansar, “Real-time detection of moving objects in a dynamic scene from moving robotic vehicles” In: Proc. of IEEE Int’l Conf. on Intelligent Robots and Systems (IROS), pp. 1308–1313, October 2003.

10- A. Talukder, L. Matties, “Real-time detection of moving objects from moving vehicles using dense stereo and optical flow” In: Proc. of IEEE Int’l Conf. on Intelligent Robots and Systems (IROS), pp. 3718–3725, October 2004.

11- C. Braillon, K. Usher, C. Pradalier, J. L. Crowley, C. Laugier, “Fusion of stereo and optical flow data using occupancy grid” In: Proc. of IEEE Int’l Conf. on Intelligent Robots and Systems (IROS), pp. 2302–2307, 2006.

12- J. Fasola, M. Veloso, “Real-time object detection using segmented and grayscale images” In: Proc. of IEEE Int’l Conf. on Robotics and Automations (ICRA), pp. 4088–4090, 2006.

13- A. Howard, E. Tunstel, D. Edwards, A. Carlson, “Enhancing fuzzy robot navigation systems by mimicking human visual perception of natural terrain traversability” In: IFSA World Congress and 20th NAFIPS International Conference, vol. 1, pp. 7–12, 2001.

14- A.J. Perez, F. Lopez, J.V. Benlloch, S. Christensen, “Colour and shape analysis techniques for weed detection in cereal fields” Comput. Electron. Agric. 25, 197–212. 2000.

15- H.T. Sogaard, H.J. Olsen, “Determination of crop rows by image analysis without segmentation” Comput. Electron. Agric. 38, 141–158, 2003.

16- C.C. Yang, S.O. Prasher, J.A. Landry, H.S. Ramaswamy, “Development of an image processing system and a fuzzy algorithm for site-specific herbicide applications” Precision Agric. 4, 5–18, 2003.

17- R. Gerhards, H. Oebel, “Practical experiences with a system for site-specific weed control in arable crops using real-time image analysis and GPS-controlled patch spraying”. Weed Res. 46, 185–193, 2006.

18- A. Tellaeche, X.P. BurgosArtizzu, G. Pajares, A.Ribeiro, C. Fernandez, “A new vision-based approach to differential spraying in precision agriculture” Computers and Electronics in Agriculture, v 60, n 2, p 144-55, 2008.

19- CNH farm field north of Saskatoon, Saskatchewan, Canada.

20- Campus farm field, University of Saskatchewan, Saskatchewan, Canada.

21- K. Youngshik, M.A. Minor, “Path manifold-based kinematic control of wheeled mobile robots considering physical constraints” International Journal of Robotics Research, v 26, n 9, p 955-75, 2007.

22- D.M. Flickinger, M.A. Minor, “Remote low frequency state feedback kinematic motion control for mobile robot trajectory tracking” IEEE International Conference on Robotics and Automation, 6 pp., 2007.

23- O. Barawid, A. Mizushima, K. Ishii, N. Noguchi, “Development of an Autonomous Navigation System using a Two-dimensional Laser Scanner in an Orchard Application”, Biosystems Engineering, v 96, n 2, p 139-149, 2007.

24- Heidari F., Fotouhi R., “Point-to-point and path following navigation of mobile robot in farm settings”, submitted to International Journal of Robotics and Automation, 2013.

# Chapter 6: Closing

## 6.1. Summary and Conclusion

In conclusion, this research was focused on introducing an autonomous navigation strategy for a mobile robot in outdoor terrains. The proposed navigation approach was composed of different modules to deal with diverse situations; sensors data processing, environment mapping, obstacle detection, obstacle avoidance, goal seeking, path planning, and path following were the main modules in the navigation strategy.

In Chapter 2, a new fuzzy-logic based (FLB) method was developed for real-time point-to-point motion planning of a mobile robot in unstructured environment. In this approach, sonar sensors were utilized to perceive the environment and detect obstacles. This method required no prior knowledge of the environment (such as a map) for navigation. Adjusting a safety margin enabled the navigation system to cope with different dynamic and unforeseen situations. The proposed method was validated using simulation and experimental tests on PowerBot mobile robot (shown in Fig. 1-1a). The kinematics model of the PowerBot was developed in Chapter 2. The results of this chapter were compared with vector field histogram and preference-based fuzzy approaches; the comparison revealed that our proposed approach produced shorter and smoother paths toward the goal in almost all of the test cases examined which was an advantage of this method. The suggested fuzzy method was applied in the rest of the chapters for mobile robot navigation in point-to-point motion and path following studies, as well.

In chapter 3, a novel human-inspired method (HIM) was introduced for mobile robot navigation. HIM was inspired by human behavior in navigation from one point to a specified goal point. HIM endowed the robot a human-like ability for reasoning about the

situations to reach a predefined goal point while avoiding any static or unforeseen obstacles; imitating human behavior in navigation enabled the robot to avoid to get trapped in deadlocks and impassable conditions which made the proposed strategy efficient and effective. In this chapter, FLB and HIM were applied for point-to-point motion planning of the robot PowerBot in the presence of static and moving obstacles. Distance-based sensory data from a laser range-finder were used for navigation of the PowerBot in unknown and cluttered settings. Experimental evaluation of HIM indicated that HIM was capable of creating smooth (no oscillations) paths for safely navigating the robot, and coping with fluctuating and imprecise sensory data from uncertain environment.

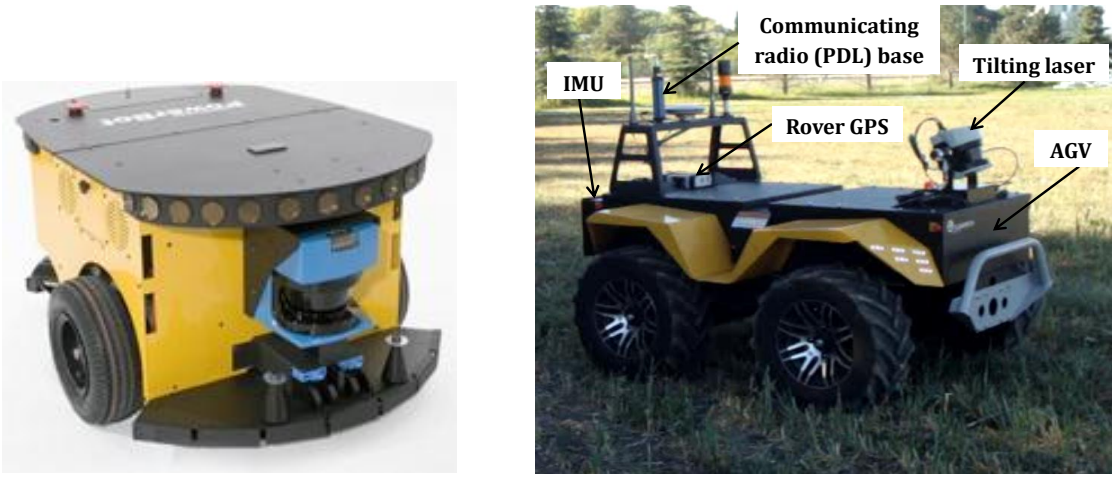


(a) (b)

Fig. 1-1: (a) PowerBot, (b) Grizzly mobile robots used for simulation and experimental tests

In Chapter 4, path following and row following navigation systems for mobile robots in farm fields were presented. Hough transform was developed for recognition of plant rows from 3D laser range finder data. This technique is used for autonomous spraying of crops and plant rows. In addition, this chapter presented experimental evaluation of the

navigation strategy on a Grizzly robot (shown in Fig. 1-1b) in variety of tests such as point-to-point motion, row-detection and path following tests.

In Chapter 5, the row following navigation system, which was introduced in Chapter 4, has been extended for rut following and proximity-following missions. In rut following system, the robot kept an existing rut in middle of the robot's wheels when possible; and in proximity-following, the robot followed the plant row while keeping a predefined proximity distance with the row. A new curve fitting method was introduced for producing a piecewise smooth path for the robot to follow. This technique removed abrupt changes in the heading angle of the robot in path following. Also in this chapter, a new method for detection of negative obstacles, such as holes and ground depressions, was introduced and experimentally tested. Experimental evaluation on Grizzly robot showed that the proposed navigation strategy was capable of detecting and following plant rows, and ruts in different scenarios.

## 6.2. Contributions of the research

The contributions of the candidate's research cover the objectives defined for her thesis. The major contributions of this thesis are:

**1)** Developed a new human-inspired method (HIM) for point-to-point navigation and control of a wheeled mobile robot in outdoor and unstructured settings.

**2)** Path following navigation of a wheeled mobile robot in farm setting.

**3)** Developed a new method for negative obstacle detection and avoidance, such as holes, ditches and ground depressions.

**4)** Developed strategies for navigation of a mobile robot in proximity-following and rut following in farm fields. A rut is a long deep track formed by the repeated passage of wheeled vehicles in soft terrains such as mud, sand, and snow.

The major contributions of this thesis are explained in more detail as follow:

**1)** The first objective was covered by introducing a fuzzy-logic based (FLB) approach that used sonar data for real-time navigation of a mobile robot in point-to-point motion in an unknown farm setting. This contribution was discussed in Chapter 2. The major advantages of the proposed approach over existing methods were that:

i. The number of fuzzy logic rules used for navigation of the robot was less than other techniques; these rules were simple and easily applicable for real-time navigation; this made a big reduction in execution time.

ii. FLB approach required no prior knowledge of the environment such as maps or landmarks and by adjusting a safety margin, the proposed approach was safely and efficiently able to cope with uncertainty and imprecision in sensory data in dynamic and unforeseen conditions.

iii. The simulation and experimental results revealed that FLB approach in comparison with vector field histogram and preference-based fuzzy approaches produced shorter and smoother paths toward a goal in almost all of the test cases examined.

**2)** In chapter 3, a new human-inspired method (HIM) was introduced for mobile robot navigation in outdoor settings. HIM, was designed to imitate behavior of a wise

human in navigation to a predefined goal point. The major advantages of HIM over existing methods are that:

i. HIM gave the robot a human-like ability of reasoning about the environment which provided uncertainty management ability for the system. HIM enabled the robot to deal with imprecise and uncertain information, therefore the navigation system handled the error from laser readings and GPS data.

ii. HIM has a modular structure which makes it easy to add new modules that develop additional behaviors to the navigation system. This makes the proposed strategy easily extensible.

iii. The proposed human-inspired navigation strategy is computationally fast and efficient, since it uses very simple and easily applicable rules for real-time robot navigation.

iv. The local minimum problem which is also called the deadlock, or dead end problem was solved in HIM, since HIM specifies the best path ahead, according to the situation of encountered obstacles, preventing the robot to get trapped in deadlock and impassable conditions.

v. Compared with FLB, the navigation time, energy consumption and the path length are less in HIM. This progress is mainly because of human-like performance of HIM which navigates the robot to take an obstacle-free path from the start point with no need to go around the obstacles during the navigation.

**3)** In Chapter 4, a navigation strategy was introduced for path following of a wheeled mobile robot in farm fields. This chapter gave the results related to the second objective of this research. The main contributions of this chapter are:

i. The proposed navigation system is robust to weather conditions and time of day, as we used an active sensor (3D laser range-finder), which does not depend on ambient illumination and can work at night time.

ii. In this chapter, Hough transform algorithm was developed for row-detection in farm field using 3D laser data.

iii. The other novelty of the suggested navigation strategy is that in row-detection module, the ends of the plant rows were identified and the robot turned to the next plant row autonomously. Therefore the designed system is capable of autonomously traversing entire farm for spraying, mowing and seeding.

iv. Experimental evaluations of the navigation strategy in different scenarios such as point-to-point motion, row-detection and row tracking tasks were performed in farm fields.

**4)** In Chapter 5, a navigation system was developed for proximity-following and rut following in farm fields. The contents of this chapter were related to the objectives 3 and 4. The novelties of this chapter are summarized as following:

i. A new approach for robust recognition of plant rows based on the modified Hough transform was proposed.

ii. A new curve fitting technique for row detection and following was presented. The proposed method generates piecewise smooth path for the robot to follow and it does not have the shortages of Hough transform in line recognition.

iii. Other advantage of the proposed strategy over existing methods is that negative obstacles such as holes, ditches and ground depressions, which are inherent part of the off-road terrains, were detected and avoided in real-time. This contribution was explained in detail in Chapter 5.

iv. The capabilities of the suggested navigation system in row detection, row, rut and proximity following were evaluated in different test situations in farm fields. Experiments were conducted on Grizzly robot and showed that the proposed strategy was able to handle different scenarios such as: diverse obstacle configuration in point-to-point motion tests; S-shape, curvy and unknown shapes of path following tests; and even navigation on hilly and uneven surfaces.

These contributions resulted in one published conference paper which is Chapter 2, and three submitted journal papers which are Chapters 3, 4 and 5 of this thesis.

## 6.3. Future possible works

The extension of the presented research can be in the theoretical and the experimental parts.

1. Future work will involve the improvement of the navigation strategy in handling holes and negative obstacles more wisely. For example, if the width of a hole is less than a threshold value then the robot can pass over the hole safely without turning around it.
2. In addition, we would like to enhance the rut following approach to manage the scenarios with more than one rut which makes the robot to place the wheels in the ruts and move in the ruts. This can reduce lateral slippage of the robot and improve the vehicle energy efficiency by reducing the energy wasted on compacting the ground, especially in off-road terrains navigation.
3. Furthermore, as a possible extension, the applications of the proposed navigation strategy can be extended in towing and plowing tasks in farm fields. It is planned to develop the current system to consider effect of interaction forces of towing till and soil on robot navigation as well.
4. Currently, our navigation system is not able to follow a desired profile for the velocity of the robot. Velocity and stability control of the robot is another part of our future research.
5. Finally, the dynamic model of the mobile robot can be used for the control and navigation of AGV in both point-to-point motion and trajectory tracking actions. Therefore, by designing a controller based on dynamic model of the robot, the stability and slippage of AGV and the forces acting on it will be considered; these can be used for the following future research.

# Appendix

Abstract of the candidate's publications on topics that are not directly related to this thesis, but related in broad robotics research are presented here. The full papers are available online, or upon request. These publications are listed as follow:

1. Vakil M., Sharbati E., Vakil A., **Heidari F.**, Fotouhi R. "Vibration analysis of a Timoshenko beam on a moving base", Journal of Vibration and Control, DOI: 10.1177/ 1077546313492808, **2013**.

2. **Heidari F.**, Vakil M., Fotouhi R., Nikiforuk P. N., "Truncation error of assumed mode modeling for flexible-link manipulators", Journal of Mechanical Engineering Science, 226 (11), 2627-2644, **2012**.

3. Vakil M., Fotouhi R., Nikiforuk P. N., **Heidari, F.** "A study on the free vibration of flexible-link flexible-joint manipulators", Journal of Mechanical Engineering Science, 225(6), 1361-1371, **2011.**

4. **Heidari, F.**, Vakil M., Fotouhi R., "On the Accuracy of Assumed Mode Modeling For Flexible Manipulators", ASME 2011 International Design Engineering Technical Conferences, Washington, DC, USA, August 29-31, **2011**.

Original Article

Institution of MECHANICAL ENGINEERS

Journal of MECHANICAL ENGINEERING SCIENCE

Proc IMechE Part C:
J Mechanical Engineering Science
226(11) 2627–2644

DOI: 10.1177/0954406212437296
pic.sagepub.com

SAGE

# Truncation errors of assumed shape modeling for flexible-link manipulators

**Fatemeh Heidari, Mohammad Vakil, Reza Fotouhi and Peter N Nikiforuk**

**Abstract**

The assumed mode shape method has been widely used to derive finite degree-of-freedom dynamic models for flexible-link manipulators, which theoretically have infinite degree-of-freedom dynamics. For a single flexible manipulator, this approximation changes locations of the zeros of transfer functions between base torque and end-effector displacement. The change in locations of zeros considerably affects accuracy of the model and therefore the performance of model-based controllers. This article presents a comprehensive study on the change in locations of zeros due to the truncation associated with assumed mode shape method. It is shown that the locations of approximate zeros depend on four non-dimensional parameters, whereas the locations of analytical zeros depend on only two non-dimensional parameters. Approximate zeros are obtained from assumed mode shape method models, whereas analytical zeros are derived from infinite order models. A thorough study of the differences between approximate zeros and analytical zeros versus the number of mode shapes as well as all the physical parameters is performed. Moreover, guidelines are provided to select the numbers of mode shapes such that the approximate zeros become close to the analytical zeros. These guidelines can easily be used by control and modeling engineers, making them valuable for modeling and control of flexible robot manipulators.

**Keywords**

Flexible robot manipulator, assumed mode shape modeling

Date received: 4 August 2011; accepted: 10 January 2012

## Introduction

The governing dynamic equations of the single flexible link manipulator (SFLM), shown in Figure 1, are infinite dimensional.[1] However, truncated dynamic models using the assumed mode shape method (AMM) are widely used for modeling of flexible robot manipulators.[2,3] The AMM is of particular interest for analysis of flexible manipulators[4–6] as it changes an infinite dimensional model into a finite dimensional one. However, AMM is an approximate truncated dynamic model as it eliminates the mode shapes that are out of the bandwidth of interest.[7] This approximation affects the accuracy of the dynamic model.[8] Since the performance of the controllers designed based on the AMM depends on the accuracy of the model,[7,9] the precision of the approximated AMM model is important.

For the SFLM shown in Figure 1, the transfer function between the base torque and the end-effector displacement $y$ can be obtained adopting the AMM approximation[10] or using the infinite dimensional model.[11] These transfer functions have zeros and poles that are, respectively, the roots of the numerator and denominator of the transfer function.[10] The transfer function derived based on the infinite dimensional model well represents the behavior of an experimental setup, and hence its poles and zeros are more accurate than those of the AMM. If exact modes of vibration are employed in the AMM,[12] the locations of the poles will be as those associated with the infinite dimensional model. However, AMM can considerably change the locations of zeros.[8] As an example, the zeros of an SFLM which is modeled by an infinite mode of vibration must all be real,[11] but when AMM is adopted, these zeros can be imaginary as well.[10]

Department of Mechanical Engineering, University of Saskatchewan, Canada

**Corresponding author:**
R Fotouhi, Department of Mechanical Engineering, University of Saskatchewan, Saskatoon, SK, S7N 5A9, Canada.
Email: reza.fotouhi@usask.ca

# A study of the free vibration of flexible-link flexible-joint manipulators

**M Vakil, R Fotouhi*, P N Nikiforuk,** and **F Heidari**
Department of Mechanical Engineering, University of Saskatchewan, Saskatoon, Canada

*The manuscript was received on 10 November 2010 and was accepted after revision for publication on 17 January 2011.*

DOI: 10.1177/0954406211399517

**Abstract:** In this article, explicit expressions for the frequency equation, mode shapes, and orthogonality of the mode shapes of a Single Flexible-link Flexible-joint manipulator (SFF) are presented. These explicit expressions are derived in terms of non-dimensional parameters which make them suitable for a sensitivity study; sensitivity study addresses the degree of dependence of the system's characteristics to each of the parameters. The SFF carries a payload which has both mass and mass moment of inertia. Hence, the closed-form expressions incorporate the effect of payload mass and its mass moment of inertia, that is, the payload mass and its size. To check the accuracy of the derived analytical expressions, the results from these analytical expressions were compared with those obtained from the finite element method. These comparisons showed excellent agreement. By using the closed-form frequency equation presented in this article, a study on the changes in the natural frequencies due to the changes in the joint stiffness is performed. An upper limit for the joint stiffness of a SFF is established such that for the joint stiffness above this limit, the natural frequencies of a SFF are very close to those of its flexible-link rigid-joint counterpart. Therefore, the value of this limit can be used to distinguish a SFF from its flexible-link rigid-joint manipulator counterpart. The findings presented in this article enhance the accuracy and time-efficiency of the dynamic modeling of flexible-link flexible-joint manipulators. These findings also improve the performance of model-based controllers, as the more accurate the dynamic model, the better the performance of the model-based controllers.

**Keywords:** flexible-link flexible-joint manipulator, natural frequency, mode shapes

## 1 INTRODUCTION

The dynamic model derivation of flexible-link flexible-joint manipulators is the first step before their model-based research, such as model-based controller research in [**1**, **2**]. The dynamic model of manipulators with links' flexibility, which is preferred for the controller analysis, is almost always derived by the assumed mode shape method [**3**, **4**]. In the assumed mode shape method, each link's lateral deflection is represented by a series of mode shapes multiplied by time-varying weight functions. The Closer the selected mode shapes to the real mode shapes of the system, the more accurate the assumed mode shape modeling [**4**] and more precise the dynamic analysis [**5**]. This article presents the *exact* closed-form mode shapes of a Single Flexible-link Flexible-joint manipulator (SFF) where these mode shapes can be used for the precise dynamic modeling. Consequently, a controller whose design is based on this model will have a better performance in the experimental verification [**6**].

While there are reports on the natural frequencies and mode shapes of a SFF [**7**–**10**], these reports do not present closed-form expressions for the natural frequencies and mode shapes considering both the payload mass and its mass moment of inertia. However, closed-form expressions not only can be used as benchmarks to validate the numerical analysis [**11**]

**Corresponding author: Department of Mechanical Engineering, University of Saskatchewan, Saskatoon, Canada.*
*email: reza.fotouhi@usask.ca*

Article

Journal of Vibration and Control
0(0) 1–18

DOI: 10.1177/1077546313492808
jvc.sagepub.com

# Vibration analysis of a Timoshenko beam on a moving base

**M Vakil[1], E Sharbati[1], A Vakil[2], F Heidari[1] and R Fotouhi[1]**

**Abstract**

In this paper free vibration of a Timoshenko beam with a tip payload, which is mounted on a cart (referred to as TBC) is studied. The cart (base) can only have lateral displacement and the tip payload has both mass and mass moment of inertia. The center of mass of the payload does not coincide with the point where the beam connects to the payload. Therefore, the tip of the beam is exposed to an extra bending moment due to the inertial force of the payload.

By employing Hamilton's principle, the governing equations of motion and the associated boundary conditions for the TBC are first derived and then transferred into dimensionless forms. By using these governing equations and their associated boundary conditions, the closed-form frequency equation (characteristic equation) of the TBC is derived. This closed-form frequency equation is validated both analytically and numerically. The closed-form expressions for the mode shapes of the TBC and their orthogonality are also presented.

By using the closed-form characteristic equation, a sensitivity study is performed and the changes in the natural frequencies versus changes in the physical parameters are investigated.

The results presented in this paper are valuable for precise dynamic modeling and model-based control of flexible mobile manipulators; a flexible mobile manipulator is a flexible link manipulator with a moving base.

**Keywords**

Closed-form frequency equation, mode shapes, orthogonality, Timoshenko beam

## 1. Introduction

The behavioral analysis of flexible structures is an ever-demanding research endeavor which must be implemented for the proper design of components utilized in machines, robots (Salarieh and Ghorashi, 2006), helicopter rotors, compressor blades (Ozgumus and Kaya, 2007), etc. These behavioral analyses can be done numerically or analytically. Although analytical relations can be obtained for simple systems, numerical analysis may be the only available option for complex systems. Although analytical methods have practical limitations, if they can be derived, they offer advantages that (i) – can be used as a benchmark to verify the numerical analysis (Oguamanam, 2003) and (ii) – can be used for a sensitivity analysis (Vakil et al., 2011a). In addition, the analytical (closed-form) expressions are usually computationally efficient compared with the numerical methods. Due to these advantages, there are numerous studies on the derivation of closed-form expressions for different flexible structures. Because presenting a comprehensive literature review on all these analytical studies is not the main aim of this paper, the investigations which are more relevant are summarized as follows:

The closed-form expressions for the (characteristic) frequency equations of Euler-Bernoulli beams with classical boundary conditions and elastic supports are available in Rao (2004) and Karnovsky (2004). The extensions of the results in Rao (2004) are presented in Wiedemann (2007), where the natural frequencies of an Euler-Bernoulli beam with large offset masses mounted on elastic supports are reported. The changes in the natural frequencies of an Euler-Bernoulli beam

[1]Mechanical Engineering Department, University of Saskatchewan, Canada
[2]Mechanical Engineering Department, University of British Columbia, Canada

Received: 14 September 2012; accepted: 23 April 2013

**Corresponding author:**
F Heidari, Mechanical Engineering Department, University of Saskatchewan, Saskatoon, SK, Canada.
Email: fatemeh.heidari@usask.ca

**Draft**
**Proceedings of the ASME 2011 International Design Engineering Technical Conferences & Computers and Information in Engineering Conference**
**IDETC/CIE 2011**
**August 29-31, 2011, Washington, DC, USA**

**DETC2011- 47967**

# On The Accuracy of Assumed Mode Modeling For Flexible Manipulators

**F. Heidari**
Mechanical Engineering Department,
University of Saskatchewan
Saskatoon, SK, Canada

**M. Vakil**
Mechanical Engineering Department,
University of Saskatchewan
Saskatoon, SK, Canada

**R. Fotouhi**
Mechanical Engineering Department,
University of Saskatchewan
Saskatoon, SK, Canada

## ABSTRACT

Assumed mode shape method (AMM) has been widely used to derive finite degree-of-freedom (DOF) dynamic model for flexible link manipulators, which theoretically have infinite DOF dynamics. For single flexible manipulator, this approximation changes locations of the zeros of transfer function, between base torque and end-effector displacement. The change in locations of zeros considerably affects accuracy of the model and hence the performance of model-based controllers.

This paper presents a comprehensive study on the change in location of zeros due to the truncation associated with AMM. It is shown that the locations of zeros of AMM model depend on four non-dimensional parameters while the locations of the analytical model depend on only two non-dimensional parameters; AMM zeros are obtained from AMM model while analytical zeros derived from infinite order model. A thorough study on the differences between AMM zeros and analytical zeros versus number of mode shapes as well as all the physical parameters is performed. Moreover, guidelines are provided to select the numbers of mode shapes such that the AMM zeros become close to the analytical zeros. These guidelines can easily be used by control engineers and thus makes them valuable for modeling and control of flexible robot manipulators.

**KEYWORDS:** flexible robot manipulator, assumed shape modeling

## INTRODUCTION

The governing dynamic equations of a single flexible link manipulator (SFLM) shown in Fig. 1, are infinite dimensional [1]. However, truncated dynamic models using the assumed mode shape method (AMM), are widely used for modeling flexible robot manipulators [2,3]. In the AMM, the spatial deflection of the flexible link is representing by a summation of mode shapes which are multiplied by time varying weight functions. The AMM are of particular interest for analysis of flexible manipulators [4,5,6] as it changes an infinite dimensional model into a finite dimensional model. However, AMM is an approximate truncated dynamic model as it eliminates the mode shapes that lie out of the bandwidth of interest [7]. The approximation associated with the AMM affects the accuracy of the dynamic model [8]. Since the performance of the controllers designed based on the AMM depends on the accuracy of the model [7], the precision of the approximated AMM model is important.

For a SFLM shown in Fig. 1, the transfer function between the base torque $\tau$ and the end-effector displacement $y$ can be obtained adopting the AMM approximation [9] or using the infinite dimensional model [10]. These transfer functions have zeros and poles, which are respectively the roots of the numerator and denominator of the transfer function [10]. The transfer function for a SFLM has right-hand-side (RHS) zeros in the domain S of the Laplace transform and thus has the non-minimum characteristic [11]. These RHS zeros are of critical importance as they limit the control bandwidth and deteriorate the trade-off between robustness and desirable control performance [12]. Furthermore, the locations of the (RHS) zeros considerably change the performance of the model-based controllers such as the inverse dynamic controller [13]. Hence a study in the accuracy of the AMM zeros is of crucial important. Although there are few reports on the difference between the AMM models and infinite dimensional model [7,14], there are no report on how the physical parameters and number of mode shapes can affect the accuracy of the AMM modeling. More precisely, there is not report on the changes in the locations of AMM zeros and infinite dimensional model zeros versus number of mode shapes and the physical parameters of the SFLM.

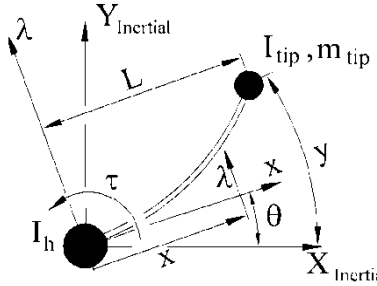


**Fig. 1: Schematic of a slewing single flexible link manipulator, SFLM**